U.S. Department of Transportation

Federal Railroad Administration

Detailed Modeling of the Train-to-Train Impact Test

Rail Passenger Equipment Impact Tests

Office of Research and Development
Washington, DC 20590

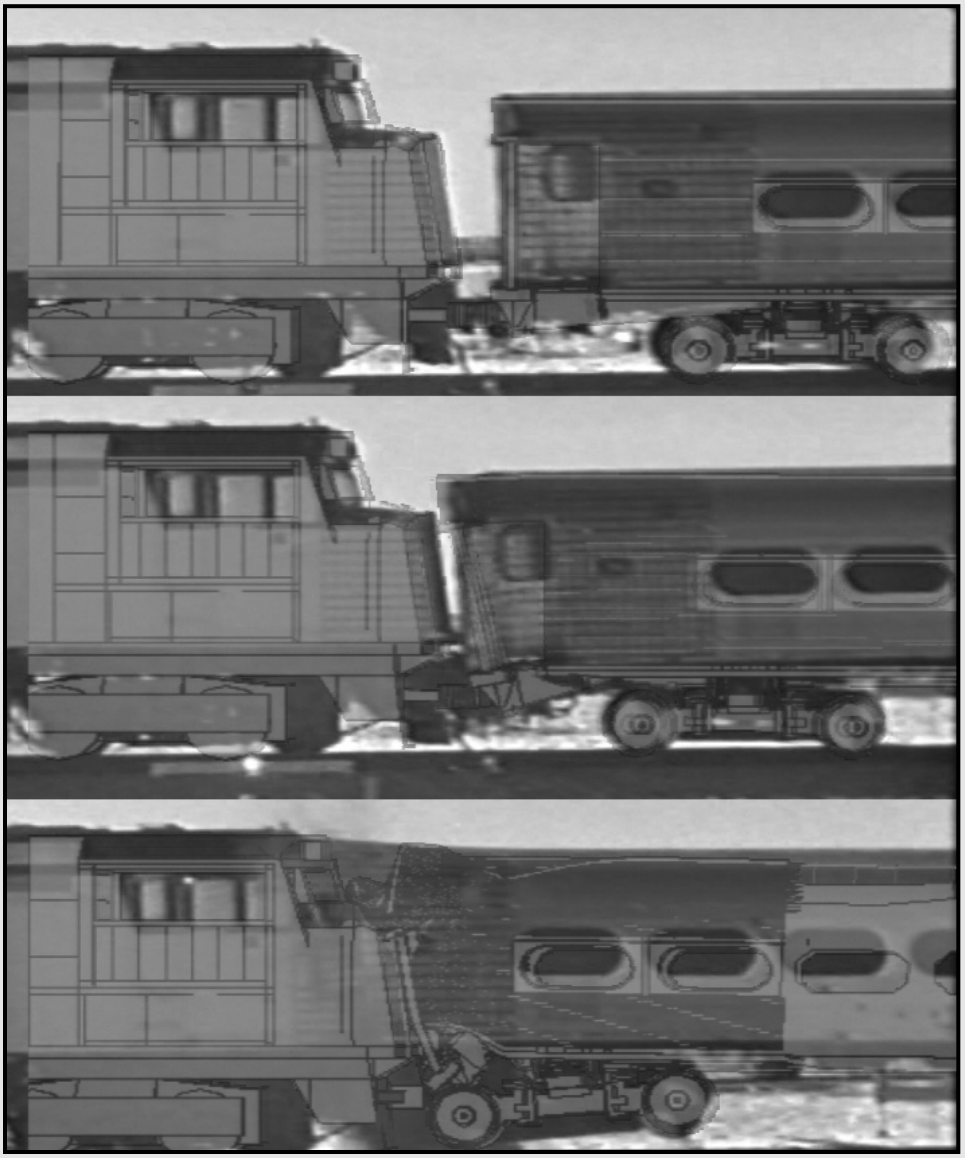

DOT/FRA/ORD-07/20

Final Report
July 2007

REPORT DOCUMENTATION PAGE

Form Approved
OMB No. 0704-0188

1. AGENCY USE ONLY (Leave blank)	2. REPORT DATE	3. REPORT TYPE AND DATES COVERED
	July 2007	Final Report November 2001-November 2002

4. TITLE AND SUBTITLE
Detailed Modeling of the Train-to-Train Impact Test

5. FUNDING NUMBERS
CB035/RR28

6. AUTHOR(S)
Richard Stringfellow and Patricia Llana

7. PERFORMING ORGANIZATION NAME(S) AND ADDRESS(ES)
TIAX LLC*
Acorn Park
Cambridge, MA 02140-2390

8. PERFORMING ORGANIZATION REPORT NUMBER
DOT-VNTSC-FRA-07-06

9. SPONSORING/MONITORING AGENCY NAME(S) AND ADDRESS(ES)
U.S. Department of Transportation
Federal Railroad Administration
1120 Vermont Avenue NW – Mail Stop 20
Washington, DC 20590

10. SPONSORING/MONITORING AGENCY REPORT NUMBER
DOT/FRA/ORD-07/20

11. SUPPLEMENTARY NOTES
*under contract to: U.S. Department of Transportation
John A. Volpe National Transportation Systems Center
55 Broadway
Cambridge, MA 02142-1093

12a. DISTRIBUTION/AVAILABILITY STATEMENT
This document is available to the public through the National Technical Information Service, Springfield, Virginia 22161.
This document is also available on the FRA Web site at www.fra.dot.gov.

12b. DISTRIBUTION CODE

13. ABSTRACT (Maximum 200 words)
This report describes the results of a finite element-based analysis of the train-to-train impact test conducted at the Federal Railroad Administration's Transportation Technology Center in Pueblo, CO, on January 31, 2002. The ABAQUS/Explicit dynamic finite element code was used to simulate the first 0.5 second (s) of the collision. The primary objective of this program was to extend the use of finite element-based models for simulating the crush of train structures to include vehicle-to-vehicle interactions.

A subset of the data collected during the test was first selected as a basis for comparison with model predictions. A finite element model of the train was then developed. This model includes detailed representations of the end structures of the cab car and the locomotive, and coarser representations of the back of these vehicle bodies and the trucks of the cab car. Connections between the cab car body and trucks were modeled to allow for lift of the body during the collision. Trailing vehicles and vehicle-to-vehicle connections were modeled using lumped mass parameters.

The results of the model were compared to the selected data. These comparisons indicate that the model captures many aspects of collision behavior, with a fair degree of accuracy, especially over the first 0.25 s of the collision.

14. SUBJECT TERMS
Transportation, safety, crashworthiness, passenger rail vehicles, cab car end structure, locomotive cab

15. NUMBER OF PAGES
84

16. PRICE CODE

17. SECURITY CLASSIFICATION OF REPORT	18. SECURITY CLASSIFICATION OF THIS PAGE	19. SECURITY CLASSIFICATION OF ABSTRACT	20. LIMITATION OF ABSTRACT
Unclassified	Unclassified	Unclassified	

METRIC/ENGLISH CONVERSION FACTORS

ENGLISH TO METRIC

LENGTH (APPROXIMATE)

1 inch (in)	=	2.5 centimeters (cm)
1 foot (ft)	=	30 centimeters (cm)
1 yard (yd)	=	0.9 meter (m)
1 mile (mi)	=	1.6 kilometers (km)

AREA (APPROXIMATE)

1 square inch (sq in, in^2)	=	6.5 square centimeters (cm^2)
1 square foot (sq ft, ft^2)	=	0.09 square meter (m^2)
1 square yard (sq yd, yd^2)	=	0.8 square meter (m^2)
1 square mile (sq mi, mi^2)	=	2.6 square kilometers (km^2)
1 acre = 0.4 hectare (he)	=	4,000 square meters (m^2)

MASS - WEIGHT (APPROXIMATE)

1 ounce (oz)	=	28 grams (gm)
1 pound (lb)	=	0.45 kilogram (kg)
1 short ton = 2,000 pounds (lb)	=	0.9 tonne (t)

VOLUME (APPROXIMATE)

1 teaspoon (tsp)	=	5 milliliters (ml)
1 tablespoon (tbsp)	=	15 milliliters (ml)
1 fluid ounce (fl oz)	=	30 milliliters (ml)
1 cup ©	=	0.24 liter (l)
1 pint (pt)	=	0.47 liter (l)
1 quart (qt)	=	0.96 liter (l)
1 gallon (gal)	=	3.8 liters (l)
1 cubic foot (cu ft, ft^3)	=	0.03 cubic meter (m^3)
1 cubic yard (cu yd, yd^3)	=	0.76 cubic meter (m^3)

TEMPERATURE (EXACT)

[(x-32)(5/9)] °F = y °C

METRIC TO ENGLISH

LENGTH (APPROXIMATE)

1 millimeter (mm)	=	0.04 inch (in)
1 centimeter (cm)	=	0.4 inch (in)
1 meter (m)	=	3.3 feet (ft)
1 meter (m)	=	1.1 yards (yd)
1 kilometer (km)	=	0.6 mile (mi)

AREA (APPROXIMATE)

1 square centimeter (cm^2)	=	0.16 square inch (sq in, in^2)
1 square meter (m^2)	=	1.2 square yards (sq yd, yd^2)
1 square kilometer (km^2)	=	0.4 square mile (sq mi, mi^2)
10,000 square meters (m^2)	=	1 hectare (ha) = 2.5 acres

MASS - WEIGHT (APPROXIMATE)

1 gram (gm)	=	0.036 ounce (oz)
1 kilogram (kg)	=	2.2 pounds (lb)
1 tonne (t)	=	1,000 kilograms (kg)
	=	1.1 short tons

VOLUME (APPROXIMATE)

1 milliliter (ml)	=	0.03 fluid ounce (fl oz)
1 liter (l)	=	2.1 pints (pt)
1 liter (l)	=	1.06 quarts (qt)
1 liter (l)	=	0.26 gallon (gal)
1 cubic meter (m^3)	=	36 cubic feet (cu ft, ft^3)
1 cubic meter (m^3)	=	1.3 cubic yards (cu yd, yd^3)

TEMPERATURE (EXACT)

[(9/5) y + 32] °C = x °F

QUICK INCH - CENTIMETER LENGTH CONVERSION

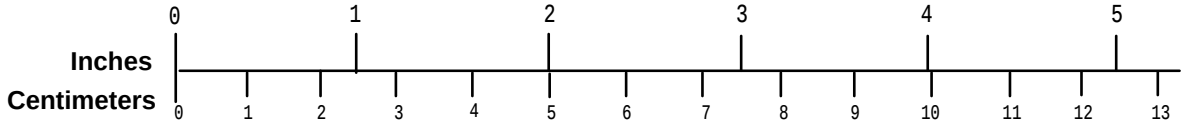

QUICK FAHRENHEIT - CELSIUS TEMPERATURE CONVERSION

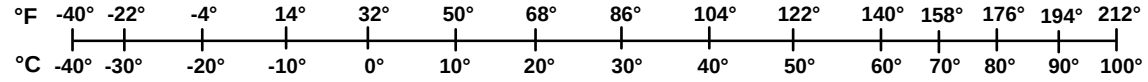

For more exact and or other conversion factors, see NIST Miscellaneous Publication 286, Units of Weights and Measures. Price $2.50 SD Catalog No. C13 10286 **Updated 6/17/98**

Preface

This report describes the results of a finite element-based analysis of the recently conducted train-to-train impact test, conducted on January 31, 2002. The first 0.5 second of the collision was simulated. Results of the analysis are compared with accelerometer and video data recorded from the test. Specific comparisons are made between test data and model predictions for colliding vehicle motions, collision forces, forces imparted by trailing equipment, and deformation modes.

This work was performed under contract for the Volpe Center as part of the Equipment Safety Research Program sponsored by the Office of Research and Development of the Federal Railroad Administration. This contract was initiated and monitored by David Tyrell, Senior Engineer, Volpe Center. The authors would like to thank Dr. Tom Tsai, Program Manager, and Claire Orth, Division Chief, Equipment and Operating Practices Research Division, Office of Research and Development, Federal Railroad Administration, for their support. The authors would also like to thank Eloy Martinez, Kari Jacobsen, and John Zolock of the Volpe Center and Benjamin Perlman of Tufts University for their helpful review and suggestions.

Table of Contents

List of Figures

List of Tables

Executive Summary

This report describes the results of a finite element-based analysis of the train-to-train impact test conducted at the Federal Railroad Administration's Transportation Technology Center (TTC) in Pueblo, CO, on January 31, 2002. The primary objective of this study was to extend the use of finite element-based models for simulating the crush of train structures to include vehicle-to-vehicle interactions. The ABAQUS/Explicit dynamic finite element code was used to simulate the first 0.5 second (s) of the collision. Finite element analysis has proven to be a useful methodology for evaluating the structural effects of a collision and improving the design of vehicle end structures so that they can better withstand the extremely high forces associated with a collision.

Data collected during the test were first selected as a basis for comparison with model results. These data include longitudinal, vertical, and lateral motions of the colliding vehicles; collision forces; high-speed video images captured during the test; and photographs of key components following the test.

A finite element model of the train was then developed. This model includes detailed representations of the end structures of the cab car and the locomotive, as well as less detailed representations of the back of these vehicle bodies and the trucks of the cab car. Connections between the cab car body and trucks were modeled to allow for lift of the body during the collision. Trailing vehicles and vehicle-to-vehicle connections were modeled using lumped mass parameters.

The model's results were compared to the selected data. These comparisons indicate that the model captures many aspects of the collision behavior. In particular, the longitudinal motions of the colliding vehicles and the collision forces were calculated with a fair degree of accuracy, especially over the first 0.25 s of the collision. Many of the key modes of deformation were also captured, including the severe folding of the draft gear, the downward bending of the end frame and its subsequent locking onto the short hood of the locomotive, the rotation of the end frame and associated off-center interaction of the collision posts with the anticlimber short hood, and the pitch rotation of the cab car body and lifting of the forward truck wheels.

The accuracy of the model begins to degrade after 0.25 s. This is principally because of the relatively simple material failure representation employed in the finite element code. In most finite element codes, including ABAQUS, DYNA3D, PAMCRASH, and others, when the magnitude of the strain in the material reaches a specified value, the material no longer supports a load. This representation is fairly accurate for tension; however, materials generally fail at significantly higher strains under compression and somewhat lower strains in shear. The simple strain-to-failure approach greatly oversimplifies material failure in complex three dimensional stress states—combinations of tension, compression, and shear. Nonetheless, the favorable comparisons between the model results and the test measurements suggest that the model can be successfully used as a tool to evaluate the consequences of a collision and, more importantly, to help improve the design of vehicle end structures.

1. Introduction

The Volpe National Transportation Systems Center (Volpe Center) is conducting ongoing research into the crashworthiness of rail vehicles in support of the Federal Railroad Administration's Office of Research and Development. Two integral components of this research include the development of computer models for simulating rail vehicle collisions and full-scale collision testing of rail equipment.

These two aspects of rail crashworthiness research go hand-in-hand. Computer models allow for study of the response of rail equipment over a wide range of collision scenarios and for assessment of the effects of vehicle modifications in a cost-effective manner. Full-scale testing (among other goals) provides a means to validate these models so that they can be applied over the desired range of collision conditions with confidence. Due to the competing modes of deformation that are associated with train collisions, sub-scale testing by itself is not adequate for this purpose.

As part of a series of full-scale tests, a train-to-train impact test was performed on January 31, 2002, at TTC in Pueblo, CO. In this test, a cab car-led passenger train, consisting of a cab car, three coach cars, and a trailing locomotive, traveling at 30 mph (48 km/h), collided with a standing locomotive-led train with two ballasted hopper cars. Figure 1 is a schematic that shows the makeup of the two trains. The total weight of each train was approximately 635,000 lb (288,000 kg). During the test, the lead cab car overrode the cab of the standing locomotive, sustaining approximately 22 ft (6.7 m) of crush (see Figures 2 and 3), while the cab of the locomotive remained essentially intact, with the anticlimber skirt and short hood denting in and the windshield center post crushing by about 1 ft (0.3 m).

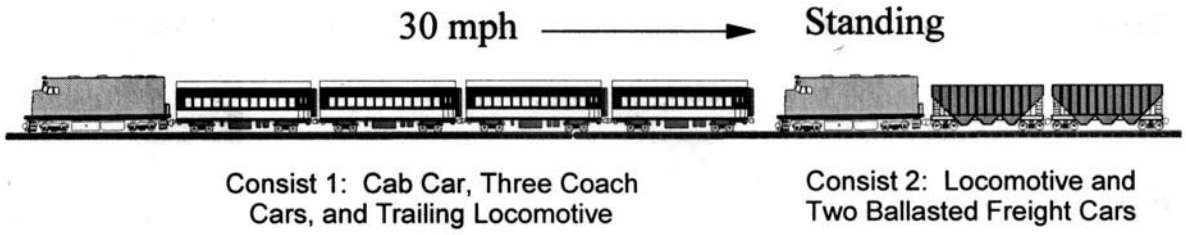

Figure 1. Schematic of the Full-Scale Train-to-Train Collision

Source: [1]

Figure 2. Images Taken from High-Speed Film Showing the Cab Car Overriding the Standing Locomotive

Source: [1]

Figure 3. Photograph of the Cab Car-Led Train Following the Collision

This study differs from previous work because the striking and struck vehicles are simulated using nonlinear explicit/dynamic finite element analysis. Both impacting vehicles were modeled as deformable bodies, rather than a deformable body impacting a rigid body [2-7].

Previous analyses of train collisions have typically broken the problem into three parts:

- The crush behavior of the cars
- The overall dynamics of the train
- The dynamics of the occupant inside the train

The crush behavior of the cars is evaluated with nonlinear finite element analysis (FEA) to determine the force required to crush the car and the shape of the car as it crushes. The collision dynamics behavior is evaluated with the lumped-parameter model to determine the distribution of crush among the cars and the trajectories of the cars during a collision, including the deceleration of the cars. The occupant dynamics behavior is evaluated with a lumped-parameter model to determine the forces and decelerations of the occupants. Comparisons with the results of full-scale testing have shown this approach to be effective in predicting impact test results [3-7].

Analysis of the train collision dynamics with a lumped-parameter model requires heuristic elements to approximate the interaction of the colliding equipment. Development of these elements relies on the interpretation of the crush analyses of the equipment and may draw on prior knowledge of the modeler about the interaction of similar equipment under similar impact conditions.

The added complexity that this new approach captures is the ability to study the interface. As key structural elements on both vehicles deform, it is now possible to study either the formation of a ramp or catapulting mechanism that can cause override to occur. This information will be useful in developing strategies to prevent this dangerous deformation mode. Additionally, it is possible to study the effect of trailing vehicles on lead vehicle crush behavior. This further provides insight into the modes of deformation and crush forces that were observed in the test.

The principal advantage of this approach lies in its ability to directly evaluate the influence of changes in the structural design of the vehicles, including geometry and materials, on the outcome of the collision. This approach, therefore, lends itself to refining a rail car's structural design more efficiently than it can be refined using typical analysis methods.

Although this approach allows for a more direct representation of the interaction of the impacting bodies, it does have potential pitfalls, including the modeling of material failure. The representation of material failure is quite simple in nonlinear FEA programs, such as ABAQUS, DYNA3D, and PAMCRASH, in comparison to the actual phenomenon. In these finite element codes, when the magnitude of the strain in the material reaches a specified value, the material no longer supports a load. This representation is fairly accurate for tension; however, materials generally fail at significantly higher strains under compression and somewhat lower strains in shear. The simple strain-to-failure approach greatly oversimplifies material failure in complex three dimensional stress states—combinations of tension, compression, and shear. In the later stages of the impact, structural components have failed, and new contact surfaces are formed. Inaccuracies in calculating the location and extent of these new contact surfaces degrade the calculations for the trajectories of the equipment.

In order to provide specific bases against which to compare the results of this model, appropriate subsets of the data that had been measured during the collision were first identified, collected, and organized. The test vehicles were each instrumented with a number of accelerometers, string potentiometers, and strain gages. In addition, high-speed film was taken of the collision from several perspectives. The high-speed film was reviewed, and still photographs were extracted for comparisons with the model results. The data was also reviewed, and selections were imported into spreadsheets, also for comparison with the model results.

Next, the finite element model of the two trains was developed. The models that had been developed in earlier programs for crush analysis of each of the two lead vehicles–the cab car and the standing locomotive–were used as starting points. A significant number of modifications were made to each of these models. New sub-models were developed defining truck-to-body connections for the cab car and defining the behavior of the colliding couplers. Lumped mass elements were used to model trailing vehicles and coupled vehicle connections.

The model was exercised, and the results compared to the test data that had previously been identified. This was an iterative process that resulted in a number of modifications to the model. The goal was to simulate, with reasonable accuracy, the first 0.25 s of the collision, during which the colliding vehicles crushed approximately 7.6 ft (2.3 m).

This report is organized as follows. Chapter 1 introduces the passenger vehicle crashworthiness test program and the approaches used in modeling and simulating the crashes using FEA and dynamic analysis applications. Chapter 2 summarizes the results of the data collected and how data was gathered using accelerometers and video cameras. Chapter 3 summarizes how components and vehicle structure were modeled using FEA and dynamic modeling programs. Chapter 4 compares the results obtained from the model to the actual test data and video stills. Chapter 5 presents conclusions from the comparison. The Appendix provides supporting data that expands on information already presented in the main text.

2. Reduction of the Train-to-Train Test Measurements

Comparisons between the model and the test were made in terms of four different measures of collision behavior:

1. Deformation modes—The deformed shape of the forward end of the cab car and the forward end of the standing locomotive as a function of time during the collision.
2. Colliding vehicle motions—Longitudinal, vertical and lateral displacements, velocities, and accelerations of the cab car and the standing locomotive.
3. Collision force—Longitudinal force between the cab car and the standing locomotive.
4. Forces imparted by trailing equipment—Longitudinal forces acting between the cab car and the first coach car and between the standing locomotive and the first ballasted freight car.

The approach taken to complete this task included reviewing high-speed film, developing spreadsheet data and graphics files for direct comparisons to model results, and reviewing selected data sets to ensure that appropriate measures of comparisons were selected.

2.1. Deformation Modes

Deformation modes of the colliding vehicles were captured by means of analysis of video stills taken from the high-speed film and inspection of the deformed structures following the collision. Each of these means is limited. Video stills show only a single viewpoint (in this case, primarily from the side of the impact point because the view from above the impact point is not clear enough to provide meaningful information), and they do not show deformation of key structural elements very well. On the other hand, post-mortem inspection of structures does not provide any information on the timing of the deformation. Interpretation of post-collision damage is particularly difficult for this collision because of the extreme damage suffered by the end of the cab car.

2.1.1. Video Images

Video stills showing a side view of the forward ends of the colliding vehicles were captured at several instances over the first 0.25 s of the collision (7.6 ft or 2.3 m of crush). Two sequences of images (one from each side of the impact point) were captured from high-speed video, as shown in Figures 4 and 5. These images clearly show the forward motion of the cab car and the slight backward motion of the locomotive.

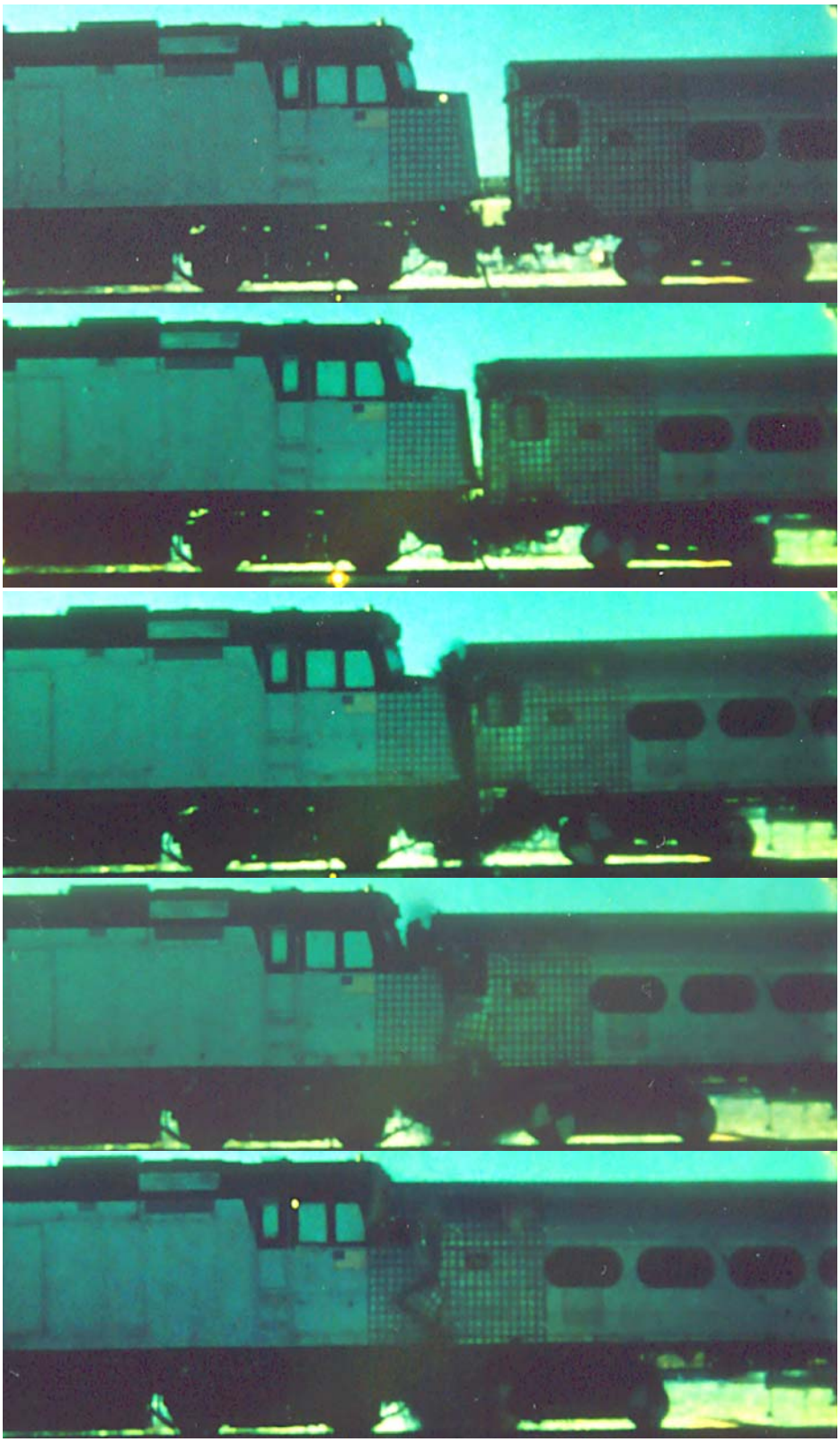

Figure 4. Sequence of Crush Over the First 0.25 s of the Collision (West Side View)

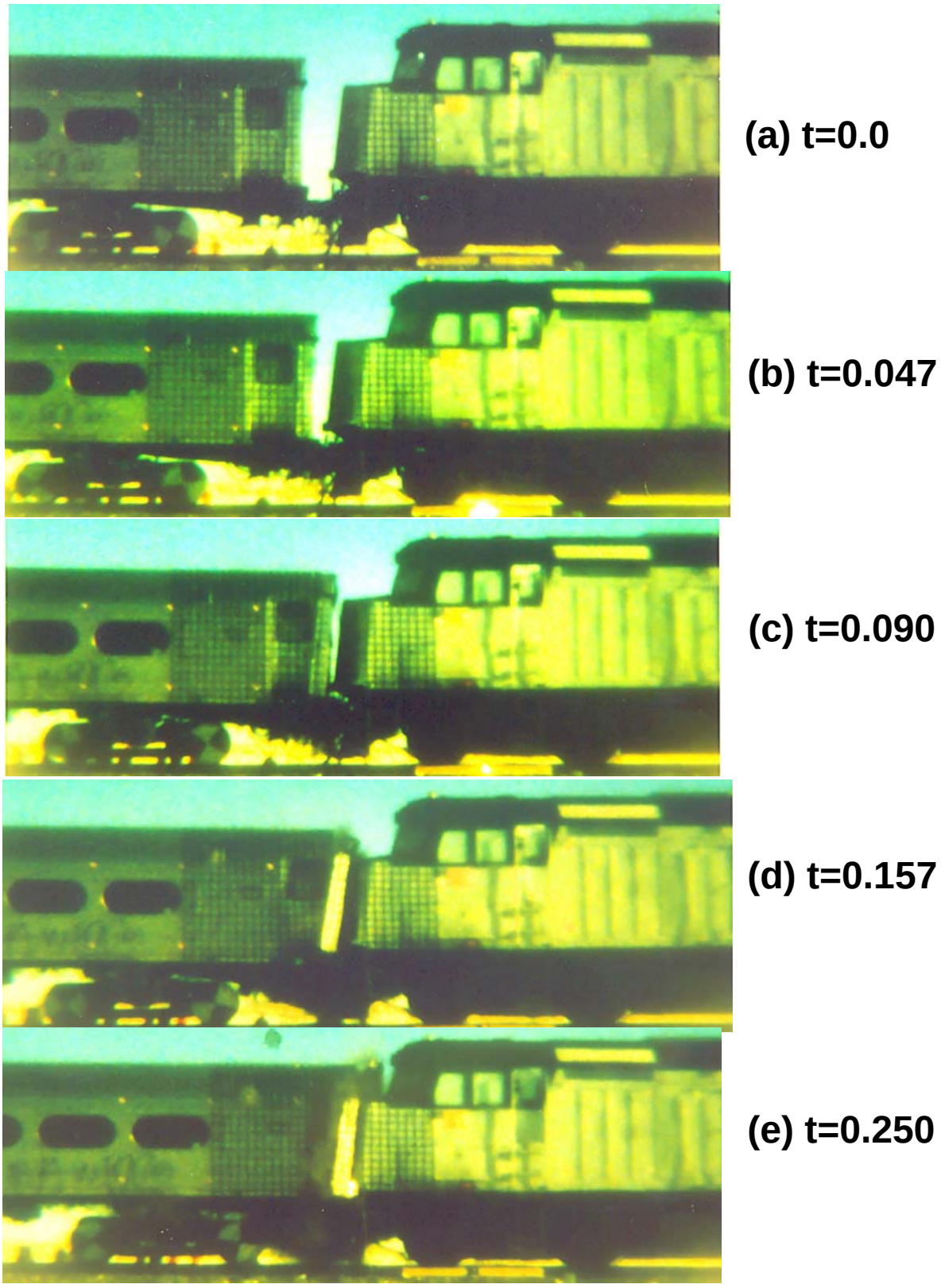

Figure 5. Sequence of Crush Over the First 0.25 s of the Collision (East Side View)

The following lists the progress of deformation that can be gleaned from these images for each of the times indicated.

0.0 s (impact)

Figures 4(a) and 5(a) show the vehicles at impact. The following details regarding the relative position of the vehicles can be obtained from these images:

- There is about a 30-in (762-mm) gap between the end of the cab car and the top front of the locomotive short hood.
- The front of the short hood is inclined by about 5 degrees relative to the front of the cab car.
- There is about an 11-in (279-mm) vertical separation between the bottom edges of the regions—gridded with 6-in (152-mm) squares—on the sides of each of the vehicles, with the locomotive grid higher.
- The bottom of the cab car draft sill is approximately 24 in (610 mm) above the rail.
- The bottom of the locomotive plow is approximately 8 in (203 mm) above the rail.

0.047 s

Figures 4(b) and 5(b) show the vehicles 0.047 s after collision when approximately 1.7 ft (0.52 m) of crush has occurred between the cab car and the standing locomotive. At this point, the following has occurred:

- The gap between the vehicle ends has closed from 30 in (672 mm) to about 10 in (254 mm).
- The end of the cab car has pitched forward slightly, lowering the inclination between it and the front of the short hood from about 5 degrees to approximately 4 degrees.
- The bottom edges of the respective grids are separated vertically by approximately 13 in (330 mm), indicating a drop of the end of the cab car body relative to the locomotive body of approximately 2 in (51 mm).
- The bottom of the cab car draft sill is closer to the rail by approximately 2 in (51 mm), indicating that the forward end of the cab car has also moved downward.
- The locomotive plow has not moved downward significantly.

0.090 s

Figures 4(c) and 5(c) show the vehicles at 0.090 s after collision when approximately 2.8 ft (0.85 m) of crush has occurred between the cab car and the standing locomotive. At this point, the following has occurred:

- The gap between the vehicle ends is nearly closed—Figure 4(c) does not show a gap, while Figure 5(c) shows a gap of only about 6 in (154 mm). (Differences may simply be due to the positions of the respective cameras but may also be indicative of some twisting of the cab car end frame.)
- The end of the cab car has pitched forward significantly, so that the inclination between it and the front of the short hood has decreased to only 1 or 2 degrees.
- The bottom edges of the respective grids are separated now by only approximately 10 in (254 mm), indicating that the cab car body has climbed about 3 in (76 mm) relative to the locomotive body.
- The forward end of the draft sill is nearly touching the rail, having moved downward by another 4 to 6 in (102 to 152 mm).
- The locomotive plow has moved downward by a few inches.

0.157 s

Figures 4(d) and 5(d) show the vehicles at 0.157 s after collision when approximately 4.7 ft (1.43 m) of crush has occurred between the cab car and the standing locomotive. At this point, the following has occurred:

- The cab car end frame has conformed to the front of the short hood.
- The bottom edges of the respective grids are separated now by only approximately 4 to 6 in (102 to 152 mm), indicating that the cab car body has climbed another 4 to 6 in (102 to 152 mm) relative to the locomotive body.
- The forward end of the draft sill has moved downward by another 4 in (102 mm) or so.
- The locomotive plow has moved downward by approximately 2 in (51 mm) more.
- The skin covering the top of the end frame has started to climb over the top of the short hood.

0.250 s

Figures 4(e) and 5(e) show the vehicles at 0.25 s after collision when approximately 7.4 ft (2.26 m) of crush has occurred between the cab car and the standing locomotive. At this point, the following has occurred:

- The cab car end frame continues to be locked to the front of the short hood.
- The bottom edges of the respective grids are nearly level, indicating that the cab car body has climbed another 4 to 6 in (102 to 152 mm) relative to the locomotive body.
- The locomotive plow is now very close to the rail.
- The skin covering the top of the end frame is beginning to interact with the locomotive cab window structure.

2.1.2. Post-Collision Inspection

A review was conducted of photographic information collected after the test for comparison to the finite element analysis. The goal was to document the key modes of final deformation and to deduce, to the extent possible, the manner in which deformation progressed during the collision.

Figure 6 shows a more detailed view of the cab car after the test (compare with Figure 3). The end frame and the underframe have been completely torn away from the superstructure of the car, and the entire car has moved off to the left of the track (looking in the direction of moving train travel). The end frame can be seen in Figure 6 lying on the left rail of the track, close to the location of initial impact. Figure 7 shows a close up of the left collision post (again looking in the direction of moving train travel); the front face of which is down toward the ground in the photograph. The position of the end frame on the track indicates that it remained in contact with the hood of the locomotive during most of the crush.

Figure 6. End Frame is Lying Face Down Over the Left Rail, Oriented Approximately 90° with Respect to the Track

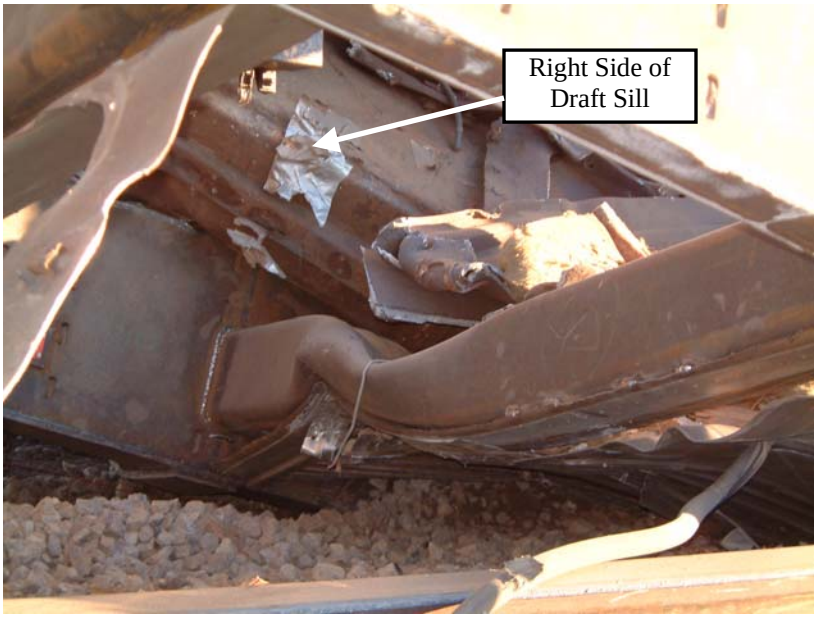

Figure 7. Left Collision Post: Front of Post is Facing Down and the End of Draft Sill Is Lying Just on Top of It

Figure 8 shows the front surface of the standing locomotive following the test. A large dent that is approximately 16 in (406 mm) is to the left of the centerline of the locomotive. It appears that this dent corresponds to the dent in the collision post (Figure 7). Substantially smaller dents exist on both the right side of the locomotive and the right collision post of the cab car (not shown). This can be explained if the cab car end frame shifted a few inches to the right as the cab car coupler draft pocket crushed. As illustrated in Figure 9, the large dent on the locomotive short hood is approximately 3 or 4 in (76 to 102 mm) closer to its centerline than one would expect if the cab car and locomotive centerlines had been coincident; the original distance between each cab car collision post and the cab car centerline was 19 in (483 mm). The angled profile (in plan view) of the locomotive anticlimber/hood would then cause the left cab car collision post to be struck first, as indicated in Figure 9, and this could then cause enough damage and weakening in the draft sill to result in a lower force impact on the right collision post. The damaged coupler pocket in the locomotive, as shown in Figure 10, provides further evidence for a shift to the right.

Figure 8. Views of Locomotive After the Test

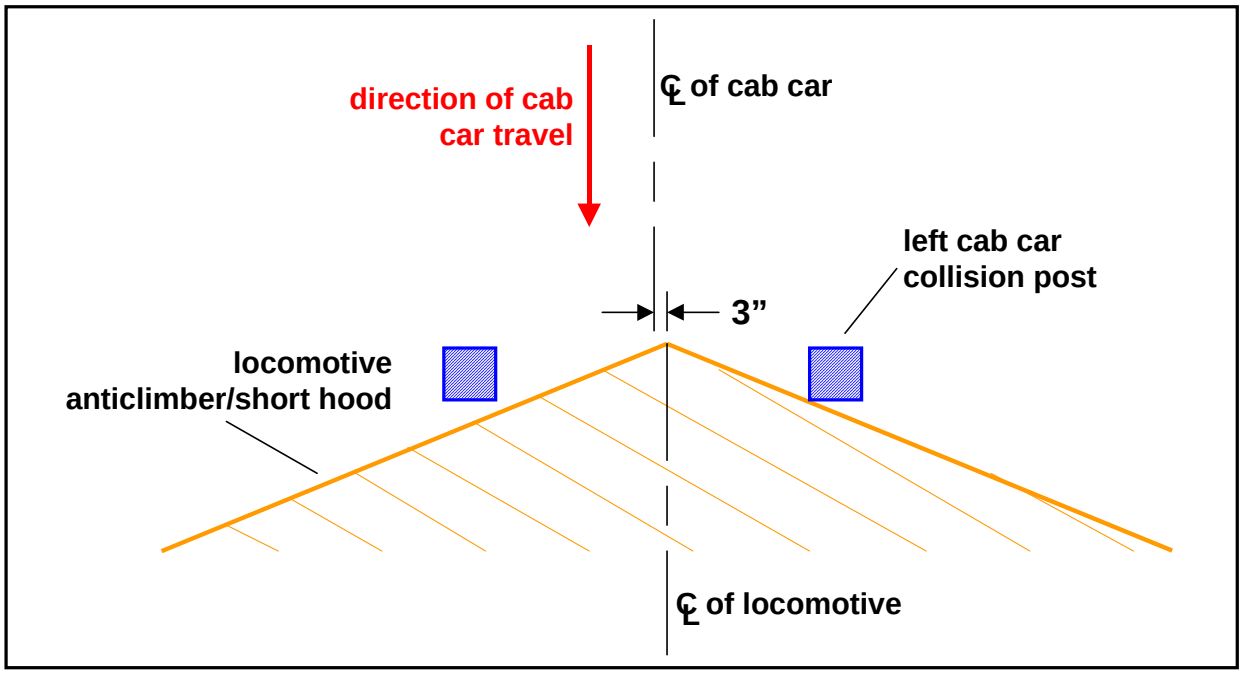

Figure 9. Illustration of a Possible Mode by which the Cab Car Collision Posts Collided with the Locomotive Anticlimber/Hood

Figure 10. Damaged Coupler Pocket of the Locomotive

Figure 9 also shows the imprint of the cab car end frame on the hood, from which it can be deduced that there was some counterclockwise rotation of the end frame about the longitudinal axis as initial deformation occurred. The end frame also appears to have rotated about a transverse horizontal axis as the bottom of the end frame was pushed inward and the end frame tilted to conform to the tilted profile of the locomotive (as is evident in Figures 4 and 5). The counterclockwise rotation may have been caused by the longitudinal load on the left collision post, which would have a component in the plane of the end frame once the end frame began to pitch. Such a component of load would tend to twist the end frame counterclockwise. (Finite element results presented in Section 4.1 also show twisting and suggest that the end frame may not be very resistant to twist.)

The manner in which the draft sill deformed during the collision is difficult to deduce because of the severe damage that occurred to all components. Observations made from the one- and two-car tests [1, 2] suggest that, in a collision in which the cab car coupler is impacted, the structure behind the draft gear fractures and pushes back. In addition, one of the sides of the draft sill can fail, and the front of the draft sill can shear downward with respect to the rear. Figures 11 and 12 show sketches made of the damaged draft sill from the one-car test that illustrates these deformation modes.

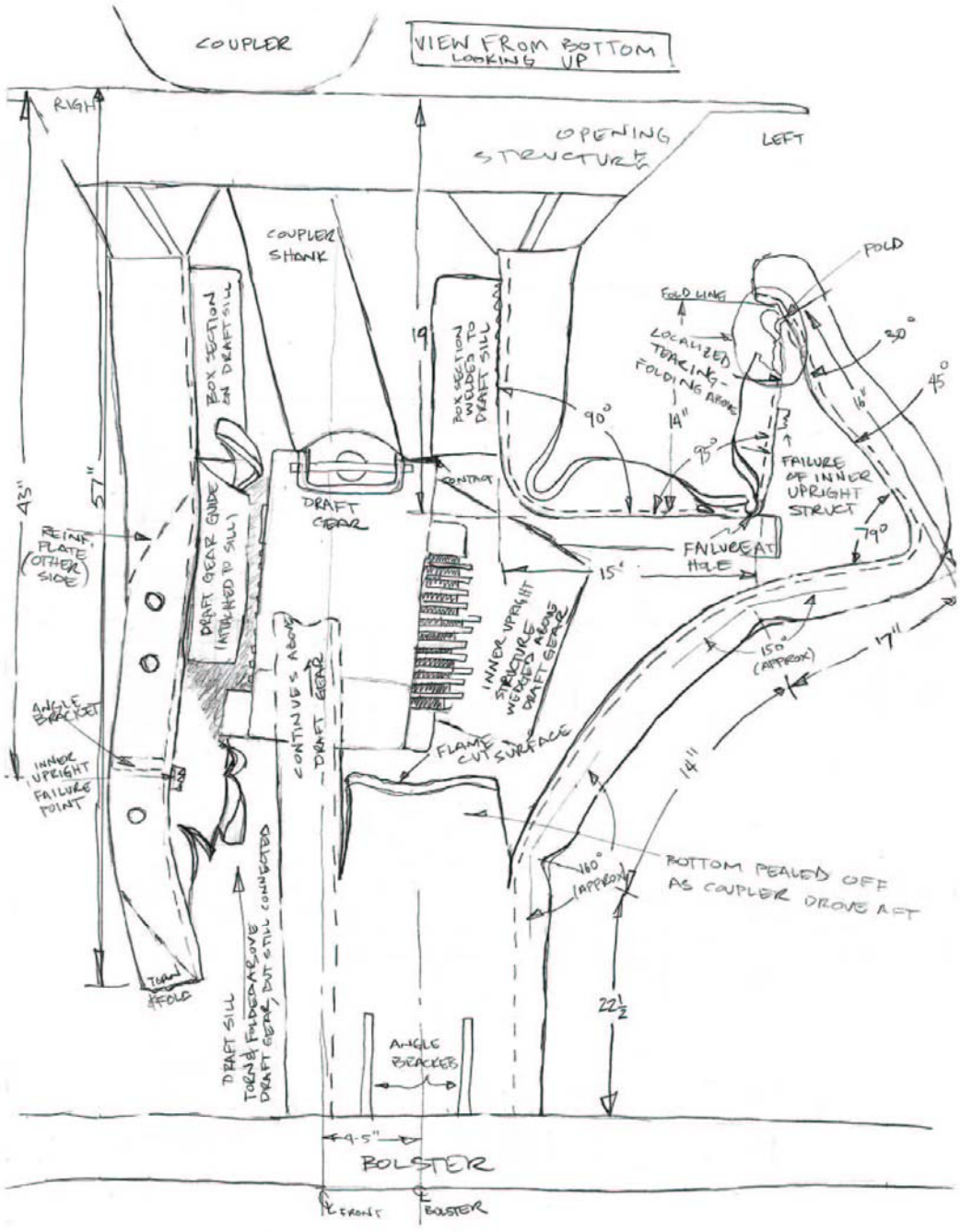

Source [3]

Figure 11. Sketches of the Damaged Draft Sill from the One-Car Test, View from Bottom

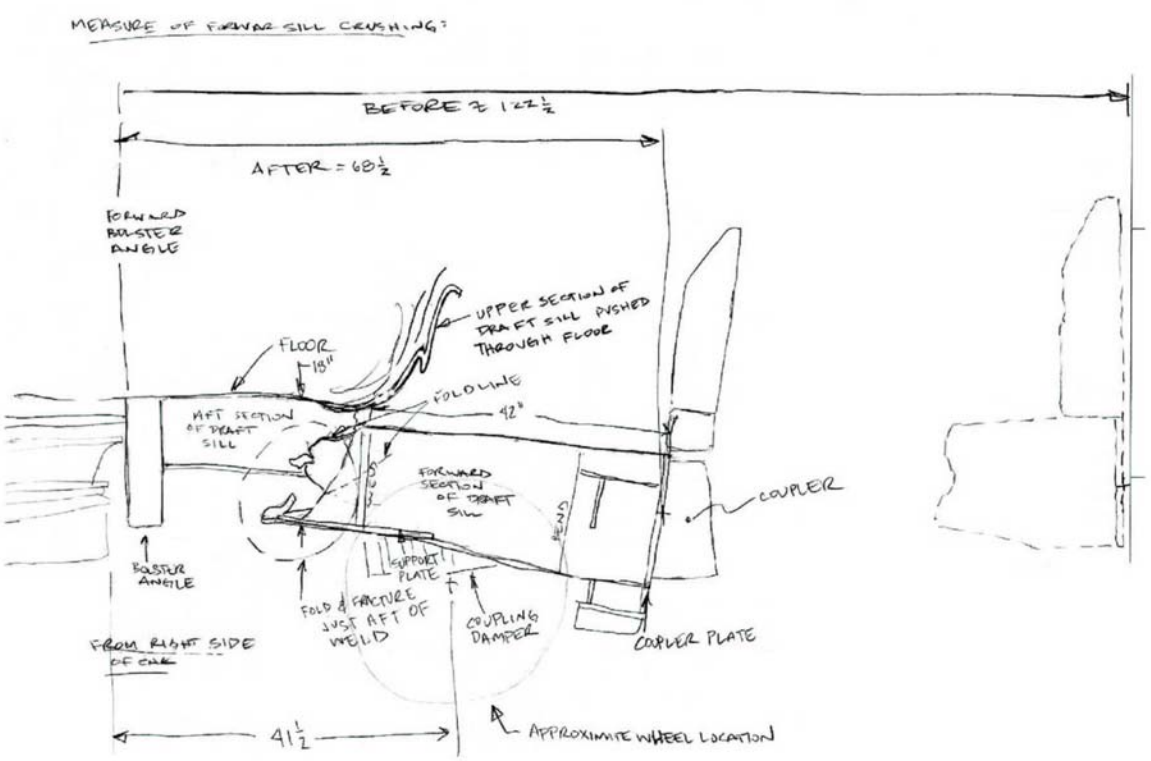

Source [3]

Figure 12. Sketches of the Damaged Draft Sill from the One-Car Test, Side View

Evidence exists that the draft sill folded to the side at some point in the collision. Figure 12 shows that the end of the draft sill and the end frame folded together on the left side of the car, which is consistent with an impact that was initially on the left side of the cab car. It also appears from Figure 13 that the draft sill folded into a Z-shape.

Finally, Figure 14 shows that the connection between the roof rails and the end frame fractured at some point on the collision.

Figure 13. Photograph of Deformed Draft Sill (Dashed Line Shows Bent Shape of the Draft Sill)

Figure 14. Location at which Roof Rail Was Connected to Left, Rear Side of Antitelescoping Plate

This photographic evidence suggests the following vehicle-to-vehicle impact and deformation sequence:

- The couplers of the cab car and the locomotive collided and transmitted substantial longitudinal force that probably fractured the structure behind the cab car draft gear.
- During this initial deformation of the draft gear support structure, a slight displacement of the cab car body to the right also occurred.
- This rightward displacement caused the left cab car collision post to be struck first by the locomotive anticlimber/hood.
- The draft sill then formed hinges as the overall crush progressed. The first of these hinges appears to be located behind the draft gear (approximately 4 ft (1.22 m) from the end).
- The higher load on the left side of the cab car end frame, combined with a tilt of the end frame, caused rotation about the longitudinal axis of the cab car.

The reason that the cab car eventually moved off to the left of the track is not clear. It appears that the initial motion of the cab car was to the right, but eventually the complex deformation and fracture that occurred in the underframe and body must have pushed its front end to the left.

2.2. Colliding Vehicle Motions

Vehicle motion data were derived from two sources: accelerometers and high-speed film. For the test, each vehicle was outfitted with a number of accelerometers. Figure 15 shows the arrangement of accelerometers on the cab car. The other vehicles had fewer accelerometers installed to adequately provide redundant measurements for the longitudinal motions of the vehicles. Accelerometer arrangement schematics for all vehicles can be found in [8].

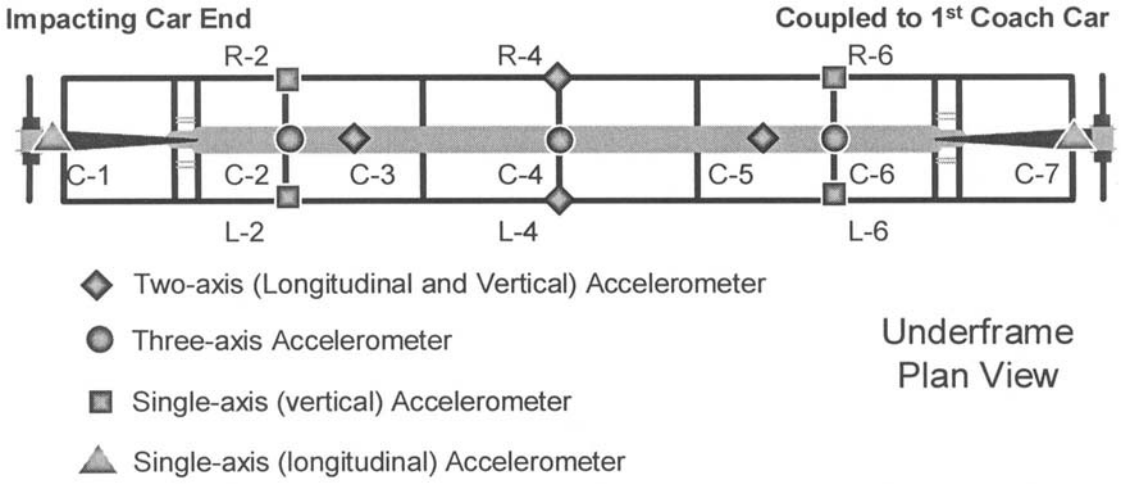

Figure 15. Schematic Showing Layout of Accelerometers for the Cab Car

The raw acceleration data were processed to remove high-frequency noise according to Society of Automotive Engineers (SAE) J211 standards. Vehicle acceleration-time histories were generated using a Channel Frequency Class (CFC) 60 (Butterworth 4-pole phaseless digital) filter. Velocity-time histories were generated using a CFC 180 filter on the acceleration data and then numerically integrating using the trapezoidal rule. Displacement-time histories were similarly generated by filtering at CFC 180 and double integrating.

Displacement data were also generated through photometric analysis of high-speed film. High-speed film cameras were placed at the locations shown in Figure 16. Through review of the movements captured on film, the following were determined:

- Longitudinal, vertical, and lateral displacements for the colliding cab car and locomotive
- Longitudinal displacements for all of the trailing vehicles

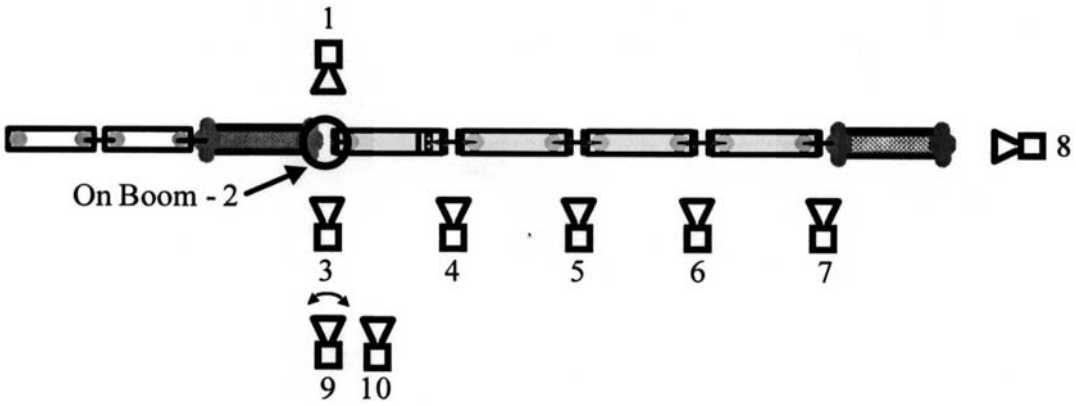

Figure 16. Schematic Showing Layout of High-Speed Cameras

Using these data, a subset of the measured motion-time histories was selected for direct comparison with finite element results. Table 1 summarizes the time-history selected for comparison with the model.

Table 1. Vehicle Motion Time-Histories Selected for Comparison to Model Predictions

Vehicle	Component	Measure
Cab Car	Longitudinal	Acceleration
		Velocity
		Displacement
	Vertical	Acceleration
		Velocity
		Displacement
	Lateral	Displacement
	Pitch Rotation	Pitch Angle
Standing Locomotive	Longitudinal	Velocity
		Displacement

The following plots, Figures 17-30, represent each of the time histories (motions and forces) selected for comparison to the model. In Figure 17, the longitudinal deceleration of the cab car exhibits an initial peak acceleration of approximately 20 G after 0.02 s. A second, smaller peak of approximately 15 G occurs at 0.04 s, followed by a negative (positive acceleration) peak of approximately 10 G at 0.07 s. Over the remainder of the first 0.5 s, the acceleration levels vary within the range of ± 6 G.

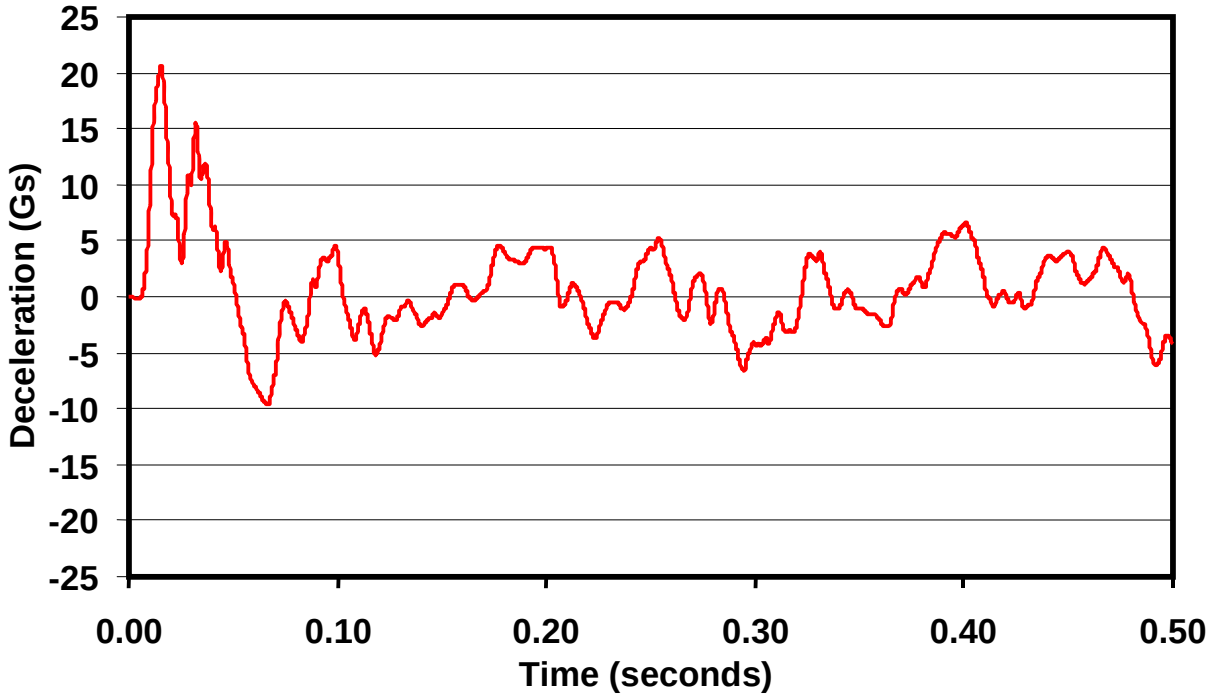

Figure 17. Measured Longitudinal Deceleration of the Cab Car

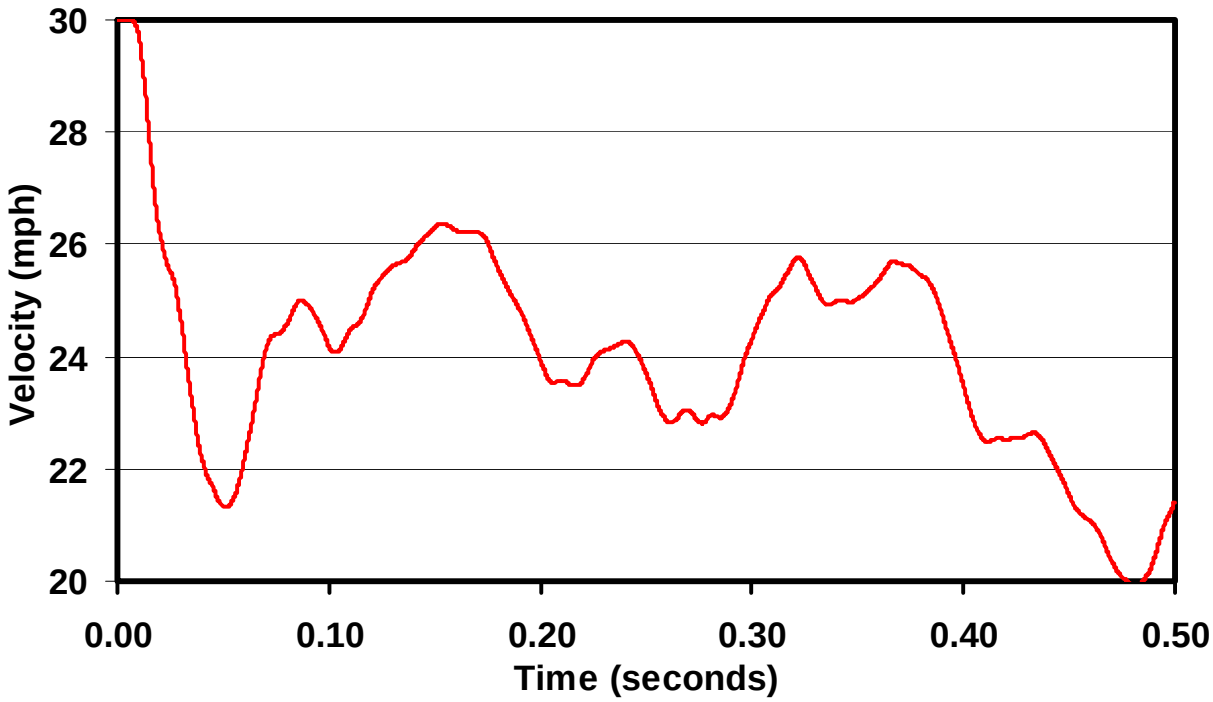

Figure 18. Measured Longitudinal Velocity of the Cab Car

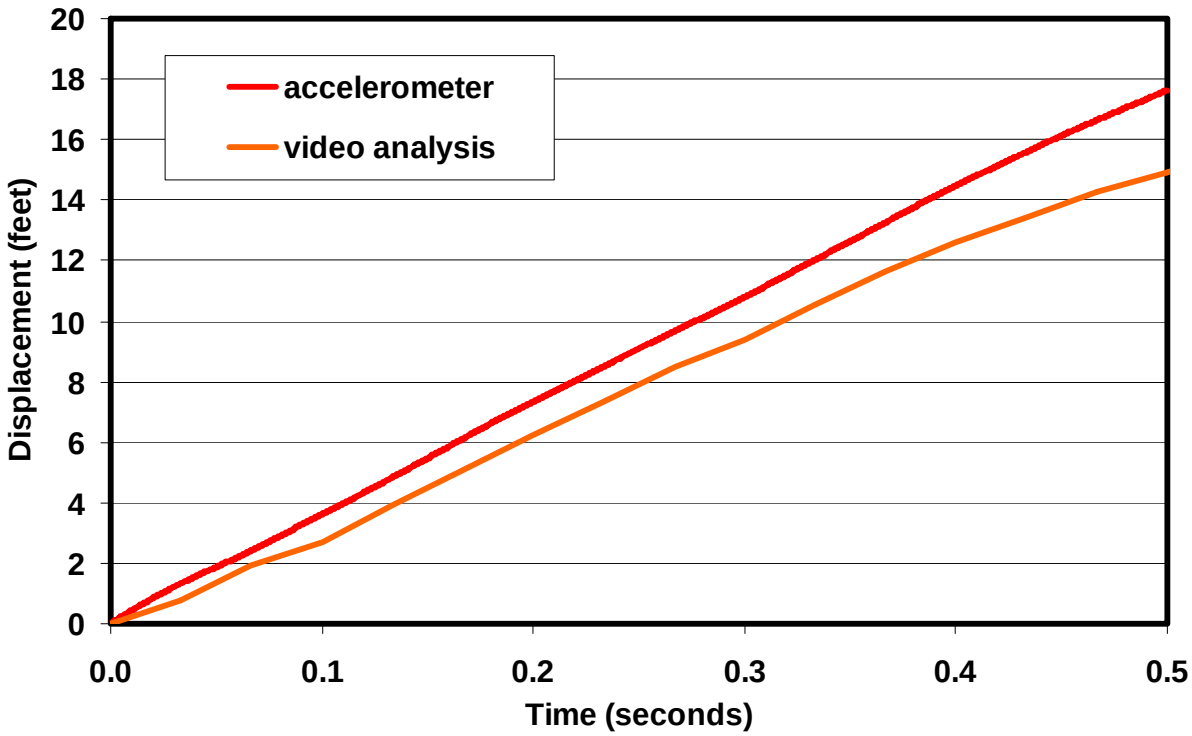

Figure 19. Measured Longitudinal Displacement of the Cab Car

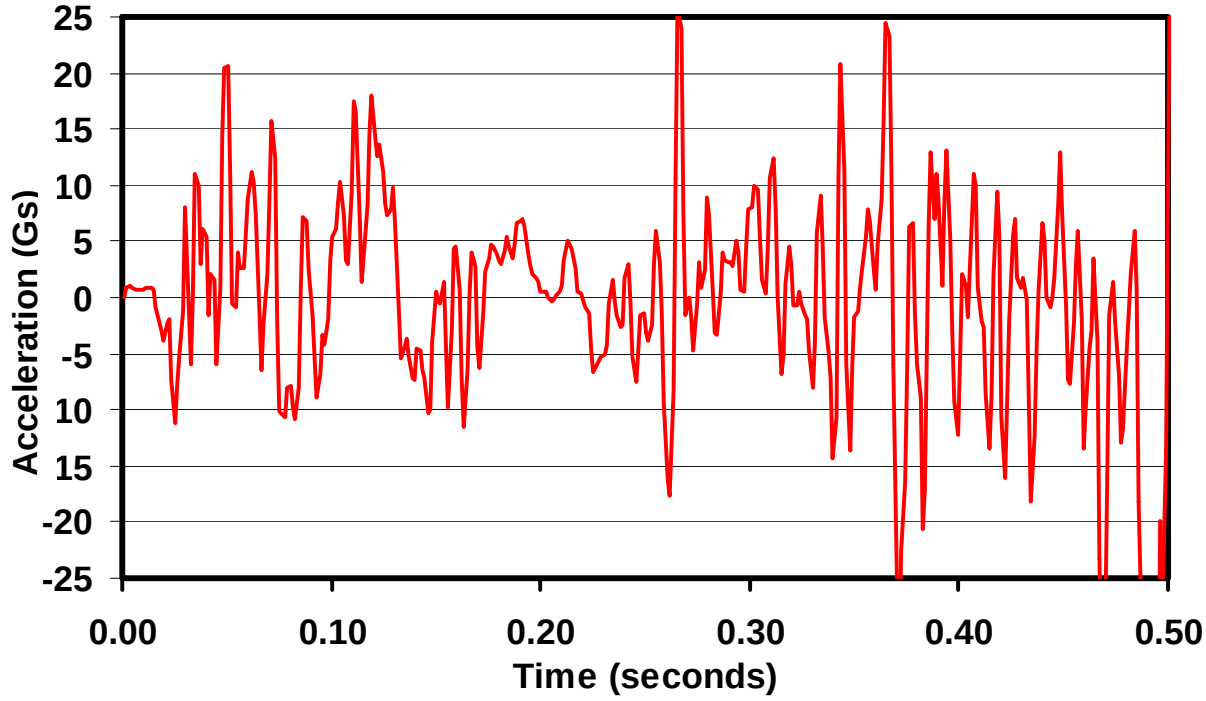

Figure 20. Measured Vertical Acceleration of the Cab Car

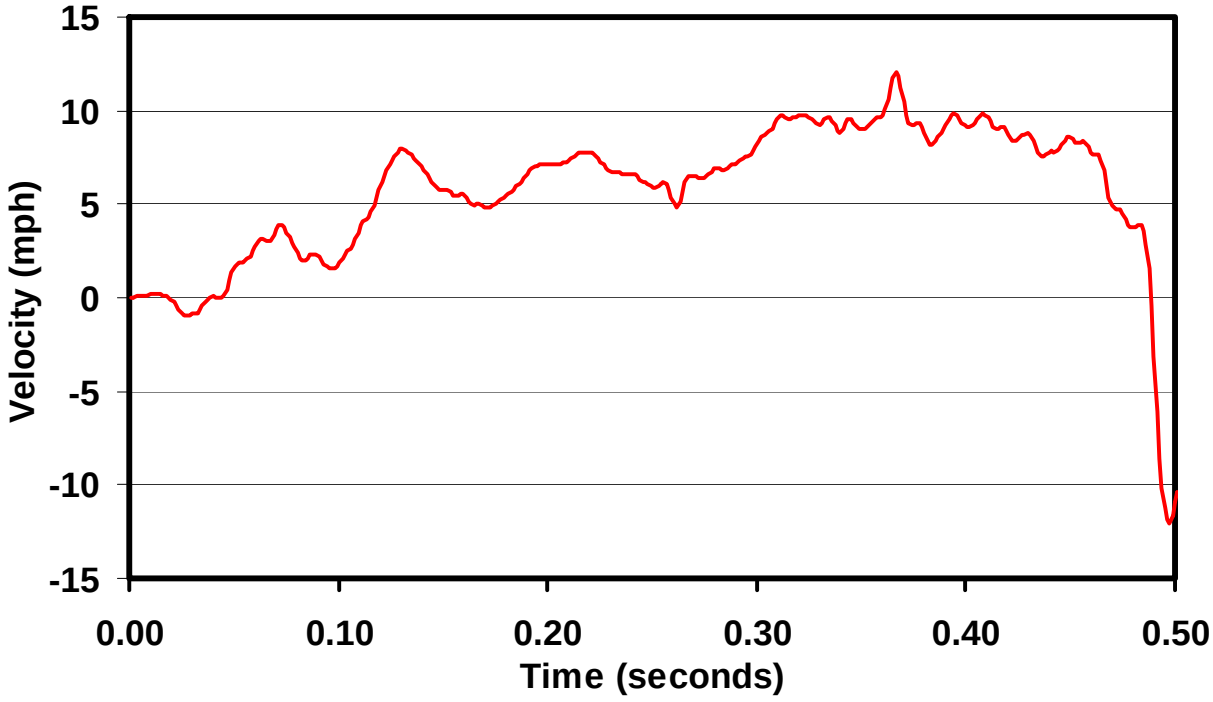

Figure 21. Measured Vertical Velocity of the Cab Car

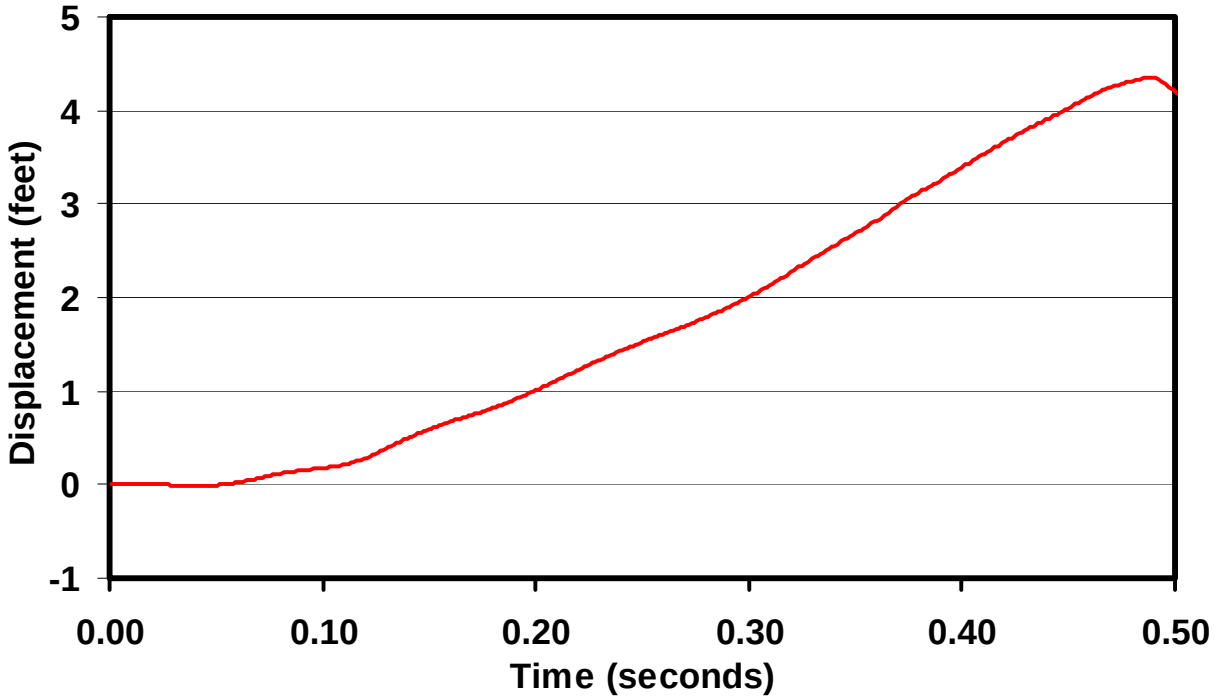

Figure 22. Measured Vertical Displacement of the Cab Car

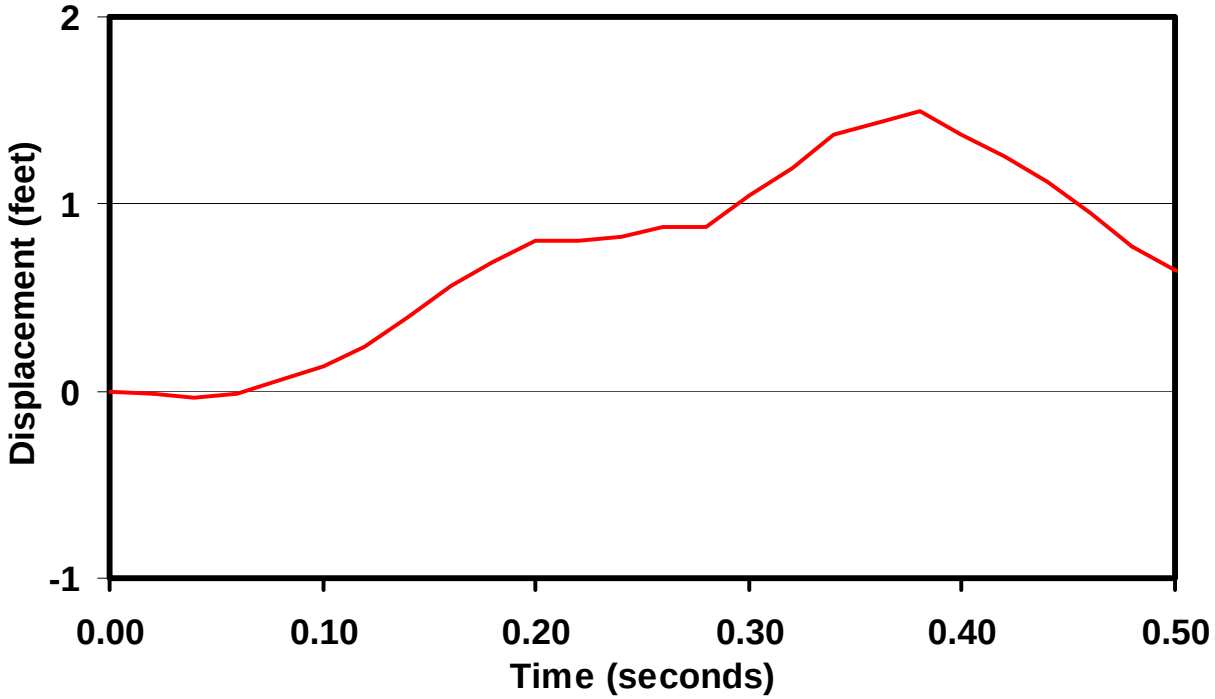

Figure 23. Measured Lateral Displacement of the Cab Car

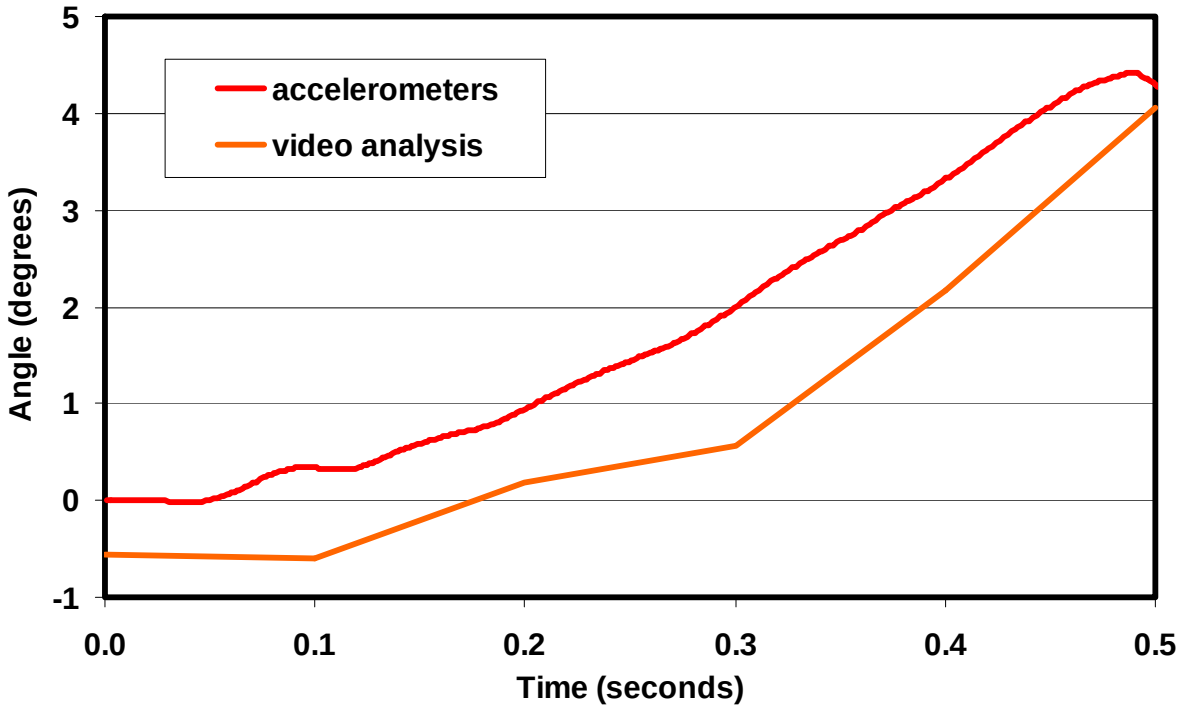

Figure 24. Measured Pitch Rotation of the Cab Car

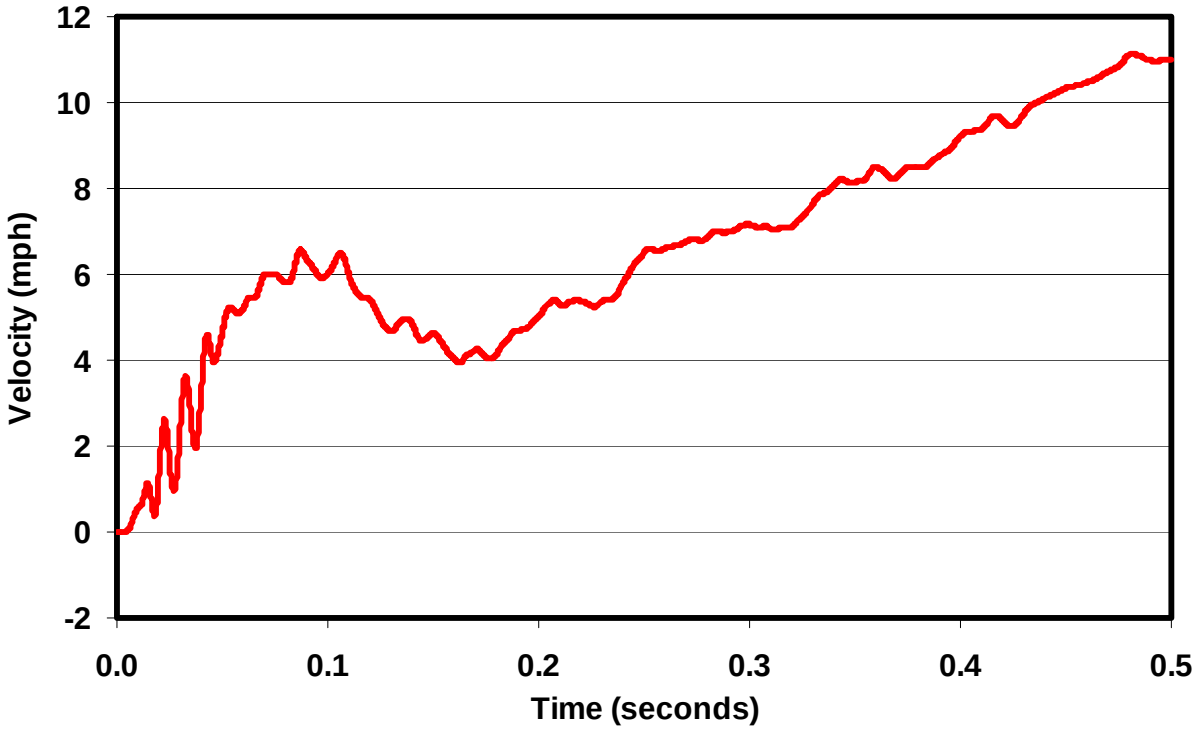

Figure 25. Measured Longitudinal Velocity of the Standing Locomotive

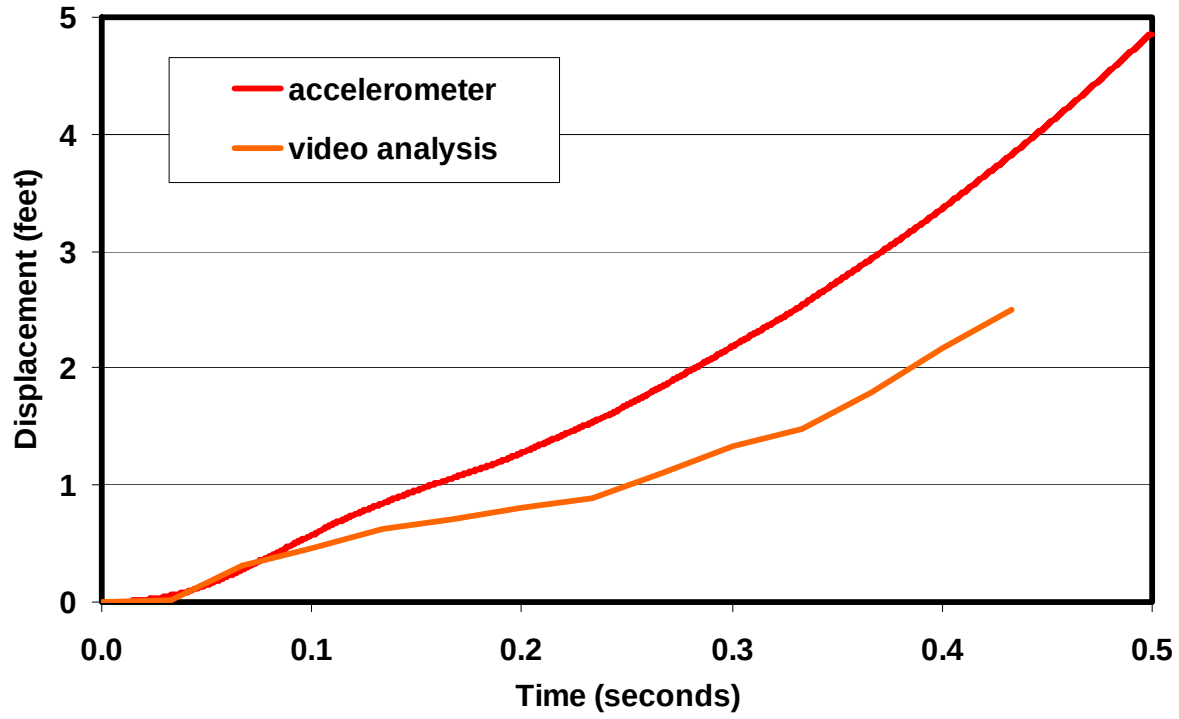

Figure 26. Measured Longitudinal Displacement of the Standing Locomotive

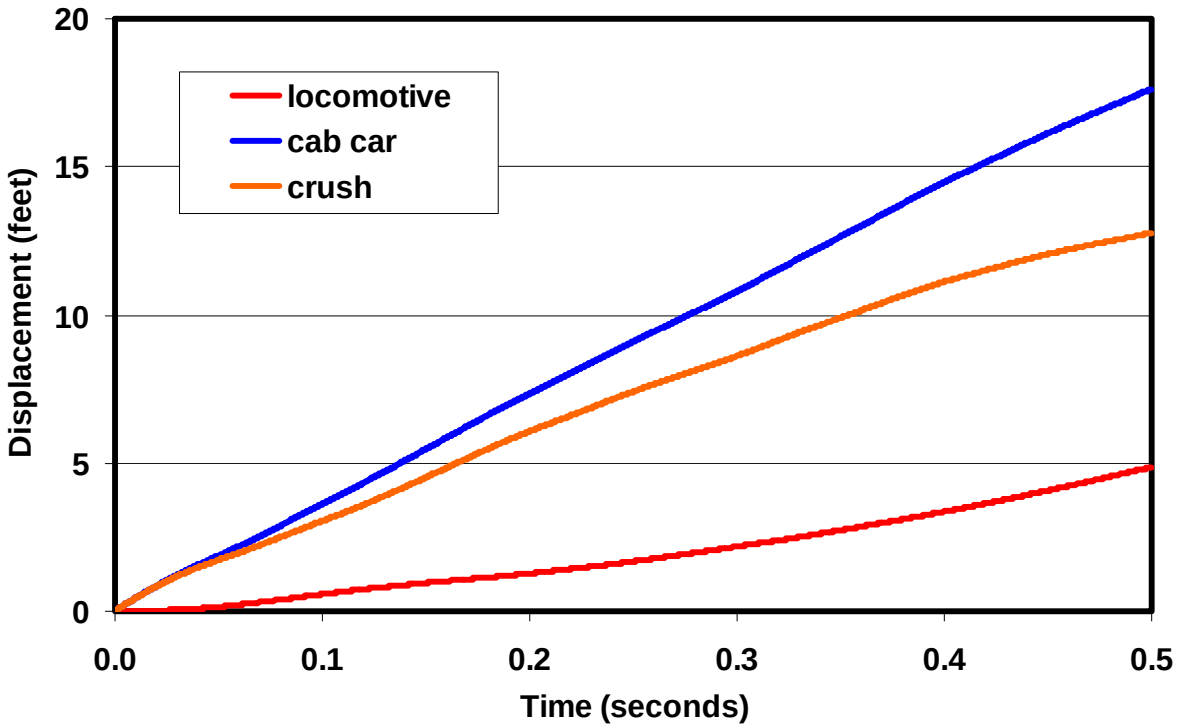

Figure 27. Measured Longitudinal Cab Car, Locomotive, and Crush Displacements

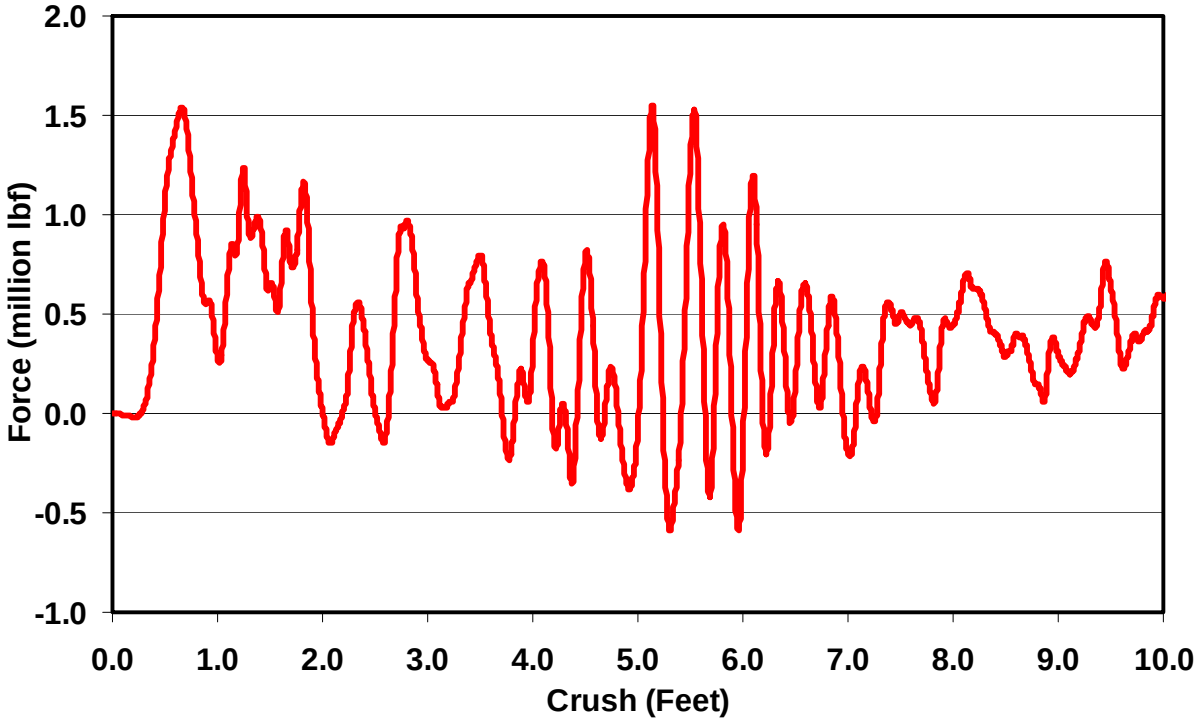

Figure 28. Measured Collision Force-Displacement Curve

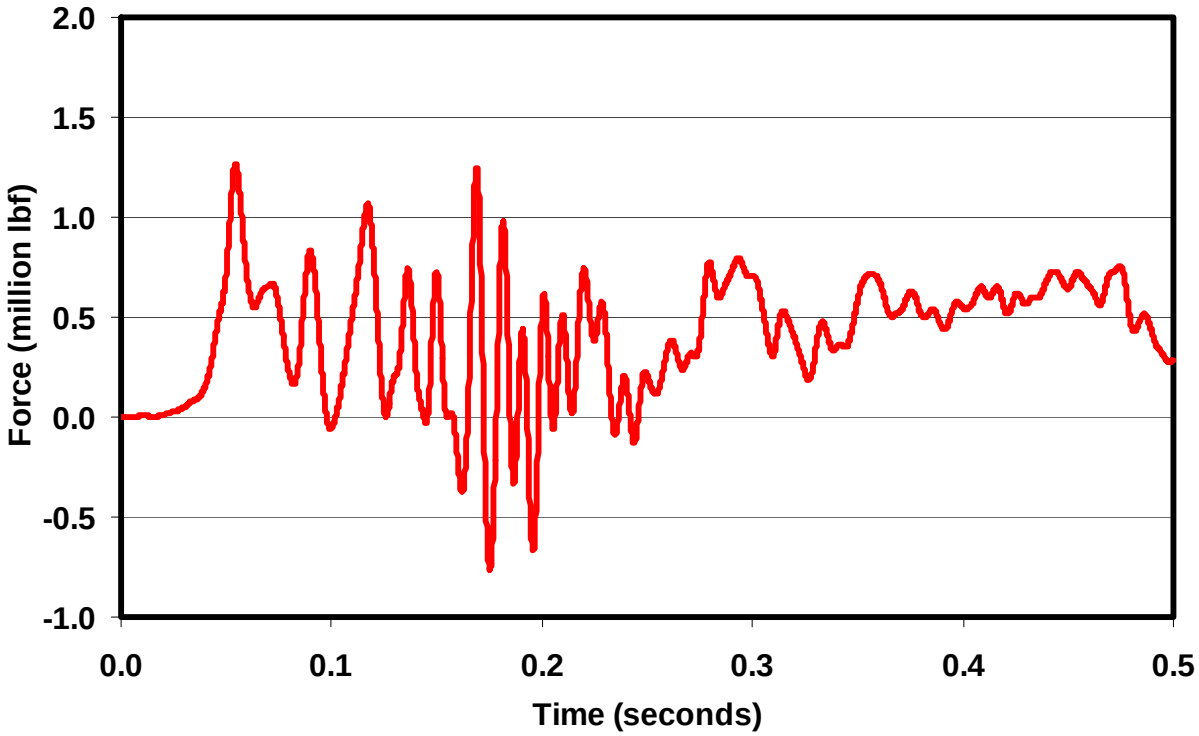

Figure 29. Measured Trailing Force on Cab Car

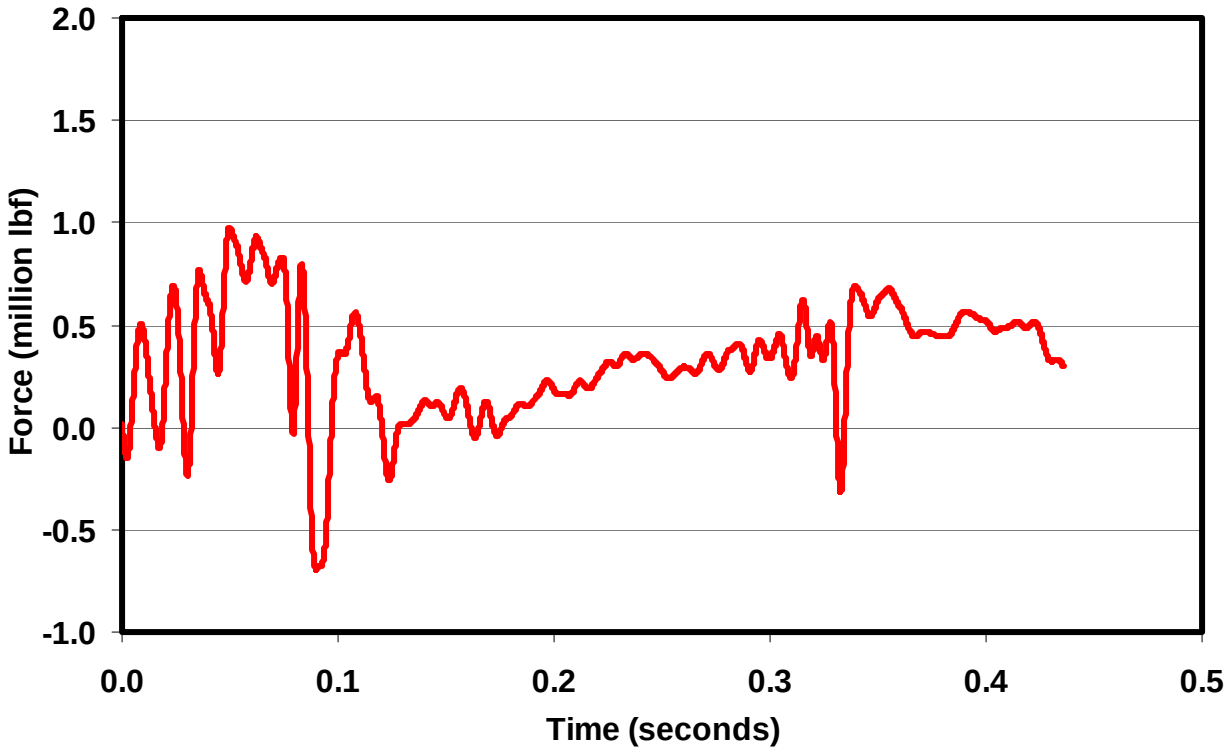

Figure 30. Measured Trailing Force on Standing Locomotive

2.3. Collision Force

Figure 31 shows the collision force-time history. It was derived from the acceleration time histories under the assumption that each consist behaves as a lumped mass system. This assumption leads to two different estimates of the collision force:

- Forward calculation: The force at the collision point is equal to the sum of the masses of the individual vehicles from the moving consist multiplied by their respective longitudinal accelerations (negated).
- Backward calculation: The force at the collision point is equal to the sum of the masses of the individual vehicles from the standing consist multiplied by their respective longitudinal accelerations.

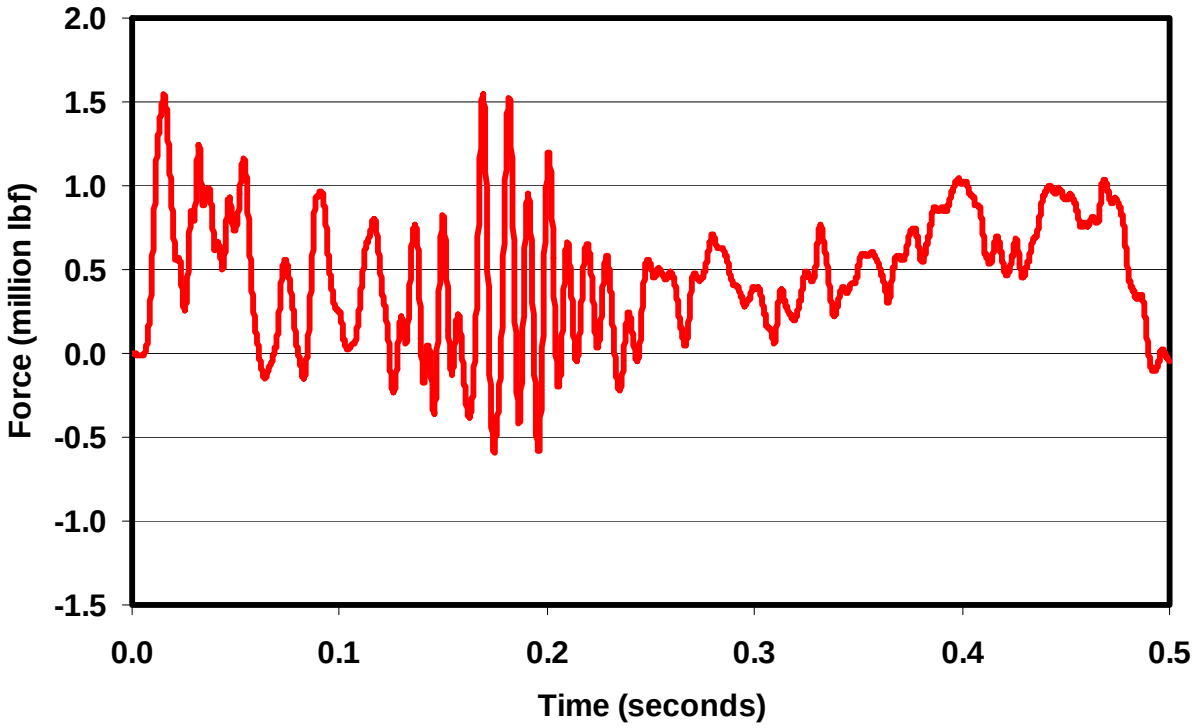

Figure 31. Collision Force-Time History

Since a coordinate system was chosen in which longitudinal motions are positive in the direction of the moving consist—hence the accelerations are negative—the forward estimate of the collision force must be negated to produce a positive force. The acceleration-time histories that were used to derive the collision force were not measured at the vehicle's center of gravity (c.g.). Rather, an implicit assumption exists that the acceleration pulse that is used is representative of the motion of the c.g.

As it happens, the acceleration measurements for the standing locomotive appear to have been corrupted because of loose engine mounts that caused excessive vibration of the engine [8]. Therefore, the backward calculation is not considered a reliable measure of collision force for this test, and it is not used for comparison with model results.

Collision force versus crush displacement curves were generated by cross-plotting force time-history data versus the time-history of the relative longitudinal displacement of the cab car and the standing locomotive. Figure 32 shows the collision force (forward estimate) versus crush curve. Because of the significant forces transmitted from the trailing vehicles (see Section 2.4), the force levels remain quite high over the first 0.5 s of the collision.

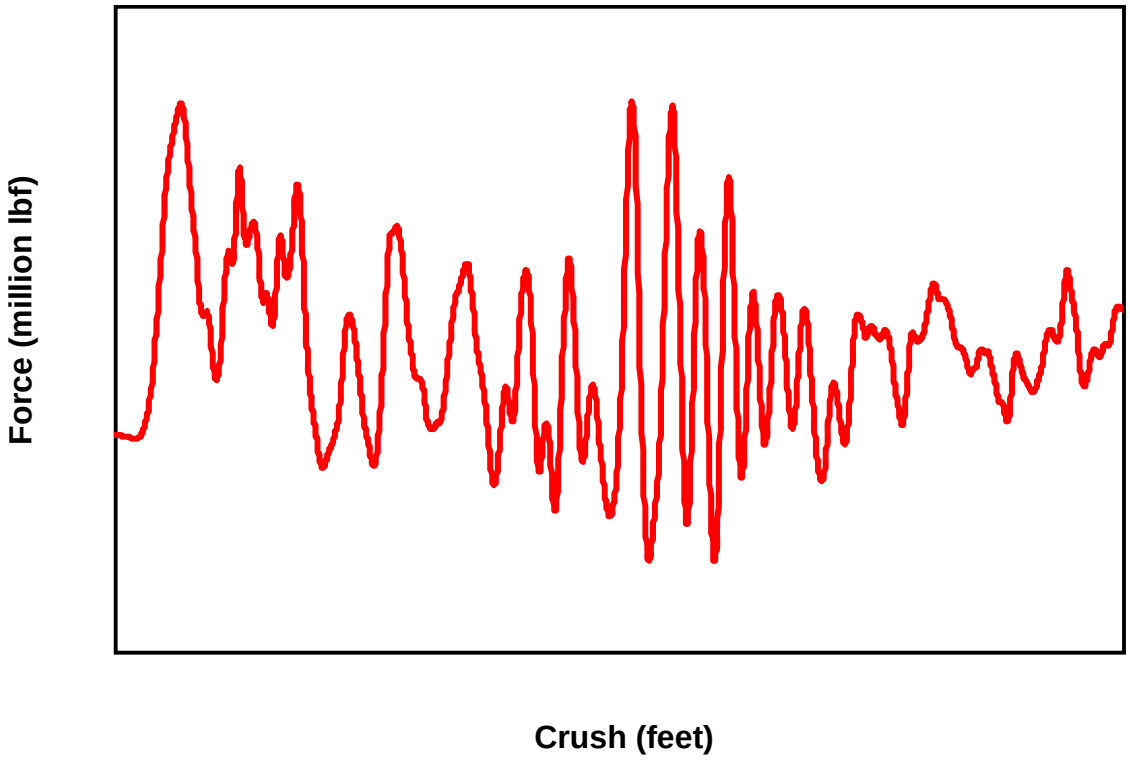

Figure 32. Collision Force versus Crush Displacement

2.4. Trailing Vehicle Forces

The forces imparted by trailing vehicles were calculated in a manner similar to that used to calculate the collision force. In this case the force on the lead vehicle is simply equal to the sum of the masses times the accelerations of each of the trailing vehicles. (Just as for the calculation of the collision force, the authors can alternatively calculate the trailing force by summing the mass × acceleration contributions of each of the vehicles forward of the trailing vehicle. For example, for the cab car, the trailing force would be equal to the sum of mass × acceleration of the vehicles in the standing consist *plus* the mass × acceleration of the cab car. Due to the engine vibration problem noted earlier, the calculation of trailing force for the test was not made in this manner.)

Figures 33 and 34 show the trailing vehicle force-time histories for the moving and standing consists, respectively. Note the delay in the initial peak force relative to the time that it occurred at the collision point (see Figure 31). In the train-to-train crash test, the trailing force has a significant effect on the collision force, as compared to the forward force (see Figures 31 and 32). Since no trailing cars are in the single car test, this force is absent in the single car test.

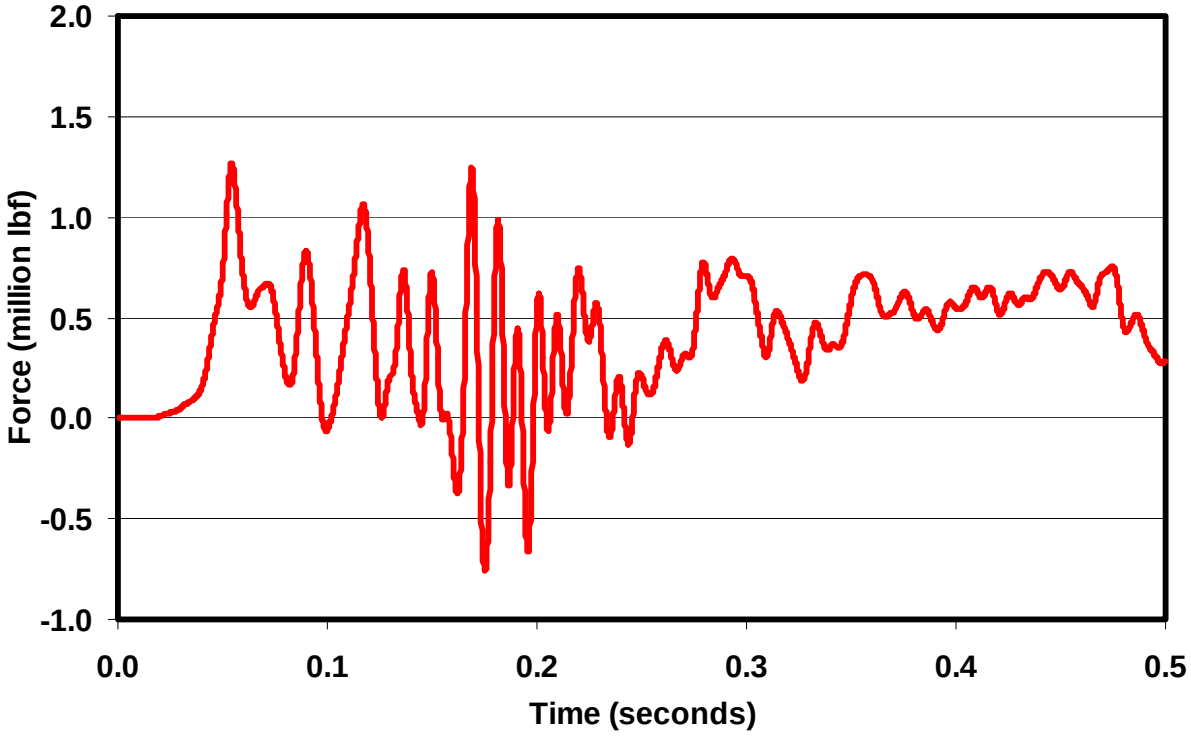

Figure 33. Trailing Force at Rear of Cab Car

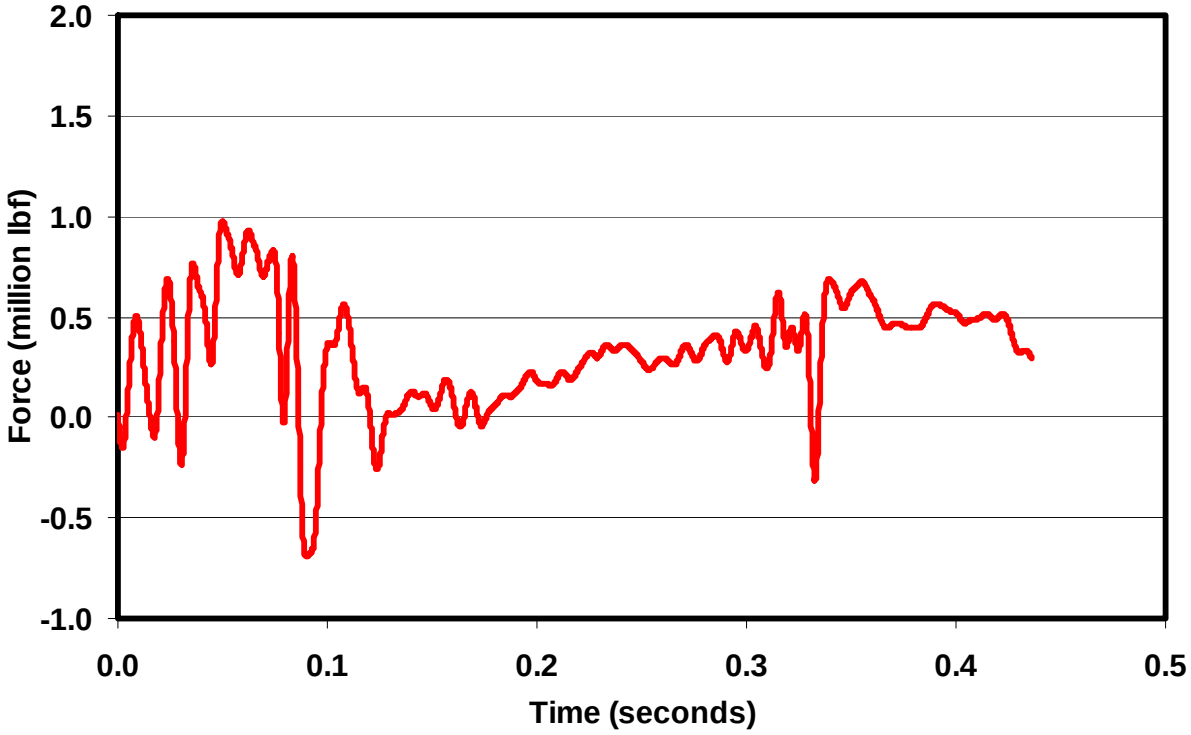

Figure 34. Trailing Force at Rear of Standing Locomotive

3. Model Development

The finite element model of the colliding trains is made up of four key elements:

1. The cab car body
2. The standing locomotive
3. The cab car trucks and truck-to-body connections
4. The trailing vehicles and vehicle-to-vehicle connections

Sections 3.1 through 3.4 discuss the development of each of these components of the full model. Section 3.5 describes the integration of these components into a complete model, as well as other more general features of the model. Finally, Section 3.6 describes the testing and implementation of the model.

3.1. Cab Car Body

The model for the cab car body was, in part, derived from models that had been developed in prior programs. As a starting point, a model was used specifically for analysis of a representative 1990s car body [3, 6]. This model features a detailed discretization of the front 20 ft (6.1 m) or so of the cab car, using a characteristic element length of approximately 1.5 in (38.1 mm). A model was then added to characterize the rear-most 60 ft (18 m) or so of the vehicle. To minimize the number of elements, this part of the vehicle was modeled in much less detail, with a characteristic element length of approximately 15 in (381 mm). A mesh transition zone about 4 ft (1.2 m) in length was developed to link the refined and coarse parts of the mesh. Figure 35 shows the mesh for the cab car. The mesh consists of approximately 125,000 shell elements, with 118,000 of these representing the more refined forward end of the cab.

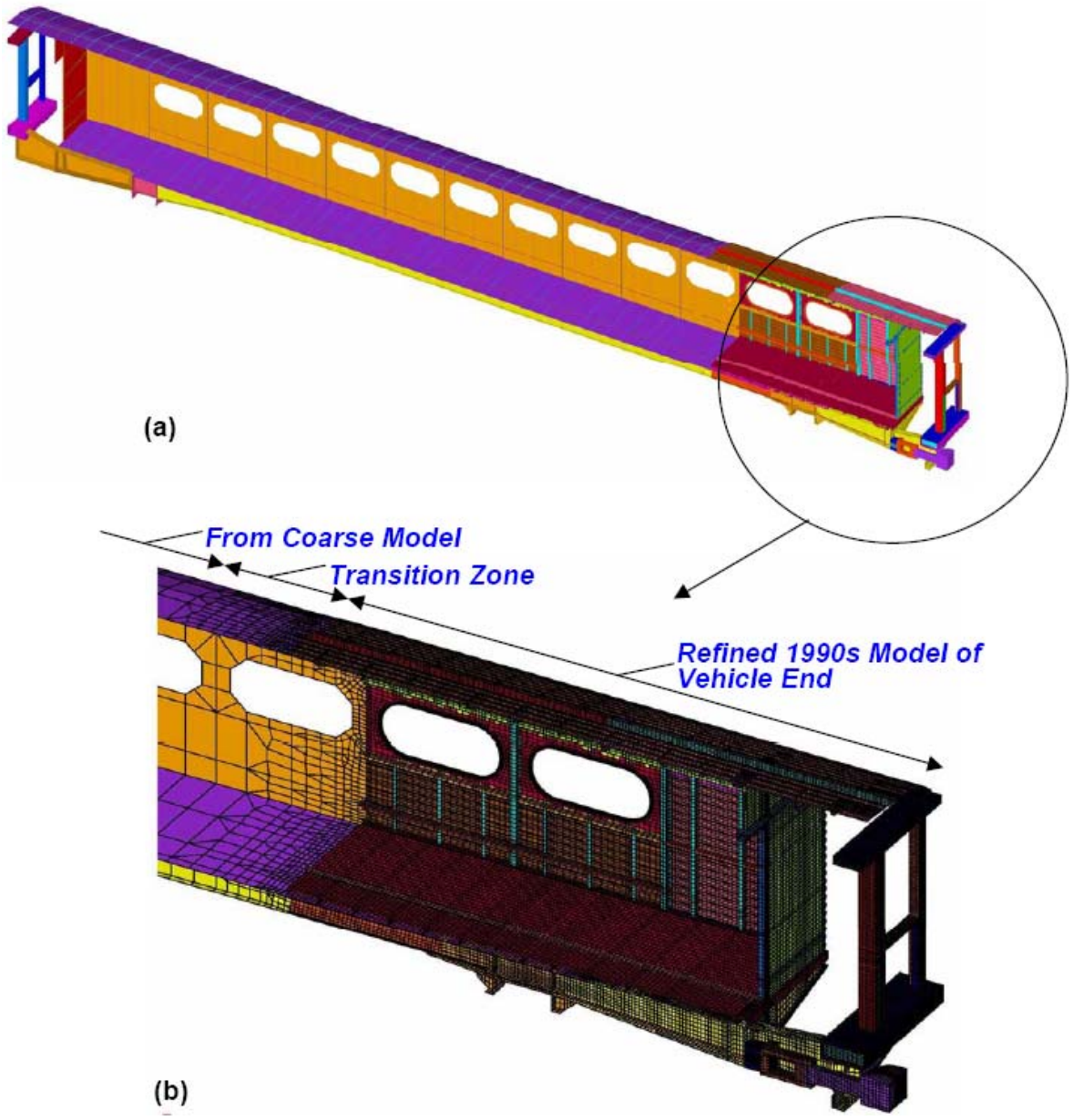

Figure 35. Finite Element Mesh for the Cab Car (a) the Entire Car (b) the Detailed Forward End

For the more refined forward end of the car, much of the development effort for this program focused on redefinition of overlapping surfaces. The automatic contact feature of ABAQUS/Explicit (see Section 3.5) does not permit the presence of any two elements whose surfaces overlap. The finite element model of the cab car from which this model was derived had many such overlapping surfaces. Each of the sets of elements that made up such overlapping surfaces had to be redefined so that only a single surface remained. Due to the detailed nature of the model, this effort was cumbersome and required the definition of hundreds of additional element sets with a single shell element representing the properties of two or more

overlapping shell elements. This was done under the assumption that the multilayer shells were fused into a single shell with the added thickness of each of the overlapping layers.

The definition of the mesh for the less refined structure of the rear end of the cab car required simplification of some structures. The one of particular note included the floor structure of the more refined forward end of the cab, with two layers separated by several inches connected with several stiffening webs along the length of the vehicle was simplified to a single layer with transverse beam elements used to represent the stiffeners. The mechanical properties of the single layer structure were modified to match the axial and bending stiffness properties of the bilayer structure. The density of the composite layer was adjusted to distribute weight along the vehicle length so that the mass of the car matched that of the cab car vehicle used in the test.

For model development and testing purposes, a coarse model of the entire vehicle was also constructed. This much more computationally efficient, but less accurate, model was used to test the behavior of various model features (see Section 3.6).

3.2. Standing Locomotive

In a like manner, the mesh for the locomotive was derived from a previous model of the cab for a Electro-Motive Diesel, Inc. (EMD) locomotive [7]. Detailed representations were added for the short hood, collision posts, anticlimber, draft pocket, and draft gear based upon drawings for the F40PH locomotive. In addition, simplified representations were added for the underframe, engine, trucks, and fuel tank. Since the damage to the locomotive was limited to the very front of the vehicle, most of the vehicle was modeled as a single rigid body. This simplification allows this part of the mesh to be represented by a single node, having the correct mass and inertia properties, greatly decreasing the solution time for the model. In the analysis, this rigid body was confined to move only in the axial direction. The mass of the portion of the locomotive that was modeled as rigid was adjusted so that the total mass of the locomotive matched that of the locomotive used in the test. Figure 36 shows the mesh for the locomotive. It consists of approximately 16,000 elements, of which about 7,000 are deformable elements.

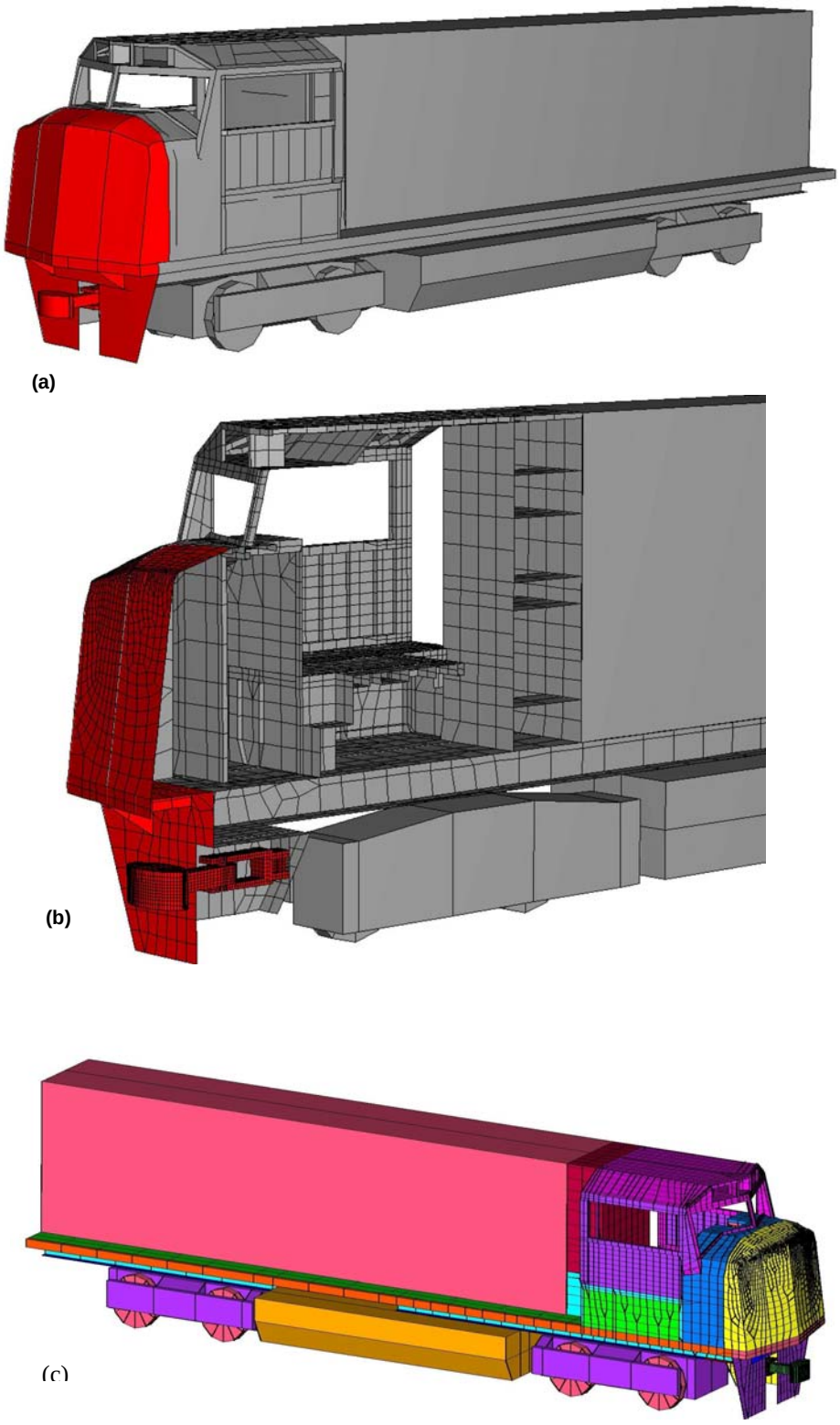

Figure 36. Finite Element Mesh for the Locomotive (a) the Entire Car, Mesh Hidden; (b) the Detailed Cab Interior; (c) the Entire Car, Mesh Visible

3.3. Cab Car Trucks and Truck-to-Body Connections

The cab car trucks were modeled as rigid bodies connected to the underframe of the cab car body through the use of ABAQUS connector elements. The structure of the truck was derived from a model developed in a previous study [6]. Figure 37 shows the mesh for the truck. This figure shows the location of the connector elements.

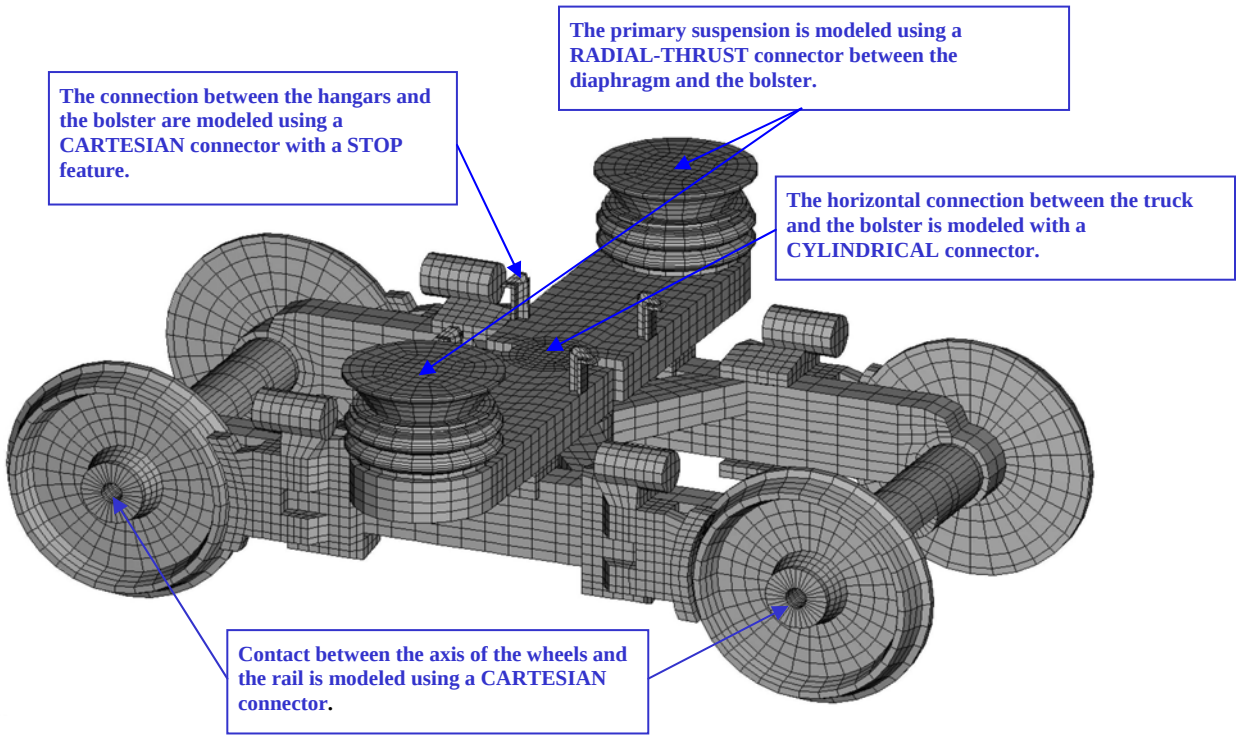

Figure 37. Finite Element Mesh for the Truck with Connector Elements Indicated

The stiff longitudinal connection of the truck to the body bolster was modeled as acting through the center pin using a 'SLIDE PLANE' connector element. This element type provides for constraining the motion of two nodes (in this case, one on the truck and one on the body bolster) to be equal in a single direction (the longitudinal direction). Relative motion in the other two directions (vertical and lateral) is unconstrained.

The much more compliant vertical and lateral connections to the body bolster acting through the diaphragms were modeled using 'RADIAL THRUST' connector elements. The radial thrust connector element provides for different behavior in the radial (lateral-horizontal plane) and thrust (vertical) directions. The radial connection was specified to have a spring stiffness of 1690 lbf/in (296,000 N/m), while the vertical connection was specified to have a spring stiffness of 3870 lbf/in (678,000 N/m) [11]. The '*CONNECTOR STOP' parameter is applied to the vertical component of motion for this element to prevent compression or extension of the secondary suspension beyond a defined maximum level of travel of ±1.0 in (25.4 mm).

In addition, connectors simulating contact between the wheel and the rail were defined between a node located at the center of each of the four truck wheels and a rigid plane representing the rail using a 'CARTESIAN' connector element. This element provides for definition of independent

behavior in three local directions. This constraint is only defined in the vertical direction, using the '*CONNECTOR STOP' parameter to limit the vertical motion of the wheel node. The connector element acts only to limit the wheel node from moving below its initial position (16 in (406 mm) above the rail).

The mesh for each truck consists of approximately 13,000 elements, all rigid. The presence of rigid elements does not significantly affect solution time.

3.4. Trailing Vehicles and Vehicle-to-Vehicle Connections

Trailing vehicles were modeled in a simplified manner using lumped masses, located at the vehicle c.g.s and matched to the measured weight of the vehicle. Table 2 lists the weights for all of the vehicles, including the colliding cab car and locomotive.

Table 2. Trailing Vehicle Masses

Vehicle	Weight, lbm (kg)
Moving Consist—Cab Car	75,014 (34,020)
Moving Consist—First Coach Car	73,427 (33,300)
Moving Consist—Second Coach Car	72,836 (33,032)
Moving Consist—Third Coach Car	148,944 (67,548)
Moving Consist—Trailing Locomotive	267,054 (121,113)
Standing Consist—Lead Locomotive	248,284 (112,600)
Standing Consist—Lead Freight Car	312,598 (141,768)
Standing Consist—Trailing Freight Car	78,459 (35,582)

Vehicle-to-vehicle connections were represented with nonlinear spring and linear dashpot elements acting in parallel. The force-deflection characteristics of the nonlinear spring elements represent, in series, the compliant behavior of the coupled draft gears and the much stiffer behavior of the vehicle underframes. Dashpot characteristics represent the damping of the vehicles and their connections, which occurs mostly through hysteresis of the draft gear pads. These elements were constrained to move only in the longitudinal direction. Specific values used in the model were chosen to be consistent to collision dynamics models that were developed by the Volpe Center [1, 8]. Table 3 lists the spring force-deflection and damping coefficients used in the model. The force-deflection and damping coefficients represent the combined characteristics of the connected vehicle ends (i.e., two couplers and draft gears acting in series).

Table 3. Coupled Vehicle Connections: Spring Force-Deflection and Damping Coefficients

Consist	Connection	Force 1000 lbf	Force (kN)	Deflection in	Deflection (mm)	Damping (lbf-sec/in)
Moving	Cab Car– 1st Coach Car	0 80 2500	(0) (356) (11,120)	0.0 3.0 7.3	(0) (76) (185)	3218
Moving	1st Coach Car– 2nd Coach Car	0	(0)	0.0	(0)	
Moving	2nd Coach Car– 3rd Coach Car	80	(356)	3.0	(76)	
Moving	2nd Coach Car– Trailing Locomotive	2500	(11,120)	9.6	(244)	8209
Standing	Locomotive– 1st Hopper Car	0 100	(0) (445)	0.0 2.4	(0) (61)	8209
Standing	1st Hopper Car– 2nd Hopper Car	2500	(11,120)	8.4	(213)	8209

3.5. Additional Model Features

A key feature of the modeling approach was the use of automatic contact, a relatively new feature of ABAQUS/Explicit. The implementation of this feature made it much easier to model the complex contact interactions between the various components of the cab car. Its use did, however, require a significant number of modifications to the models, which had not originally been set up to run with the automatic contact feature.

The model also includes limited use of one of the material failure features of ABAQUS/Explicit. Failure was restricted to the draft sill structures, using a strain-based material law with a failure strain of 30 percent. Previous experience in this program and others suggests that the use of the material failure option of ABAQUS/Explicit in conjunction with contact leads to numerical difficulties that prevent the completion of the analysis. For this reason, a more aggressive approach to modeling failure was not used. As is discussed in the next section, this leads to gradually increasing deviations between the predictions of the model and the test results once fracture begins to drive the collision behavior. This issue arose after approximately 0.25 s.

The *VARIABLE MASS SCALING option of ABAQUS/Explicit was used to limit the required processing time. This parameter imposes a minimum time step for the analysis and compares the minimum stable time step, which is based on a calculation of the stable time step for each element, to this value. If the minimum stable time step for any element falls below the imposed minimum, the density of that element is increased until the stable time step for that element equals the imposed value. A time step of 2.0E-6 s was imposed for this analysis. This resulted in an increase in the mass of the cab car of 1.2 percent as a result of density changes. Experience suggests that this small level of added mass does not appreciably affect the outcome of the model.

3.5.1. Colliding Coupler Interactions

Models for cab car and standing locomotive couplers were modified to better represent their impact and subsequent motions. The representation of the connection between the coupler shank and the yoke was enhanced so that axial force transmission and coupler rotation could be modeled. This was done by explicitly modeling a rigid-pinned connection between the yoke and the coupler shank (see Figure 38). In addition, the respective couplers were each defined to have curved heads that allow them to collide and transmit longitudinal forces but also have them rotate past one another without locking together. An initial angular offset of 5 degrees was imposed on the initial configuration of each of the couplers to promote preferential rotational motion.

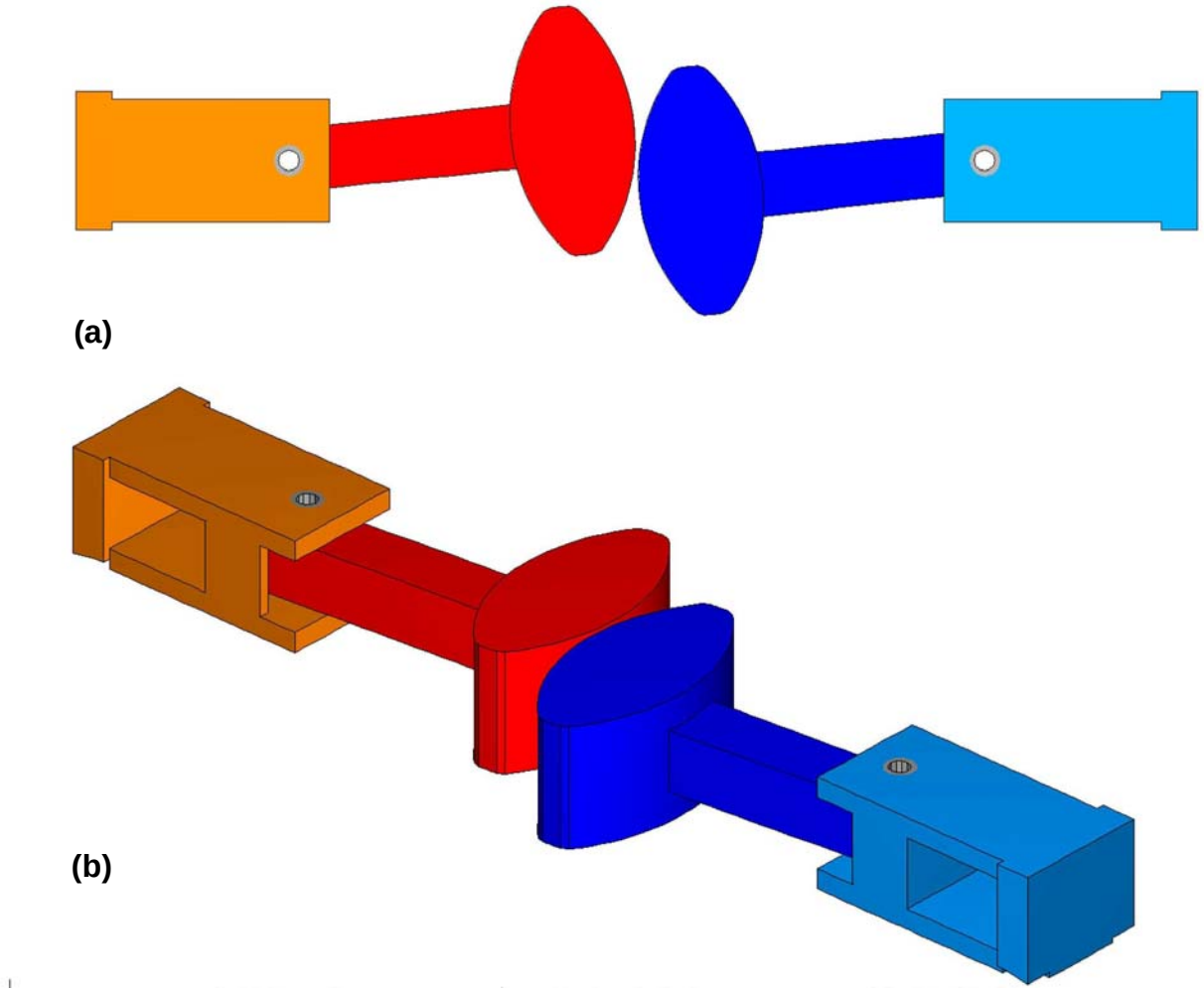

Figure 38. Finite Element Model for the Colliding Couplers (a) Plan View (b) Isometric View

3.6. Integrating, Testing, and Refining the Model

The input files for the model were constructed using a modular approach, with key model elements defined in separate files and brought into the master input file as needed. This facilitated the development of preliminary models for testing various aspects of the method. Some of the preliminary models that were constructed include:

- A coarse model of the cab car, with the full car defined with the same level of mesh refinement used to define the rear end of the final cab car vehicle mesh. This model was used to conduct preliminary collision studies examining issues related to the colliding vehicle interface, the connections to the trucks, and the connections to the lumped mass elements representing the trailing vehicles. This model was also used in a lifting simulation that was performed to study the connections of the truck to the cab car body and the truck to the ground, particularly the limits to vertical motion associated with lifting of the trucks through the hook connections, impact with the rail, and bottoming out of the suspension.
- A symmetric model of the cab car and the locomotive. This model was used for preliminary studies of the colliding interactions of the refined cab car forward end and the locomotive. The use of symmetry cut the computation time significantly.

4. Comparison of Model and Test Results

Comparisons between the model and the test were made in terms of each of the four different measures of collision behavior described in Section 2:

1. Deformation modes—Comparison of the model predicted and test results of the cab car and locomotive deformed shapes.
2. Colliding vehicle motions—Comparison of the model predicted and test results of the motions (accelerations, velocities, and displacements) of the cab car and standing locomotive.
3. Collision force—Comparison of the model predicted and test results of the longitudinal force between the cab car and the standing locomotive.
4. Forces imparted by trailing equipment—Comparison of the model predicted and test results of longitudinal forces between the cab car and the first coach car and between the standing locomotive and the first ballasted car.

Sections 4.1 through 4.4 present these comparisons.

4.1. Deformation Modes

The model was evaluated by comparing the following:

- Sequences of deformed meshes from the model and high-speed video stills (see Section 2.1.1, Figures 4 and 5).
- Deformed meshes of cab car and locomotive components with photographs of deformed structures taken after the collision (see Section 2.1.2, Figures 8, 10, 13, and 14).

4.1.1. Comparison with Video Stills

Figure 39 shows side-by-side comparisons of the model predictions and test results in terms of side views of the collision sequence at several roughly equal times during the first 0.25 s of the collision. Based upon these comparisons, one can make the following assessments regarding the model's ability to simulate the collision:

- The model appears to capture the downward bending of the end frame of the cab car onto the front of the short hood and the eventual conforming and locking of the end frame onto the short hood.
- The model also captures the downward bending of the front of the draft sill. However, the mode of deformation for the draft gear appears to differ somewhat from that of the

test. In the test, the draft gear appears to bend downward from a single plastic hinge point near the forward truck wheel. In the model, two plastic hinge points are formed above the forward wheel, so that the middle of the draft gear actually bends upward. These differences in deformation mode could easily be attributable to small differences between the characteristics of the model draft sill and the actual draft sill. This is particularly true when one considers the large extent of fracture that occurred in the draft sill.

- The model also captures the impact of the cab car roof structure against the window frame of the locomotive cab, as indicated in Figure 39(d).
- The model does not appear to capture the mode of deformation of the superstructure that surrounds the end frame of the cab car. In the test, the superstructure appears to separate from the underframe, as evidenced by the continued flatness of the roof in Figure 39(e). In the model, the superstructure deforms considerably. The likely difference in behavior lies in the fact that the superstructure clearly tore away from the underframe in the test; whereas, in the model, the superstructure is intimately connected to the underframe and is not able to tear away.
- The model results suggest that the forward truck starts to lift sometime after 0.157 s and before 0.25 s. The test results indicate that the forward truck is just starting to lift at 0.25 s.

In the test, as is evident in Figure 2, the wheels of the truck did begin to lift noticeably shortly thereafter.

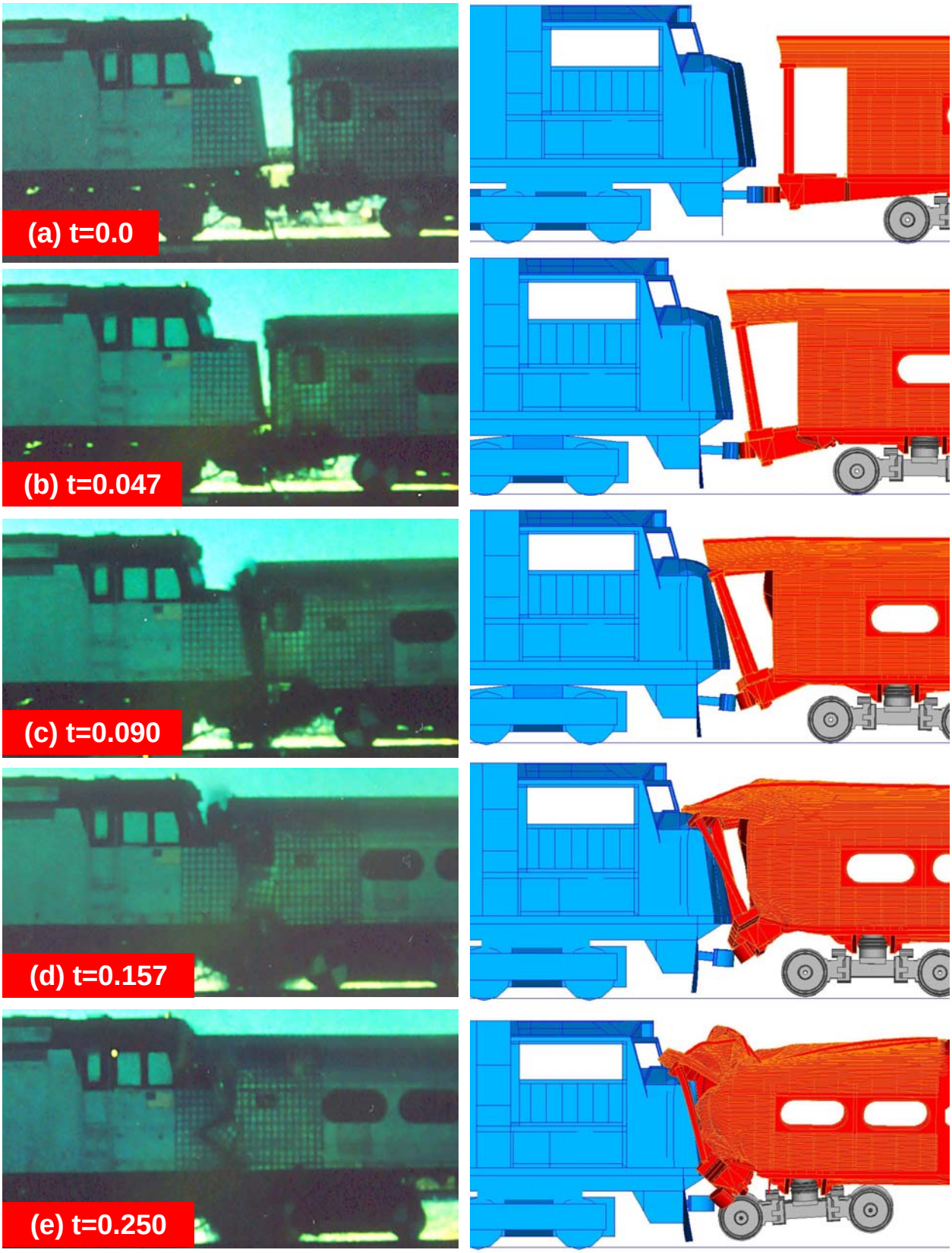

Figure 39. Comparison of Model and Test Results: Collision Sequence

4.1.2. Comparison with Post-Collision Photographs

The predicted damage to the front of the locomotive is generally consistent with the damage that occurred in the test. Figure 40 shows the deformed locomotive model end after 0.6 s. The predicted damage to the upper front face of the short hood is very consistent with the test results, as is the sideways motion of the coupler. The coupler moves in a direction that is opposite the direction that it moved in the test. This is a result of the choice for the direction of the initial angular offset that was imposed on the model couplers (Figure 24). Since the remainder of the model is symmetric, offsetting the couplers in the opposite direction would have reproduced the actual motion of the coupler.

The damage that occurs in the anticlimber also appears to be consistent with the test results. As indicated in Figure 40, the model anticlimber experiences damage in two locations—one near the center of the locomotive and one more toward the left side. It is clear that this damage arises due to collision of the collision posts of the cab car. In fact, if one examines the sequence of images shown in Figure 41 in which the collision posts of the cab car are superimposed onto the locomotive, it is clear that the collision posts and, for that matter the entire end frame, roll during the collision.

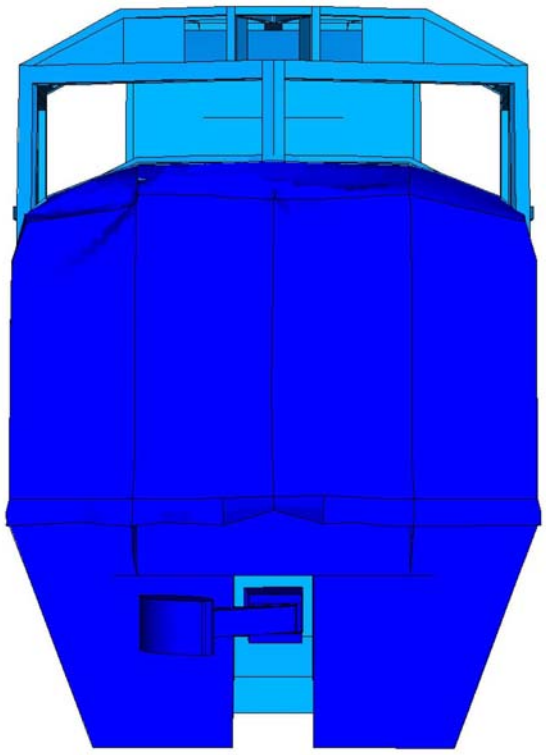

Figure 40. Model Prediction for Deformation of Standing Locomotive Front End After 0.6 s (Deformable Structure Indicated in Dark Blue)

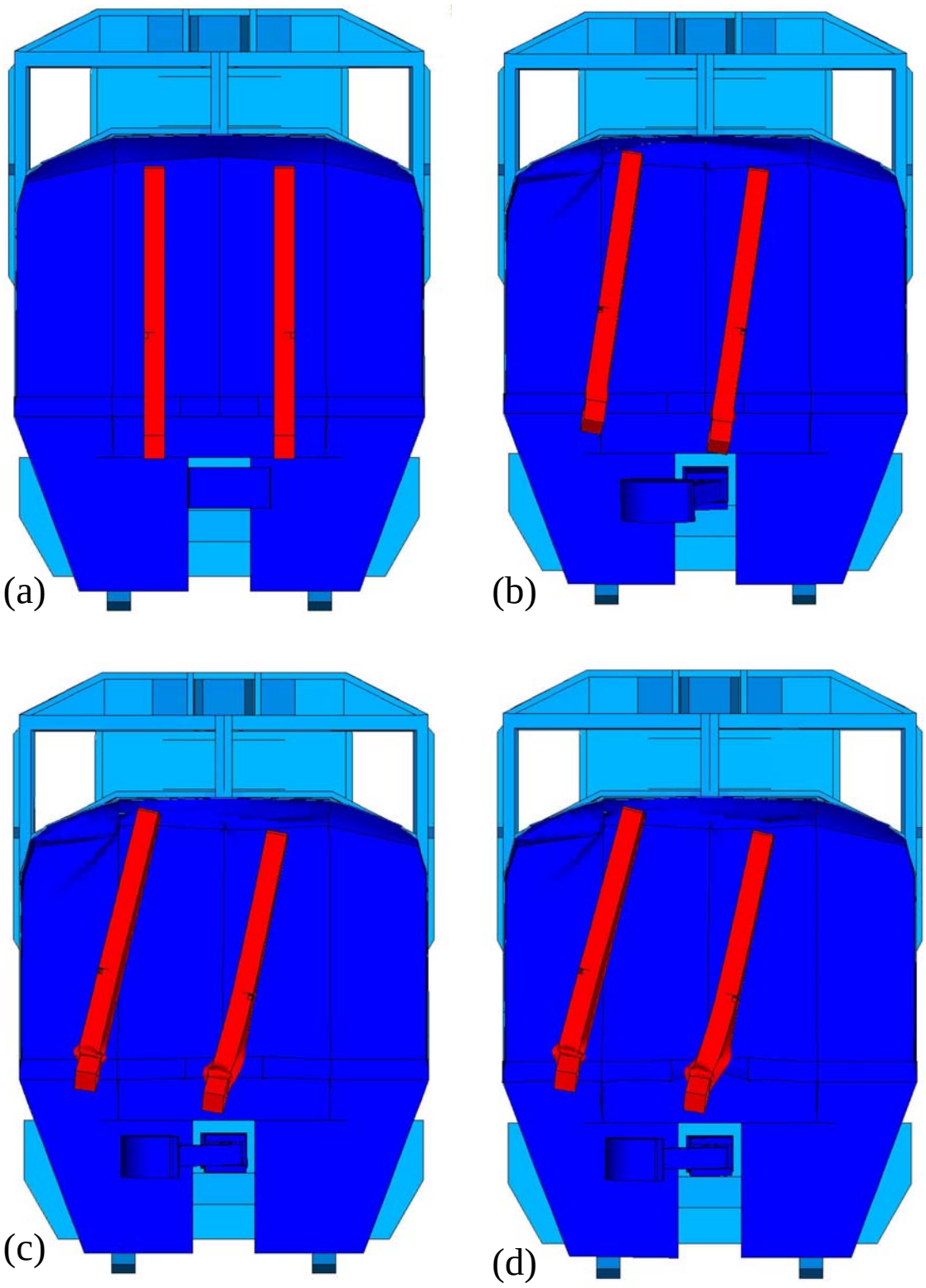

Figure 41. Sequence of Images Showing Deformation of Collision Posts onto the Short Hood of the Standing Locomotive (a) 0.0 s, (b) 0.156 s, (c) 0.3 s, (d) 0.6 s

Figure 41(d) shows that the damage to the anticlimber matches up very nicely with the motion of the collision posts. Moreover, it appears that the lateral shift and the angular rotation of the collision posts are consistent with the post-mortem evidence illustrated in Figures 8 and 9. It appears that much of the rotation occurs early in the collision. After 0.156 s (Figure 41(b)), the collision posts have rotated about 8 degrees from vertical. After 0.3 s (Figure 41(c)), the rotation has increased to approximately 11 degrees; after 0.6 s, it has increased to only about 12 degrees.

An image of the lower end of the cab car collision posts (Figure 42) indicates that the damage to the posts is similar in mode and location to that shown in Figure 7. It appears, however, that the local deformation is more severe in the model. The test damage may be less severe because the local forces on the collision post are relieved through fracture of other components (such as the anticlimber). It could also be less severe simply because the interaction of the end frame with the anticlimber is different because of the manner in which the draft sill deforms and fractures.

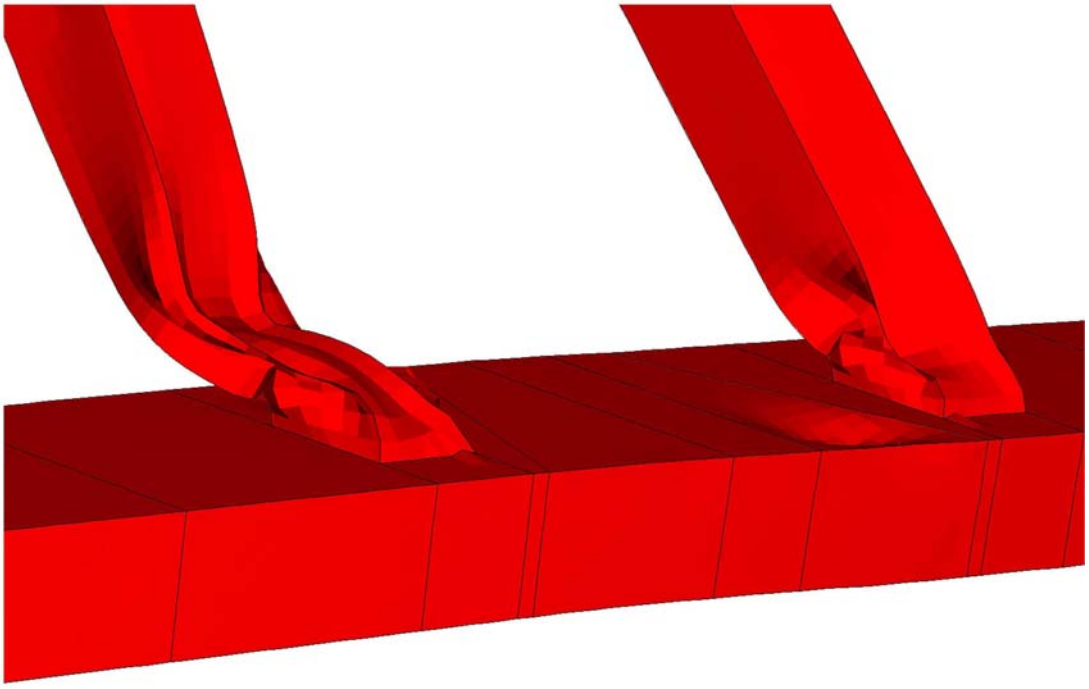

Figure 42. A Closeup of the Model Collision Posts After 0.6 s

Finally, one can compare the test and model with respect to damage to the draft sill. Figure 43 shows a sequence of images that illustrate the evolution of damage in the draft sill. In comparison to Figure 13, it is clear that the model captures both the severe deformation of the draft sill and its tendency to fold into a Z-shape. Due to the extreme levels of deformation, it is difficult to surmise the exact deformation pattern in the demolished draft sill, but it appears that the folding may have occurred primarily in a horizontal plane. In contrast, it appears that, in the model collision, the folding occurs primarily (but not entirely) in a vertical plane.

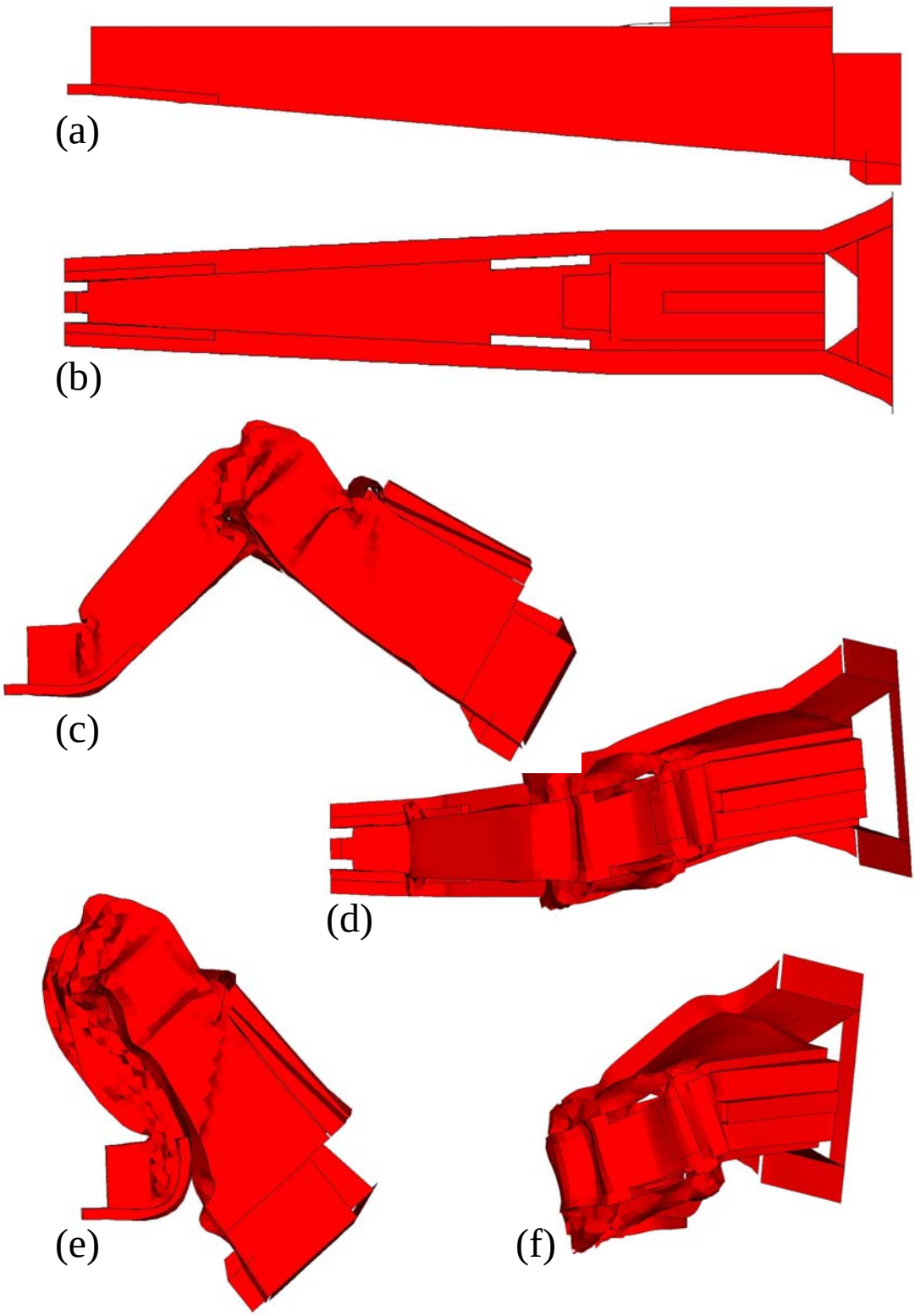

Figure 43. Sequence of Images Showing Deformation of the Cab Car Draft Sill (a) Undeformed Side View; (b) Undeformed, Top View; (c) 0.156 s, Side View; (d) 0.156 s, Top View; (e) 0.3 s, Side View; (f) 0.3 s, Top View

4.2. Colliding Vehicle Motions

In order to produce meaningful comparisons to test results, model predictions of acceleration were also filtered using SAE J211/CFC 60. SAE filtering can be done within the ABAQUS/Viewer post-processing program. Appendix A presents plots showing comparisons between model and test results for each of the selected time histories (motions and forces). Figure 44 shows a visual representation of the complete finite element model. The cab car-led consist is comprised of a detailed model of the cab car and a series of springs representing the trailing cars. The locomotive consist is comprised of a detailed model of the locomotive and a series of springs representing the ballast cars.

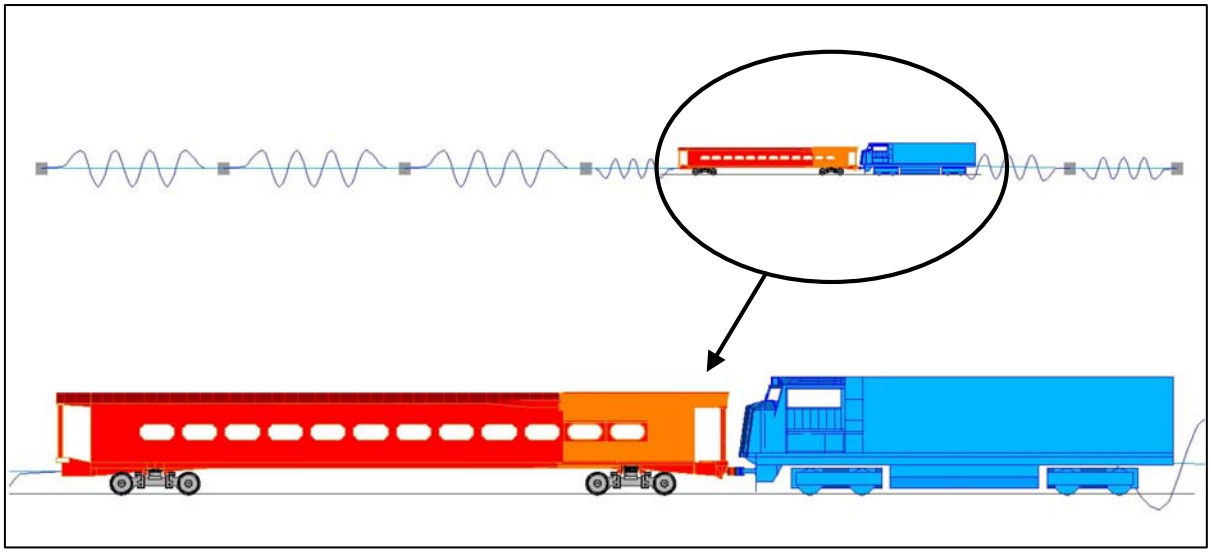

Figure 44. Complete Finite Element Model of the Cab Car-Led Train with the Standing Locomotive-Led Train

Figure 45 shows a comparison of the filtered longitudinal deceleration time histories for the cab car. In general, the model follows the trend of the test data over this 0.5-second interval. It captures the peak deceleration of about 20 G quite well, though the timing appears to be off by a few milliseconds. This may simply be due to a shift in the time of impact recorded in the test or slack in the colliding couplers. The model also captures the 10 G negative deceleration (positive acceleration) that occurs at 0.07 s. After about 0.3 s, the model-predicted accelerations rise above the test data. This is an indication that the model is not picking up the extent of fracture that is occurring during this time period. As noted in Section 3, the model restricts failure to the draft sill only; clearly, as evidenced by Figure 2, extensive fracture is occurring elsewhere in the end frame by this time. Plots for the cab car longitudinal, vertical, and lateral accelerations; velocities; and displacement motions (Figures 46-51) are also included.

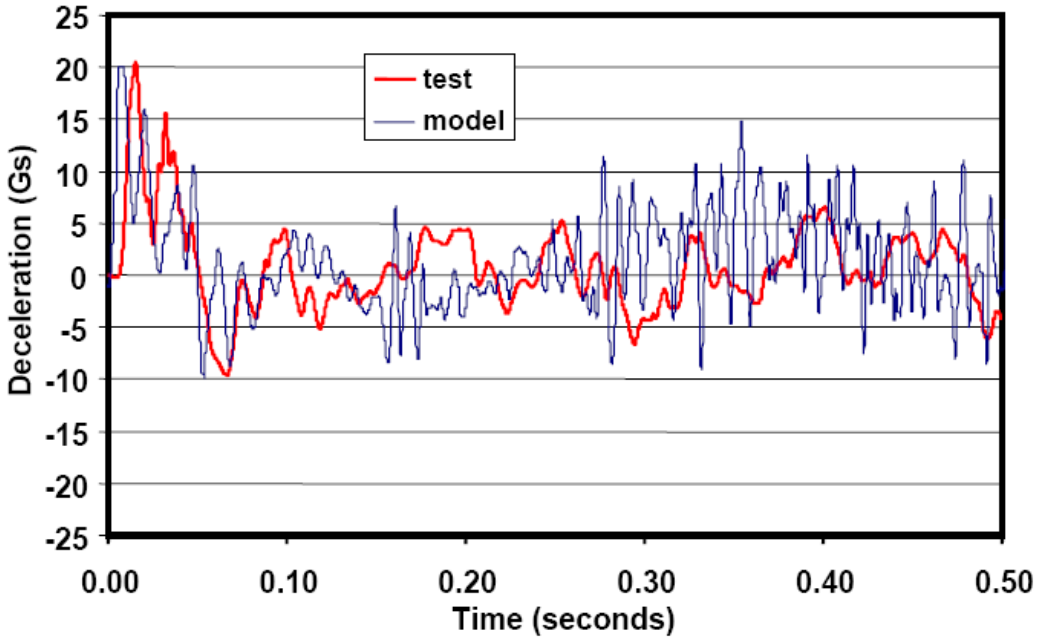

Figure 45. Comparison of Test and Model: Longitudinal Acceleration of Cab Car

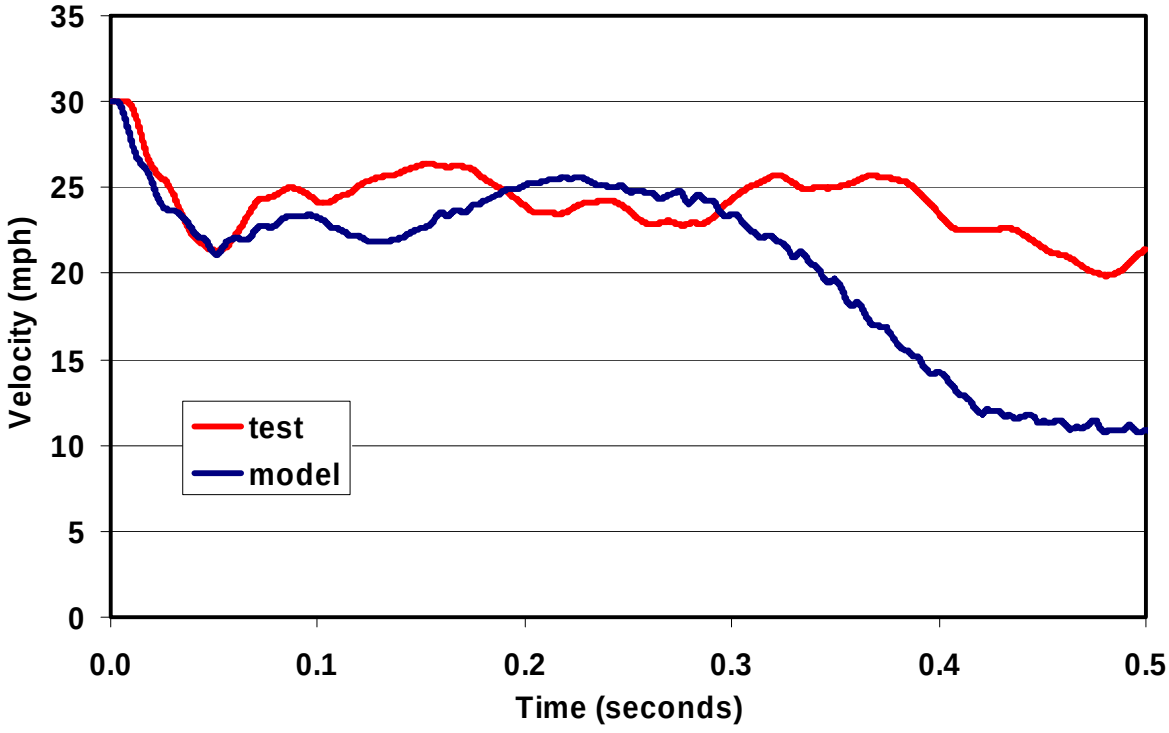

Figure 46. Comparison of Model and Test: Longitudinal Velocity of the Cab Car

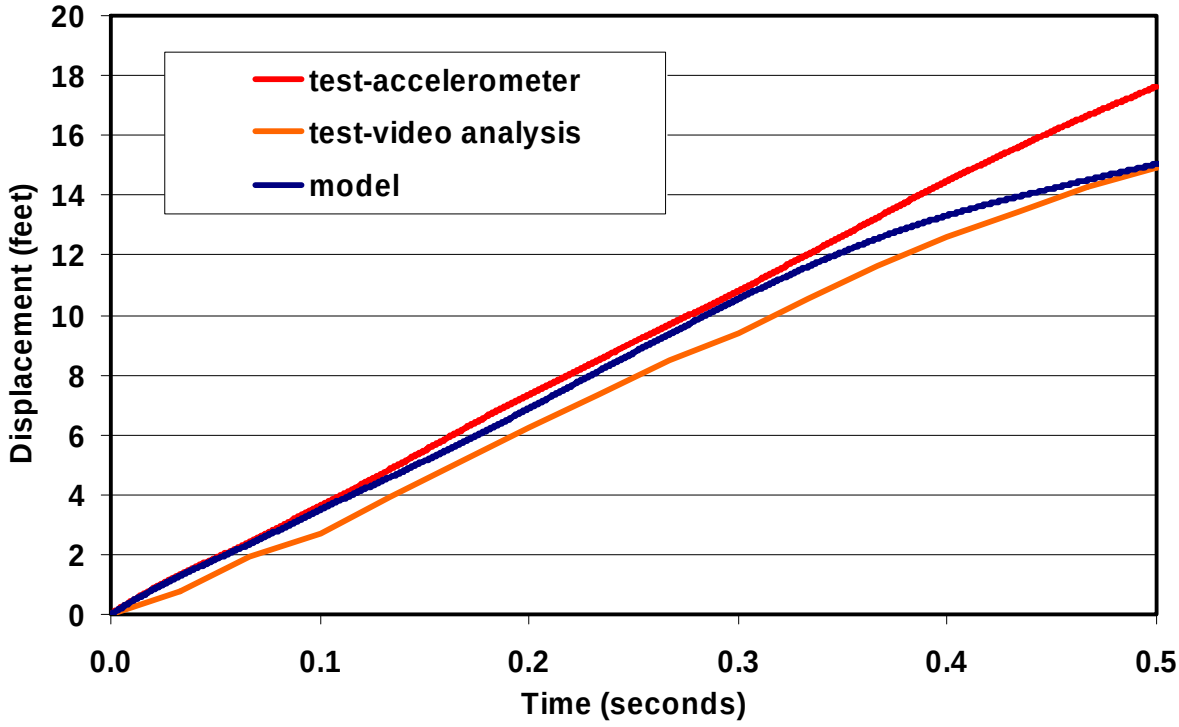

Figure 47. Comparison of Model and Test: Longitudinal Displacement of the Cab Car

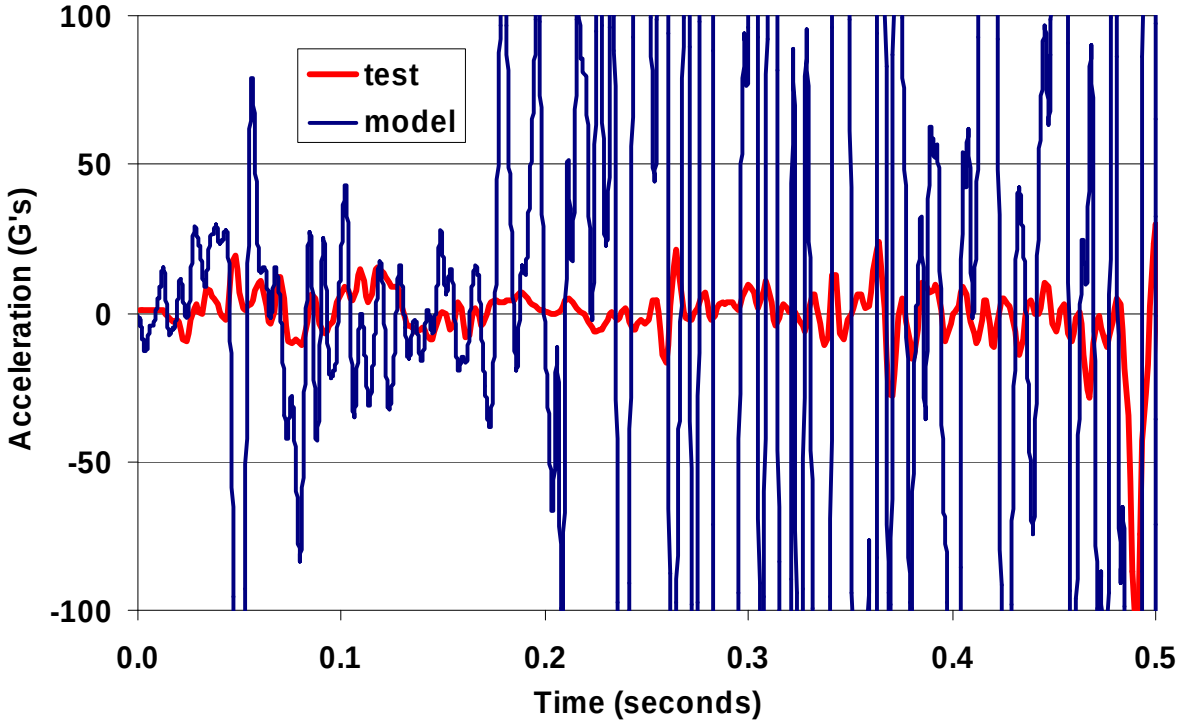

Figure 48. Comparison of Model and Test: Vertical Acceleration of the Cab Car

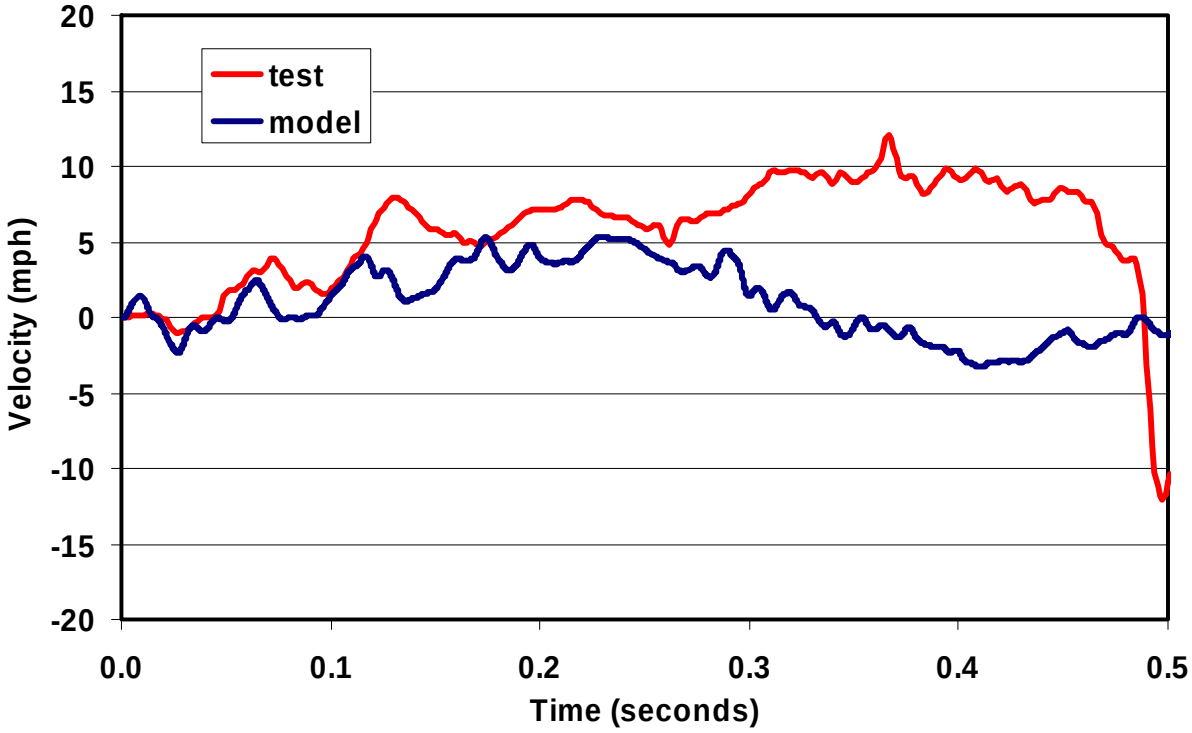

Figure 49. Comparison of Model and Test: Vertical Velocity of the Cab Car

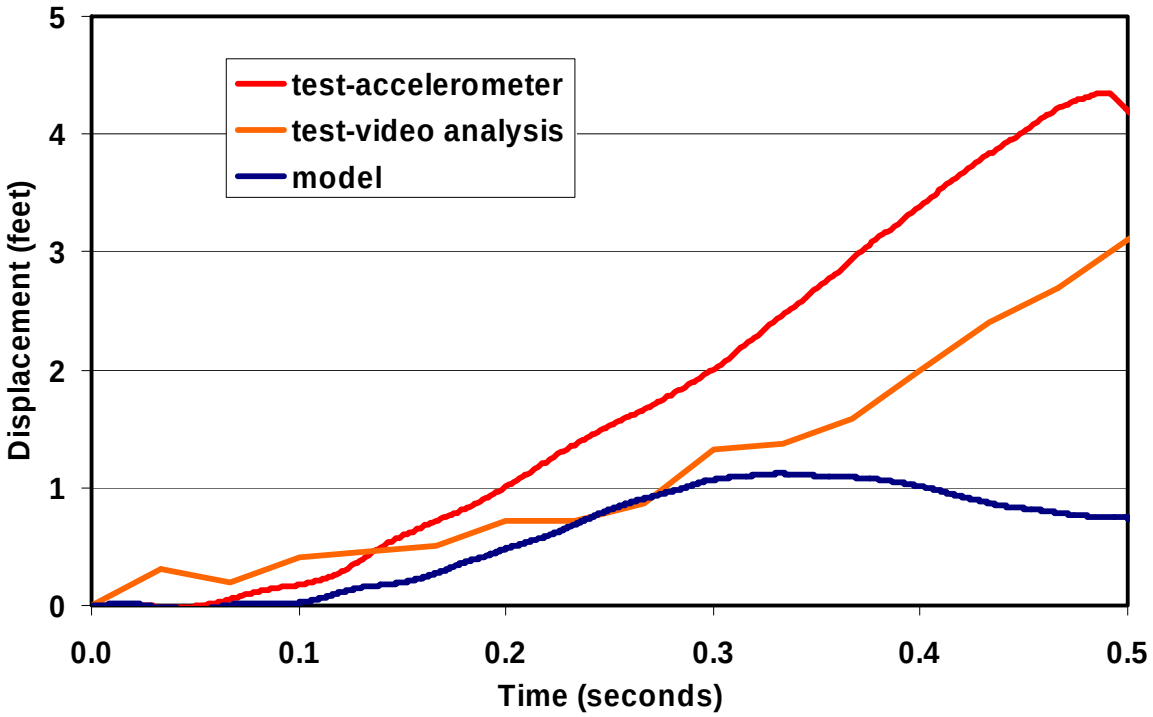

Figure 50. Comparison of Model and Test: Vertical Displacement of the Cab Car

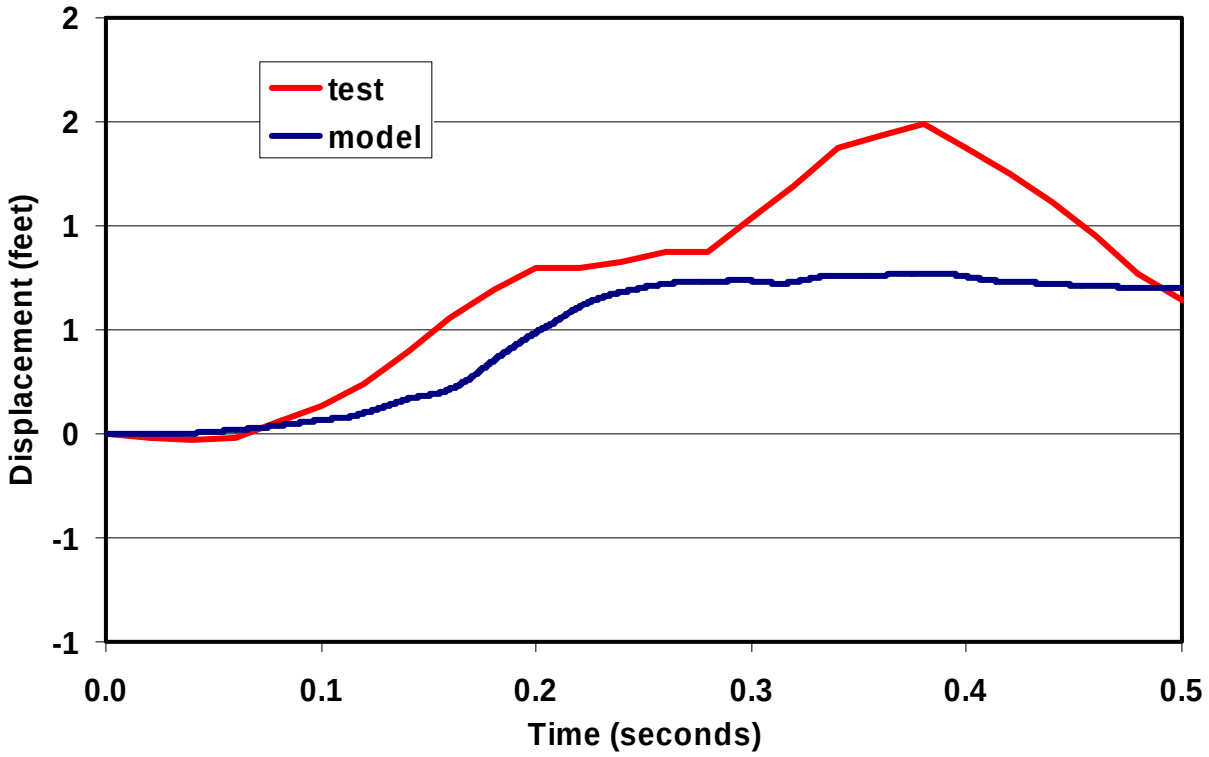

Figure 51. Comparison of Model and Test: Lateral Displacement of the Cab Car

Figure 52 compares the pitch angle that develops during the collision. The results shown in the figure indicate that the model captures the climb of the forward end of the cab car over the first 0.2 s or so of the collision but not after that. In the model, the entire cab car appears to become trapped on the short hood of the locomotive, limiting further upward motion; whereas, in the test, the superstructure of the cab car appears to have torn away from the underframe and continued to climb. To capture the behavior exhibited in the test, more careful attention must be paid to modeling the details of the connections between the cab car superstructure and the underframe.

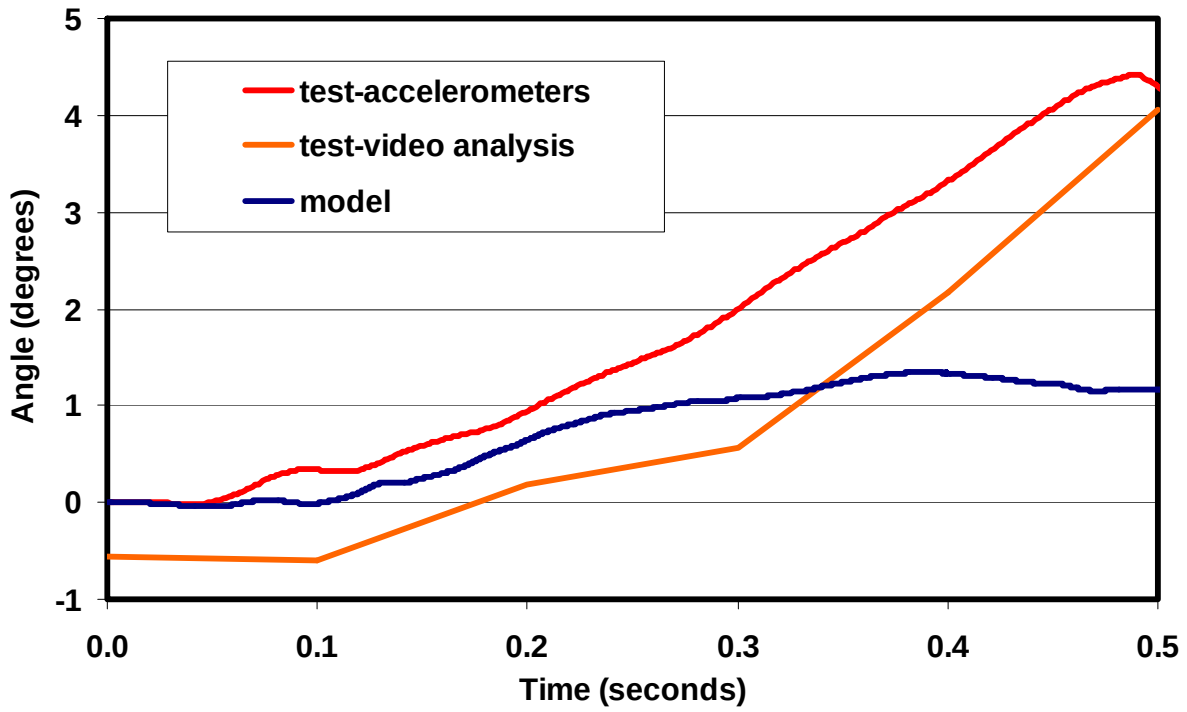

Figure 52. Comparison of Test and Model: Pitch Angle of Cab Car

As noted in Chapter 2, the accelerometer on the locomotive had problems associated with vibration due to loose engine mounts. For this reason, the accelerometer data are noisy and do not lend themselves to comparisons with model predictions. The longitudinal velocity data, which are still considered to be valid, are compared with model predictions in Figure 53. The results indicate that the shape of the velocity history is captured but that its magnitude is underestimated by approximately 50 percent. Model predictions for the longitudinal displacement of the locomotive (Figure 54) seem to be more consistent with video data, indicating that the accelerometer-derived velocity estimation may be overestimating the actual test velocity.

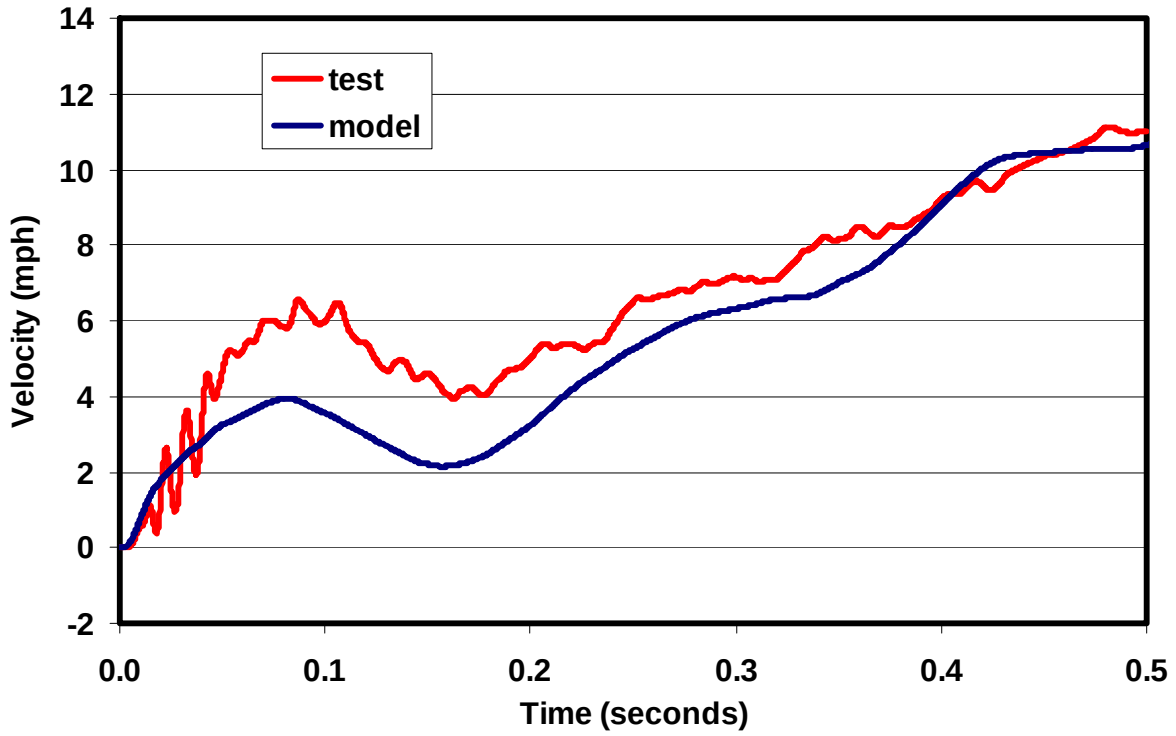

Figure 53. Comparison of Test and Model: Longitudinal Velocity of Locomotive

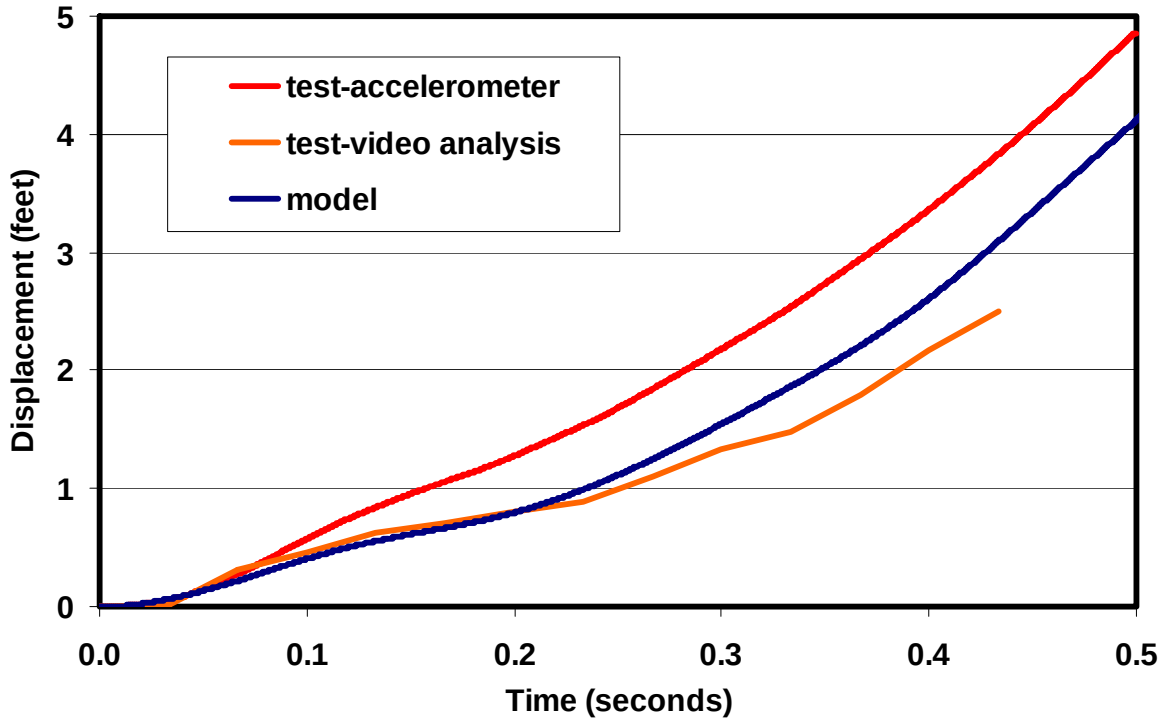

Figure 54. Comparison of Test and Model: Longitudinal Displacement of Locomotive

Subtracting the longitudinal displacement time history of the cab car from that of the standing locomotive provides an indication of the crush displacement time history. Figure 55 shows a comparison of cab car, locomotive, and crush (cab car minus locomotive) displacements versus time. As is evident in this figure, the model and test crush displacements compare quite favorably over the first 0.25 s or so. After this time, the respective curves begin to deviate from one another as the model loses accuracy due to the significant extent of fracture that arises, which the model does not accurately capture. The extensive fracture lowers the resistance of the cab car structure, therefore promoting additional displacement with time.

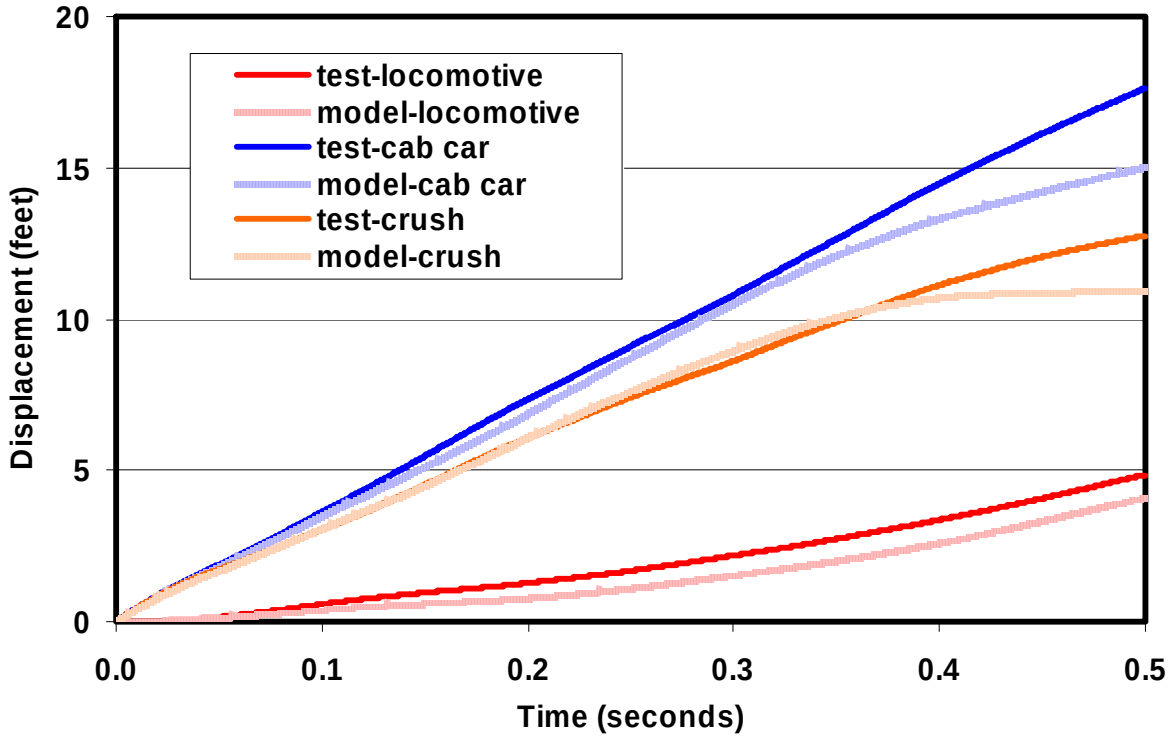

Figure 55. Comparison of Test and Model: Longitudinal Displacement of Locomotive, Cab Car, and Crush

4.3. Collision Force

For the model, the collision force-time history was derived from the acceleration-time histories in the same manner that it was for the test data—under the assumption that each consist behaves as a lumped mass system.

Figure 56 shows a comparison of the collision force based upon test and model-predicted accelerations. For the model, force estimates can be derived from accelerations of both the moving and standing consists (the so-called forward and backward estimates). As the plot indicates, better agreement exists between the model and the test when the model's standing consist acceleration data (the backward calculation) is used. In a lumped mass model, these two

measures of force are equal. In the FEA model, differences between the two curves arise from two sources:

- The change in momentum of the cab car (or locomotive) is not exactly equal to the acceleration of a point near the center of gravity of that vehicle multiplied by the mass of the vehicle.
- The momentum of the moving consist is not conserved—an impulse is applied to ground through contact forces acting through the wheels.

Further investigation indicates that using the acceleration at a single nodal location produces noise in the force prediction but does not significantly affect the trend of the data. However, it turns out that the impulse to the ground is significant. Correcting the force calculation by subtracting the ground's reaction force (Figure 57) results in a better comparison between the forward calculation and the test data, as well as more consistency between the forward and backward force estimates of the model.

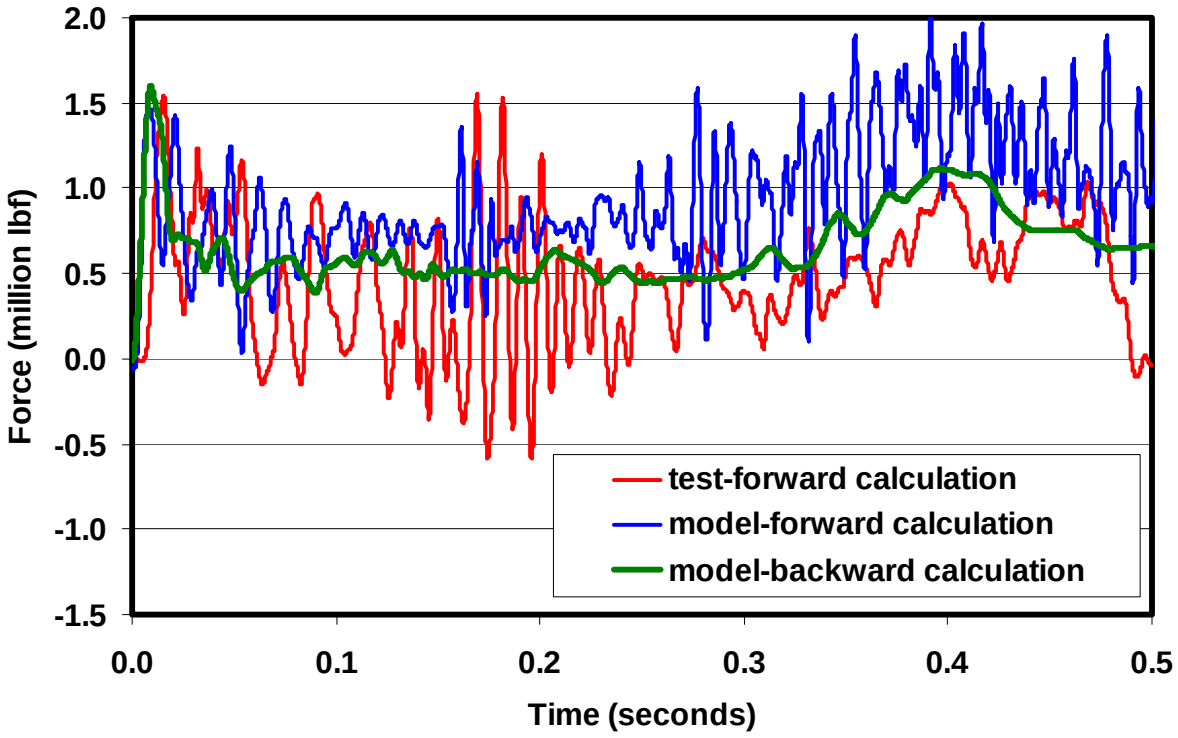

Figure 56. Comparison of Test and Model: Collision Force

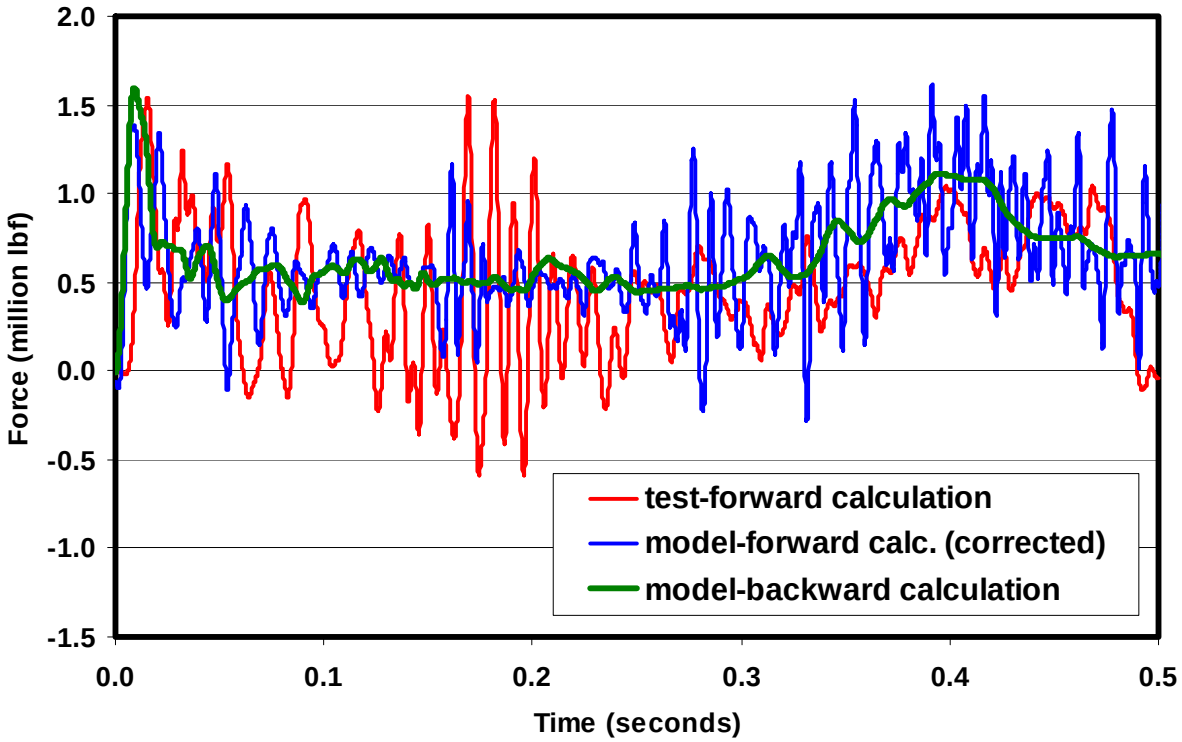

Figure 57. Comparison of Test and Model: Collision Force (Corrected)

4.4. Trailing Vehicle Forces

Trailing vehicle forces were also determined in a manner consistent to that used for the test data—the trailing force on the lead vehicle was calculated as the sum of the masses times the accelerations of each of the vehicles trailing the cab car. Or, alternatively, the sum of the masses times the accelerations of all of the vehicles forward of the first coach car (i.e., the cab car plus the entire standing consist). This estimate was also corrected by amount of the ground reaction force.

Figure 58 compares model and test results for the cab car trailing vehicle force time history. Of particular interest for this study is the large magnitude of the trailing force acting on the cab car. In comparison to a single-vehicle collision, the trailing force clearly has a significant effect on the collision force. It appears from Figure 58 that the magnitude of the model-predicted trailing vehicle force on the cab car is higher on average than the values derived from the test data, even over the first 0.25 s of the collision. This indicates that the values used for the stiffness and damping characteristics of the trailing vehicle connections may need to be modified.

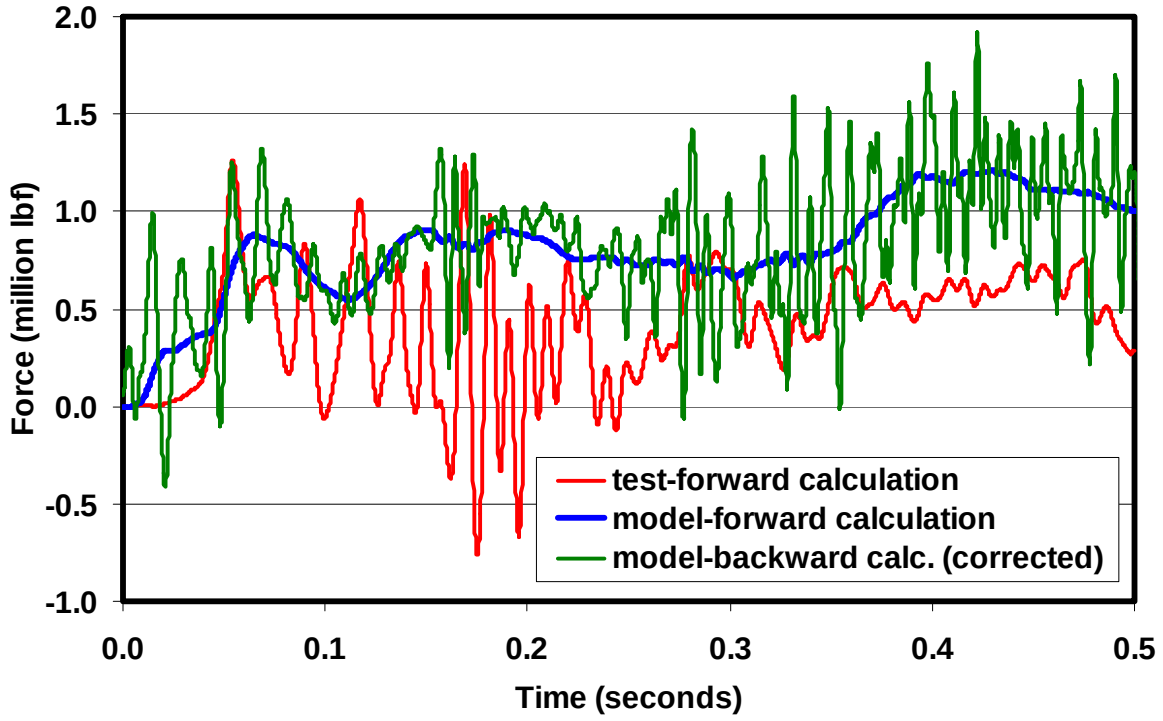

Figure 58. Comparison of Test and Model: Moving Consist—Trailing Vehicle Forces (Corrected)

Further investigation of the discrepancy between model and test predictions for the cab car trailing vehicle force over the first 0.25 s of the collision suggests that it can be explained, at least in part, by what appears to be a substantial difference between the force-deflection characteristics of the spring used to model the connection between the second and third trailing coach cars and the actual force-deflection characteristics of the connection. This difference is noticeable when comparing the model and test velocity histories for the moving consist (Figure 59).

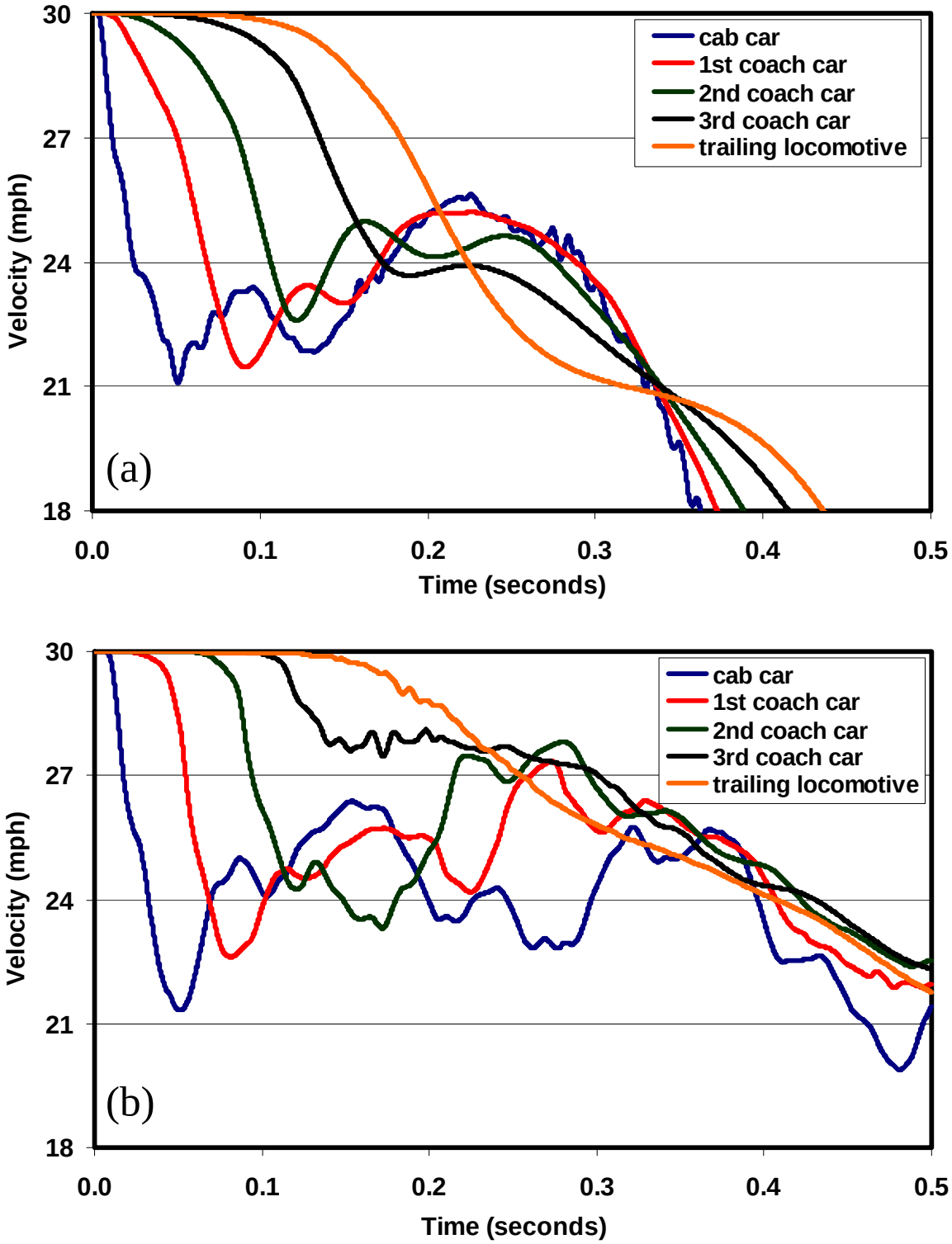

Figure 59. Comparison of Test and Model: Moving Consist—Moving Consist Vehicle Velocities (a) Test (b) Model

In examining these velocity profiles, it appears that the model captures the decrease in velocity over the first 0.2 s of the collision for the cab car and the first and second coach cars reasonably well. It appears, however, that the decrease in velocity of the fourth vehicle during this time period is not well captured. The velocity of the third coach car plateaus at about 28 mph (45 km/h) between 0.15 and 0.2 s. Clearly, little force backward exists on the third coach car from the second coach car during this time interval. A comparison of the relative longitudinal displacements of the vehicles (Figure 60) indicates that the relative displacement between the cab car and the first coach car and between the first and second coach cars stabilizes after about 5 in of crush, indicating that there is about 5 in (127 mm) of relatively compliant compression of both draft gears before the much stiffer underframes begin to deform. However, the curve is much different for the connection between the second and third coach cars, with over 8 in (203 mm) of crush occurring before the connection stiffens up. In contrast, the model connectors are defined to have 3 in (76 mm) of compliant crush before they stiffen.

The trailing force appears to be greatly affected by this discrepancy. The difference between model and test results for the deceleration of the third coach car during the 0.15 to 0.20 s time interval implied by Figure 33 is nearly 4 G (4 mph, or 6.4 km/h, decrease over 0.05 s). Since the fourth coach car weighs nearly 150,000 lbm (67,000 kg), this represents a change in trailing force of nearly 600,000 lbf (2,668,800 N). This value is consistent with the difference between model and test values for trailing force during this time interval, as indicated in Figure 58.

This discrepancy can likely be mitigated to some extent by adjusting the stiffness parameters for the model connectors. (Corrections of this sort can be made only through either examination of post-test data or careful characterization of conditions prior to the test.) In any event, it is clear that collision and trailing forces are sensitive to these parameters.

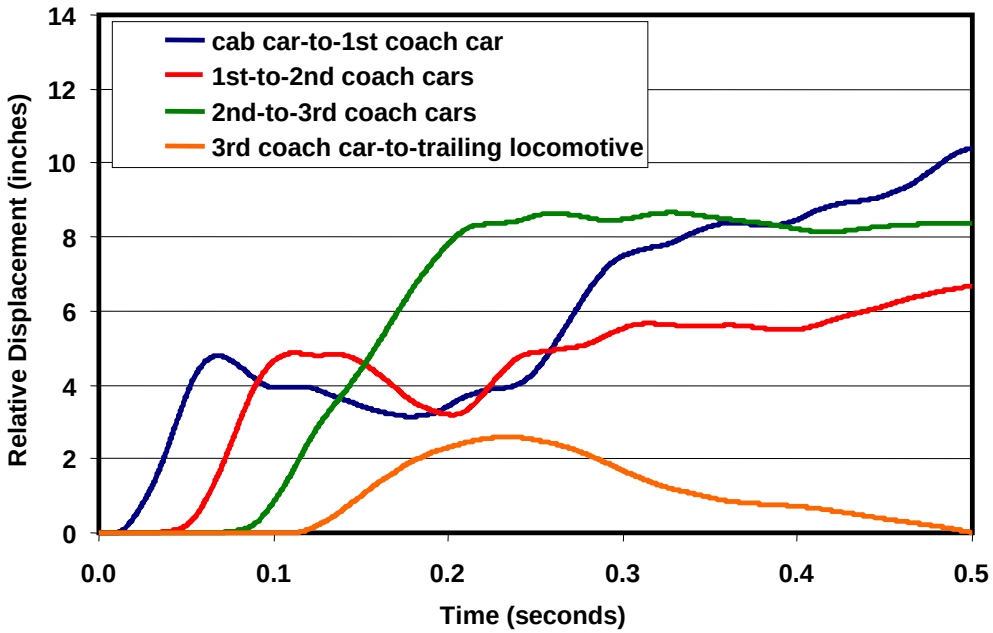

Figure 60. Test Data—Moving Consist Relative Vehicle Displacements

In contrast to the results for the moving consist, the trailing force on the standing locomotive (Figure 61) seems to be well captured by the simplified model of its trailing vehicles and vehicle-to-vehicle connections.

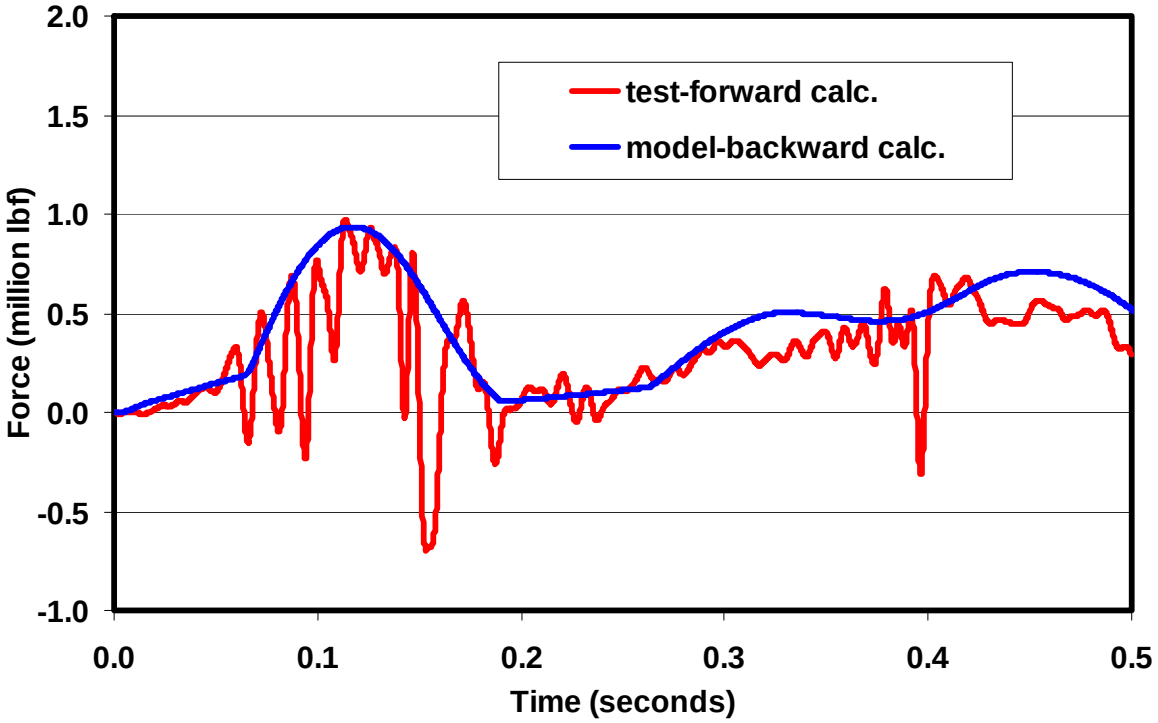

Figure 61. Comparison of Test and Model: Standing Consist—Trailing Vehicle Forces

5. Summary and Conclusions

Overall, the detailed finite element simulation of the train-to-train test collision captures many aspects of the collision behavior.

In particular, the longitudinal motions of the colliding vehicles and the collision forces were calculated with reasonable accuracy, especially at the early stages of the collision. In addition, many of the key modes of deformation were captured, including the severe folding of the draft gear (if not the precise mode), the downward bending of the end frame and its subsequent locking onto the short hood of the locomotive, the rotation of the end frame and associated off-center interaction of the collision posts with the anticlimber short hood, and the pitch rotation of the cab car body and lifting of the forward truck wheels.

The results of the model further indicate that the motion and the modes of deformation of the cab car and locomotive end frames are affected by the configuration of the couplers at the time of the collision. With misaligned initial position assumed for the colliding couplers, the model is able to produce a vehicle end trajectory that matched up with the actual trajectory very closely. Reversing the initial positions of the couplers would result in a roll rotation of the cab car end frame in the opposite direction of the test. The model was able, however, to capture this rotation without having to vary the degree of coupler misalignment, suggesting that the deformations of the cab car and locomotive may not, in fact, be very sensitive to the degree of misalignment or offset.

To simulate the later stages of the impact accurately, the model needs further development in two key areas: the representation of trailing vehicle and vehicle-to-vehicle connection parameters on collision forces and the representation of fracture on the deformation of the end frame.

The effect of trailing vehicle parameters on the prediction of collision forces is one that also affects the formulation of lumped-parameter collision dynamics models. A concurrent effort exists to refine the representation of vehicle-to-vehicle connections using the results of the two-car impact test conducted on April 4, 2000. The results of that effort were not available in time for inclusion in this model.

The material failure issue is most critical if one wishes to accurately simulate more than the first 0.25 s of the collision; however, many challenges are related to accurately modeling the effect of fracture. With respect to material behavior, one must not only characterize the fracture behavior of the components and connections as a function of stress and strain but also characterize how the variation of this behavior from place to place on a particular vehicle or with time might affect the mode of the collision. With respect to modeling, it is clear that, for these types of collisions, one needs to be able to simultaneously model fracture and contact. However, numerical issues are associated with interaction between newly created surfaces produced by fracture that still need to be resolved. The capability of finite element codes, such as ABAQUS, to handle such complex behavior has increased dramatically in recent years and is likely to continue to do so. Modeling the separation of the vehicle superstructure with the end frame is also desirable, although it is not clear that this would significantly change predictions for vehicle motions or collision forces.

In summary, the favorable comparisons between the model predictions and the test measurements over the first 0.25 s of the collision suggest that the model can be an effective tool for evaluating the consequences of a collision between two trains and, more importantly, for helping to improve the design of vehicle end structures so that they are better able to withstand such collisions.

6. References

1. Tyrell, D., Severson, K., Perlman, A.B., and Rancatore, R., "Train-to-Train Impact Tests: Analysis of Structural Measurements," Proceedings of IMECE'02, the 2002 ASME International Mechanical Engineering Congress and Exposition, November 17-22, 2002, New Orleans, LA.
2. Stringfellow, R., Mayville, R., and Rancatore, R., "Evaluation of Protection Strategies for Cab Car Crashworthiness," Arthur D. Little, Inc. Report Reference 30299-05 (January 2000).
3. Mayville, R.A., Johnson, K., and Stringfellow, R.G., "Development of Conventional Passenger Cab Car End Structure Designs for Full-Scale Testing," TIAX Final Report to the Volpe National Transportation Systems Center, Cambridge, MA, Reference 74431 (December 2002).
4. Martinez, E., Tyrell, D., and Zolock, J., "Rail-Car Impact Tests with Steel Coil: Car Crush," in Proceedings of ASME/IEEE Joint Railroad Conference, April 22-24, 2003, Chicago, IL.
5. Tyrell, D.C., Severson, K.J., Mayville, R.A., Stringfellow, R.G., Berry, S., and Perlman, A., "Evaluation of Cab Car Crashworthiness Design Modifications," in Proceedings of the 1997 IEEE/ASME Joint Railroad Conference, March 18-20, 1997, Boston, MA, pp. 49-58.
6. Kirkpatrick, S., and MacNeil, R., "Development of a Computer Model for Prediction of Collision Response of a Railroad Passenger Car," Proceedings of the 2002 ASME/IEEE Joint Railroad Conference, April 23-25, 2002, Washington, DC.
7. Tyrell, D., Severson, K., Marquis B., Martinez, E., Mayville, R., Stringfellow, R., Hammond, R., and Perlman, A.B., "Locomotive Crashworthiness Design Modifications Study," Proceedings of the 1999 IEEE/ASME Joint Railroad Conference, April 13-15, 1999, IEEE Catalog Number 99CH36340, ASME RTD Volume 16.
8. Tyrell, D., "Passenger Rail Train-to-Train Impact Test Volume I: Overview and Selected Results," U.S. Department of Transportation, DOT/FRA/ORD-03/17.I, July 2003.
9. Tyrell, D., Severson, K., and Perlman, A.B., "Single Passenger Rail Car Impact Test Volume I: Overview and Selected Results," U.S. Department of Transportation, DOT/FRA/ORD-00/02, March 2000.
10. Tyrell, D., Severson, K., and Perlman, A.B., "Passenger Rail Two-Car Impact Test Volume I: Overview and Selected Results," U.S. Department of Transportation, DOT/FRA/ORD-01/22.I, January 2002.
11. Tyrell, D., private communication, 2002.

Appendix.

Comparison of Model Predictions and Test Results for Vehicle Motions and Collision Forces

This appendix includes three pairs of curves. Each pair has an uncorrected and a corrected version.

Table A-1. Listing of Plots Comparing Test Measurements and Model Predictions

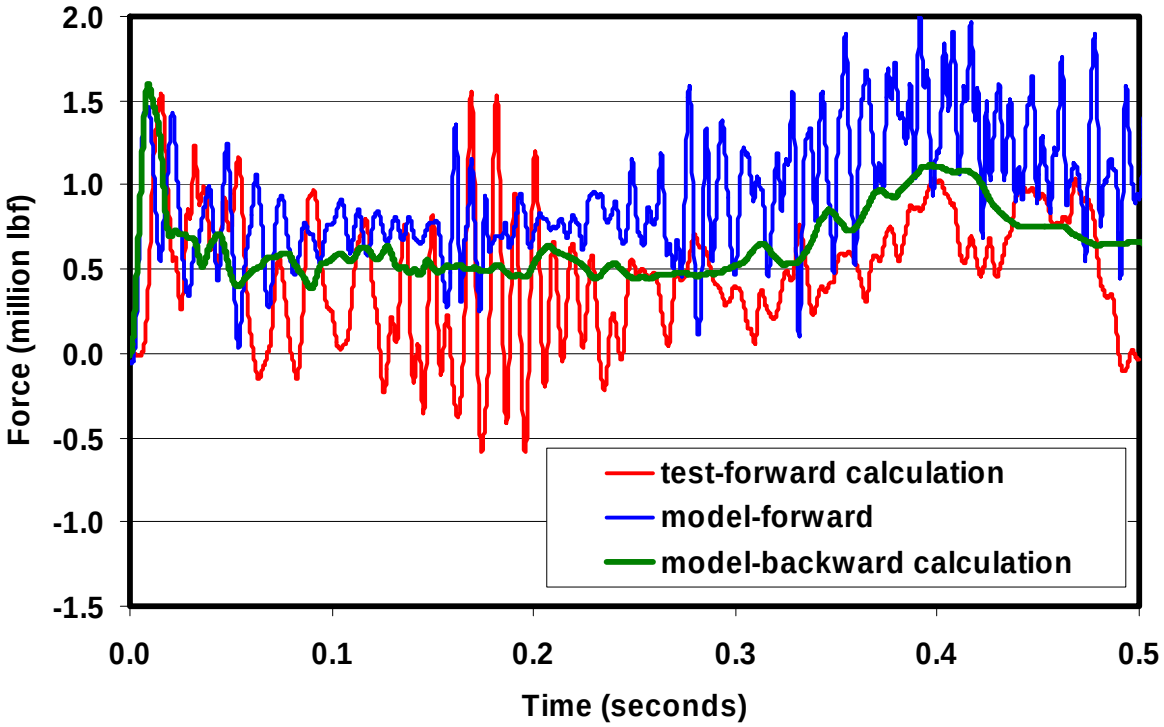

Figure A-1a. Comparison of Model and Test: Longitudinal Collision Force

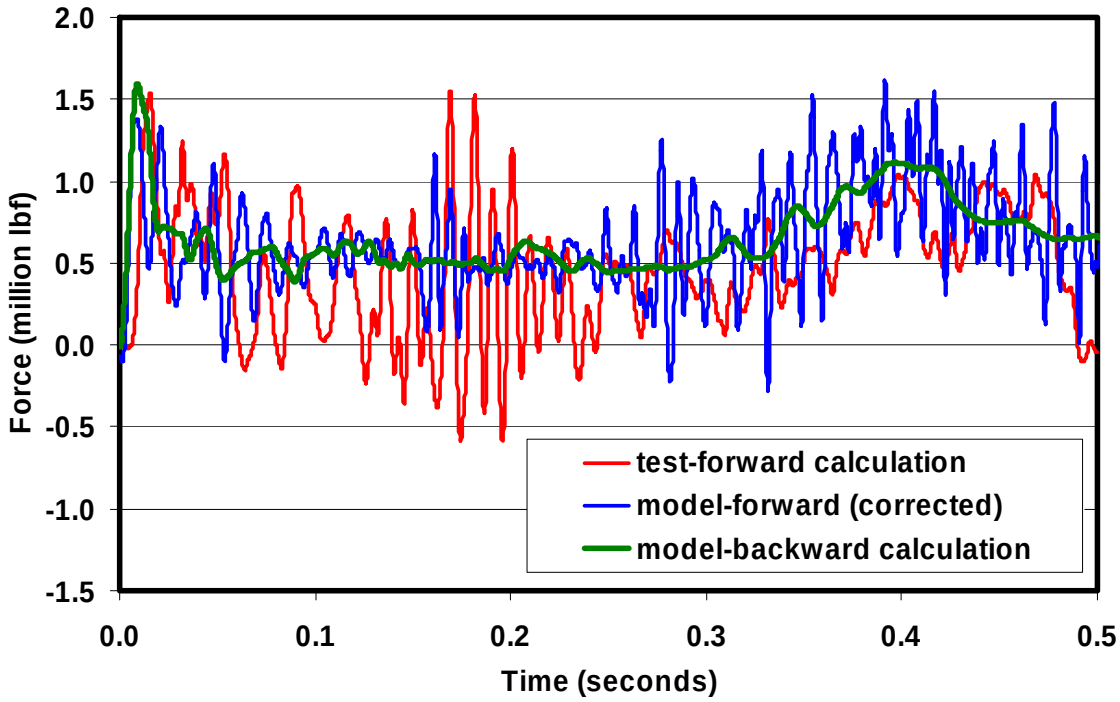

Figure A-1b. Comparison of Model and Test: Longitudinal Collision Force (Corrected)

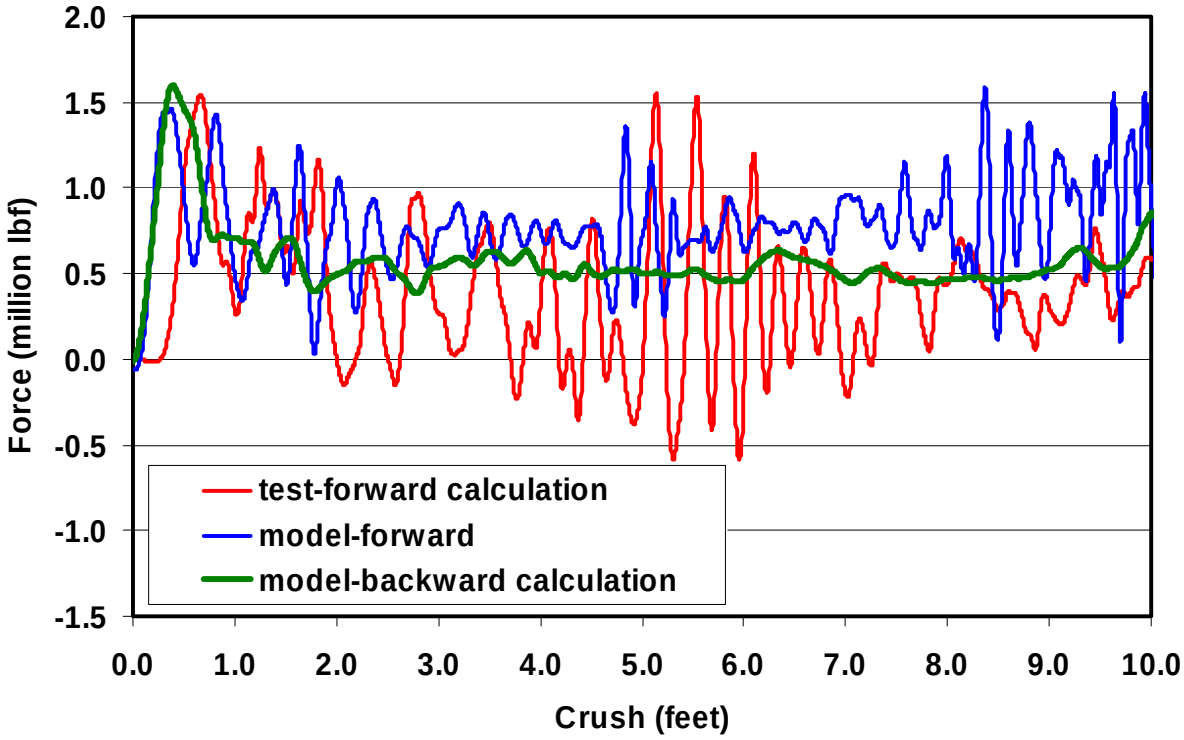

Figure A-2a. Comparison of Model and Test: Collision Force-Displacement Curve

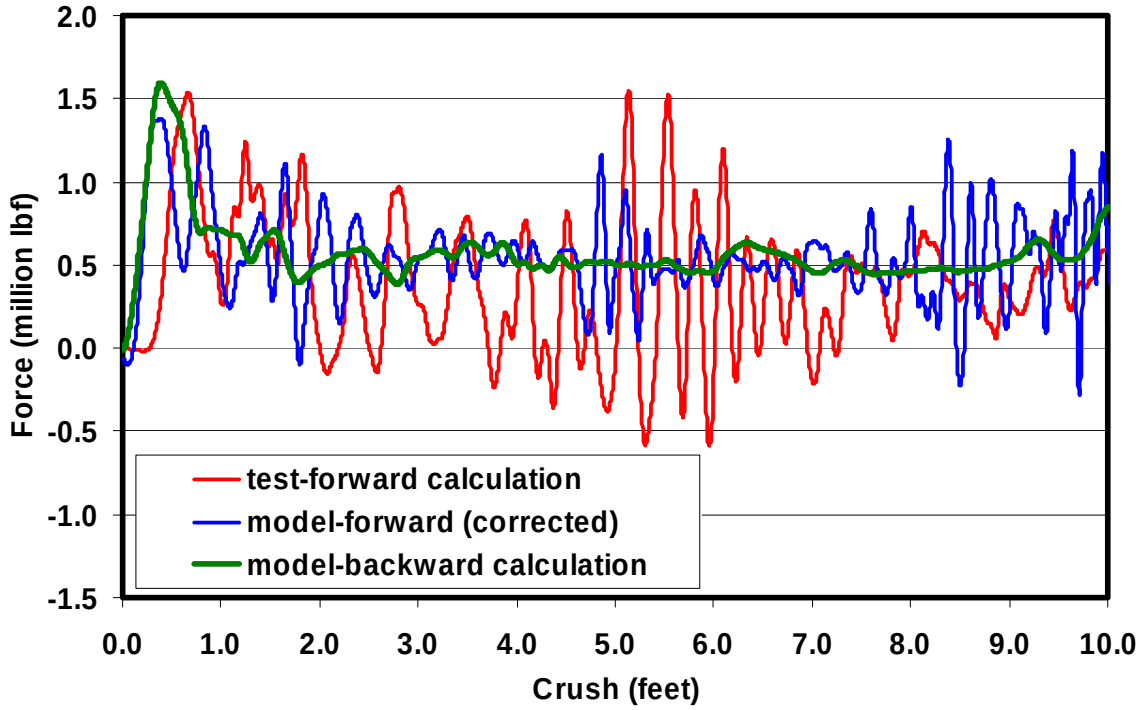

Figure A-2b. Comparison of Model and Test: Collision Force-Displacement Curve (Corrected)

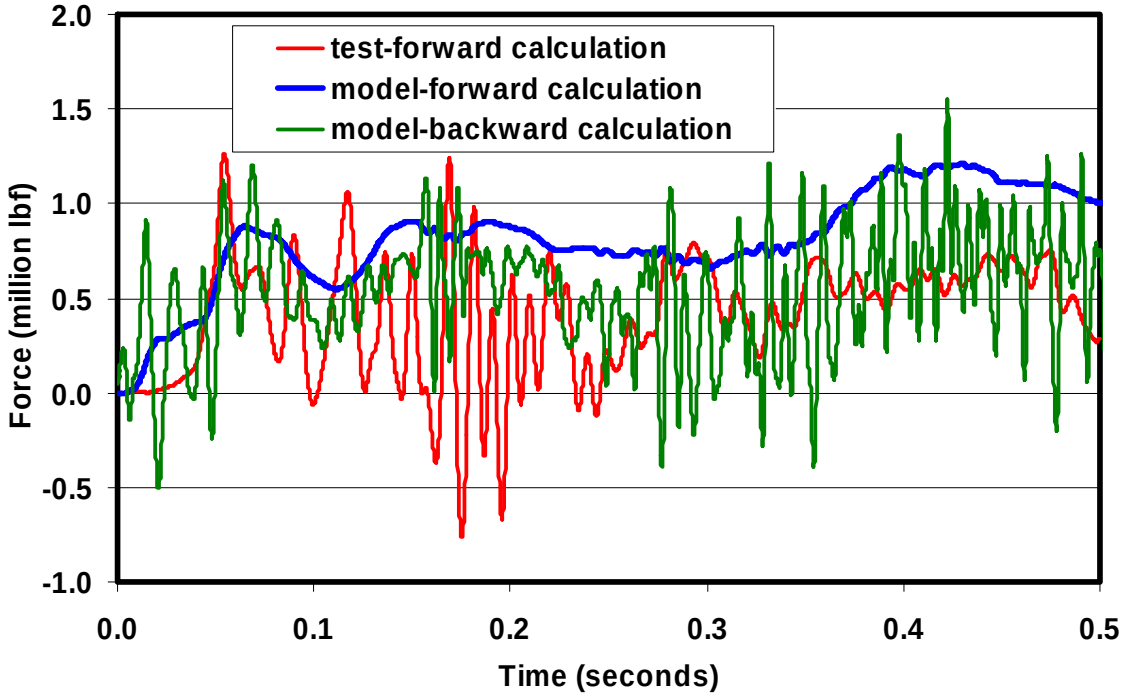

Figure A-3a. Comparison of Model and Test: Trailing Force on Cab Car

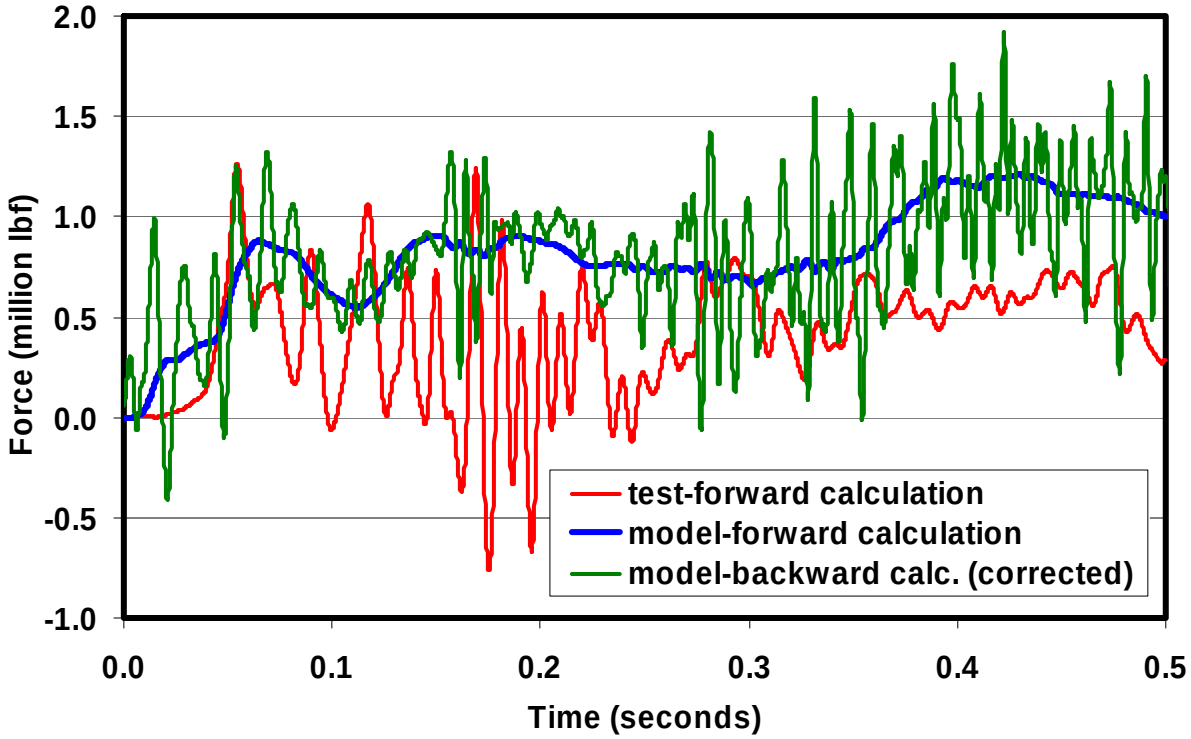

Figure A-3b. Comparison of Model and Test: Trailing Force on Cab Car (Corrected)

Acronyms

c.g.	center of gravity
CFC	Channel Frequency Class
EMD	Electro-Motive Diesel, Inc.
FEA	finite element analysis
ft	feet
G	acceleration of gravity
in	inch
SAE	Society of Automotive Engineers
TTC	Transportation Technology Center
s	second/seconds
Volpe Center	Volpe National Transportation Systems Center